UNIVERSITY OF THESSALY

SCHOOL OF ENGINEERING

DEPARTMENT OF CIVIL ENGINEERING

Master Thesis

THE EFFECT OF CONSTANT RESTORING FORCE IN A SEISMICALLY ISOLATED BRIDGE MODEL EXCITED BY NEAR-FIELD GROUND MOTIONS

by

MICHALIS EVANGELINAKIS

A Thesis
Submitted in Partial Fulfillment of the Requirements for the Degree
of Master of Science in Civil Engineering
2011

Acknowledgments

I would like to express my sincere gratitude to my advisor Associate Prof. Panagiotis Tsopelas for his support and guidance during my research experience, as well as to Prof. Eyripides Mystakides for the accommodation in the Construction Design and Analysis Lab for my simulations and analysis of my research problem.

One more personal note, I would like to thank my family for the mental support during all these years of study and of course my friends and colleagues for the courage and all the precious moments that we shared at the time of my postgraduate studies.

Table of Contents

1 Introduction

Strong far-field and near-fault ground motions could induce large accelerations and substantial internal forces into a structural system putting it at risk of not surviving them. A-seismic structural design must be able to optimize the reduction of both internal forces and displacements in a structural system. Seismic isolation is such a design approach and has been widely incorporated in seismic protection strategies, reducing those responses by lengthening the fundamental period of the structures and/or providing supplemental energy dissipation.

A variety of seismic-protection devices, classified as active, semi-active and passive, depending on performance and nature of the developing forces are employed in seismic isolation systems. Friction-type damping forces could be effective in seismic protection when long period ground (near-fault) motions are considered. However, such forces are responsible, in general, for large permanent displacements in the isolation level. Therefore, restoring forces are needed capable to re-center the isolated structure. Such a restoring force could be one which has constant amplitude throughout the displacement range.

A number of devices (Tsopelas and Constantinou 1994, Pekcan et al 1995 and Christopoulos et al. 2008), have been proposed to reduce structural responses (displacements and/or forces) under dynamic excitations which have a strong “impact/high velocity” component. Such excitations are the near-fault type of seismic motions as they have come into the earthquake and structural engineering research attention after the 1994 Northridge, 1995 Kobe, and 1999 Taiwan earthquakes.

The effect of constant restoring force of a seismic isolation system on the responses of a seismically isolated bridge model excited by near-fault and far-field seismic motions is examined extensively. In order to evaluate that effect, the system responses (isolation system displacements, deck accelerations, pier accelerations, pier shear forces) have to be compared to the responses of the isolated bridge when another isolation system (e.g. visco-elastic in nature with linearly increasing restoring force) is utilized.

Following this approach, one has to design/create a seismic isolation system which will provide similar isolation (stiffness or period) and energy dissipation (damping) properties, to the isolation system with the constant restoring force. One has to recognize that designing such system might not be possible since an isolation system with constant restoring force has a highly non-linear behavior which can only be approximated (for a given level of

displacement amplitude) by a system with effective properties, if the choice of a base system to compare against is a simple linear visco-elastic isolation system.

Two isolation systems consisting of two components are considered in the present study. The first component, which is common to both isolation systems, is the sliding bearings, which provide normal load carrying capacity as well as energy dissipation through friction. The second component, which is different for the two isolation systems, and is presented for each one below, provides restoring force and viscous damping capacity.

- In the first isolation system: Fluid Restoring Force and Damping Devices (FRFDD) providing constant restoring force and non-linear viscous damping capacity.
- In the second isolation system: visco-elastic devices provide linear restoring force (linear spring) and linear viscous damping capacity.

1.1 Effect of Constant Restoring Force

The constant restoring force mechanism of a restoring force device is depicted in Figure (1-1) as compared to the linear restoring force provided by a typical linear spring.

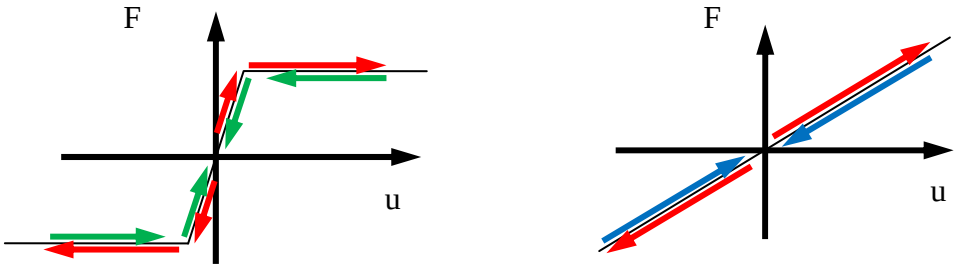

Figure (1-1) Force displacement relationship of a a) constant restoring and b) linear restoring force spring.

The restoring force provided by a linear spring is proportional to displacement, which implies that as the spring deformation increases the restoring force, the spring force imposes on the mass of a dynamic system, increase. As the spring has reached its maximum displacement and is returning towards to its initial, equilibrium position, the restoring force decreases and the only force on the mass is the "inertial force" which can be manifested as the velocity which the mass is crossing (passing through) the equilibrium position.

When considering a constant restoring force spring (CRFS), the restoring force remains constant in amplitude throughout the motion/oscillation. This property has a significant effect in the behavior of a spring-mass system: at the point of half period of an oscillation (after a mass has reached the maximum displacement and is returning towards the neutral position) the velocity which a mass crosses the neutral position is much larger than the velocity of a mass when the restoring force is provided by a linear spring. This can be easily seen when someone considers the potential energy stored in the two springs at the maximum deformation which in turn is transformed into kinetic energy at the equilibrium position.

The potential energy stored in a constant restoring force spring with force F_{max} and deformation "u_0" is : $E_{CRFS} \approx F_{\max} u_o$ and the energy stored in a linear spring extended at the same deformation level and reacting by the same force is : $E_{LS} = \frac{1}{2} F_{\max} u_o$

From that energy expression becomes clear that the potential energy to be transformed to kinetic energy, manifested by velocity, is almost twice for the constant restoring force spring. The velocity at the point of equilibrium in of an oscillatory motion is very important, since it is nothing more than the initial condition for the motion of the mass when the displacement is zero (crosses zero). If that value is high then the maximum displacement which is going to

be reached (in the following half cycle) in the oscillation in the direction of the velocity, is going to be high also. To demonstrate this point, consider a SDOF system which undergoing free vibrations with initial conditions of velocity only. The system is going to deform more in the first cycle when the initial velocity is higher. Exactly this point might be the one where an engineer has to be cautious when systems with constant restoring forces are utilized within a structural system.

2 Bridge Seismic Isolation

The seismic protective system utilized in the present study consists of:

- Flat sliding bearings, capable to support the deck weight and provide energy dissipation and through friction in.
- Fluid Restoring Force/Damping (FRFD) Devices, capable in providing constant restoring force through fluid pressurization and damping forces.

Both components contribute as isolation and energy dissipation mechanisms, to the bridge seismic protective system.

The bridge structure utilized in this study is a scaled model (length scale factor equal to 4). Thus **the results produced and discussed refer to the scaled bridge model and not to a full scale bridge**.

2.1 Sliding Bearings

The bridge model is equipped with four unidirectional sliding bearings, (Tsopelas 1994). The disk type sliding bearing consists of a bottom plate which is supported by a high hardness Adiprene disc and a shear restriction mechanism. The Adiprene disk provides rotational capability to the bottom plate thus full contact of the sliding interface is secured. A plate with PTFE or other materials is attached in the circular recessed section of the disk. A detail cross section of the sliding isolator is shown in Figure (2-1). In the present study the materials used had a coefficient of friction ranging between 7% and 15% as it is shown in Figure (2-2).

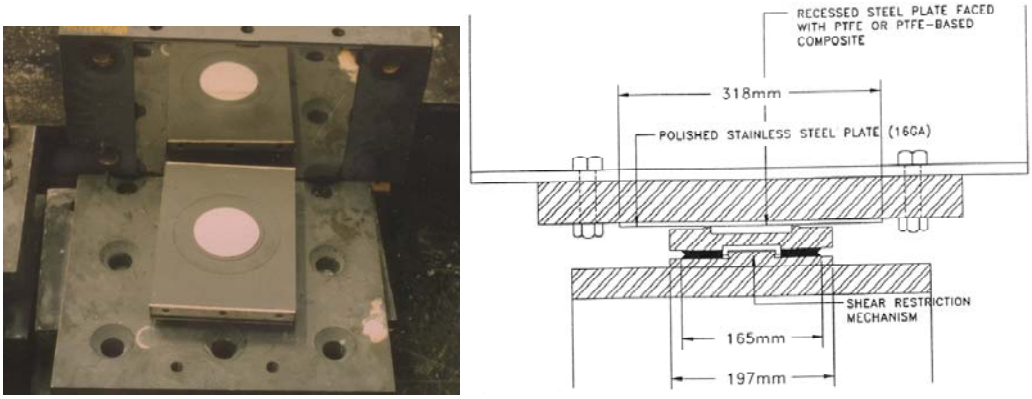

Figure (2-1) Sliding isolator: a) View of the open isolator, b) cross section of the isolator (from Tsopelas and Constantinou 1994).

The coefficient of friction "μ" of the sliding interface of the isolators is a function of the sliding velocity and follows the equation below proposed by Constantinou (1990).

$$\mu = f_{max} - (f_{max} - f_{\min})\exp(-\alpha|\dot{u}|) \quad \textbf{(2-1)}$$

Where f_{max} is the coefficient of friction at high velocity of sliding, f_{min} is the coefficient of friction at almost zero velocity of sliding, "a" is a parameter controlling the transition of the coefficient of friction from low to high sliding velocities, and "$\dot{u}$" is the velocity of sliding.

Figure (2-2) compares experimental values of the coefficient of friction with the predictions of the above equation.

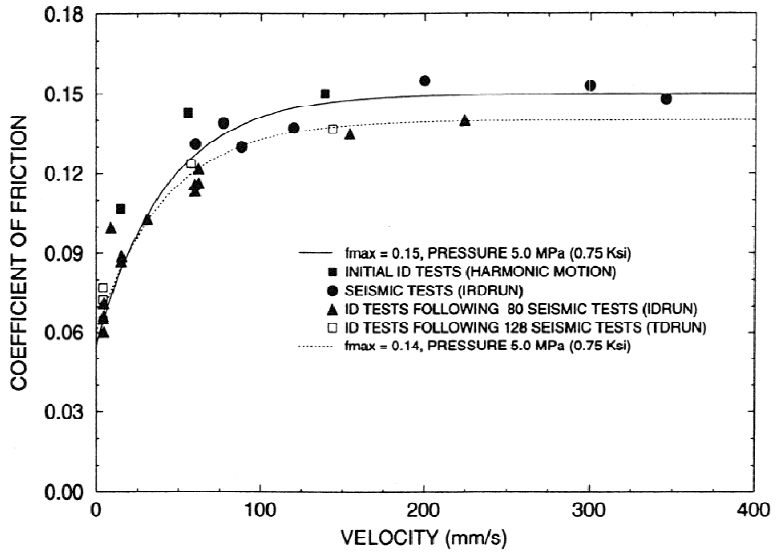

Figure (2-2) Variation of coefficient of friction with velocity (from Tsopelas and Constantinou 1994).

2.2 Fluid Restoring Force and Damping (FRFD) Device

The main difference between the common fluid viscous damping devices and the FRFD device is the restoring force which the FRFD device provides. The bridge model utilized in this study is equipped with two scaled FRFD devices, connected between the deck and the top of the piers. Figure (2-3) shows a picture of the device and a cut-out of it depicting the basic components of its construction. Each device is about 38 cm long and weights 1.7 kg, it has a stroke of $\pm 5\ cm$, and resists with maximum force of 13.5 kN at peak stroke under dynamic loading.

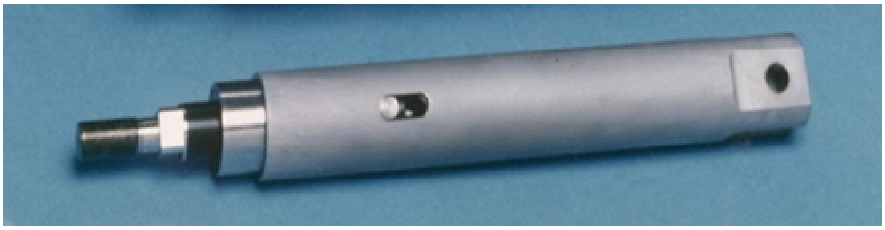

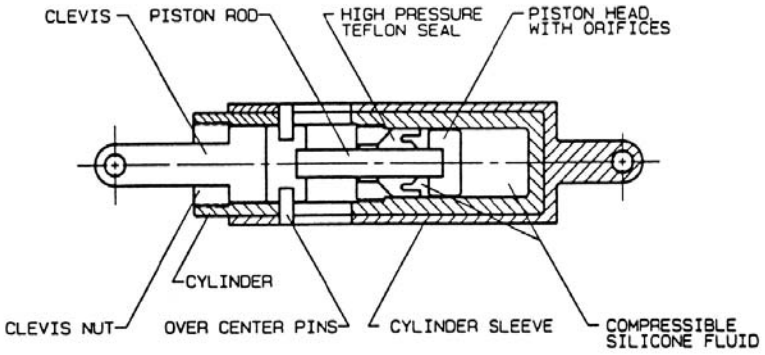

Figure (2-3) View and cut-out of the Fluid Restoring Force and Damping Device (Tsopelas and Constantinou 1994).

The bridge model is supported on sliding bearings, thus a re-centering force is needed in the isolation system to minimize or eliminate potential permanent displacements at the isolation interface. Each FRFD device features a constant restoring force at zero displacement equal to $F_0 = 4.75\ kN$ which may be exceeded for further deformation, restoring force with stiffness $K_0 = 100\ N/mm$ and a non-linear viscous force which depends on the velocity the device undergoes. The preload force has been determined to be larger than the minimum frictional force from the sliding isolators in order to eliminate permanent deformations of the deck during a seismic excitation. Thus, force of $2F_0$ (two devices are used) equals $9.5\ kN$, is slightly larger than the frictional force of the sliding bearings which equals to $f_{min}W_d = 0.06 \cdot 143 = 8.58\ kN$, where f_{min} the "static" friction coefficient and W_d the deck weight. The following figure demonstrates the response of the FRFD device to a static and a dynamic loading.

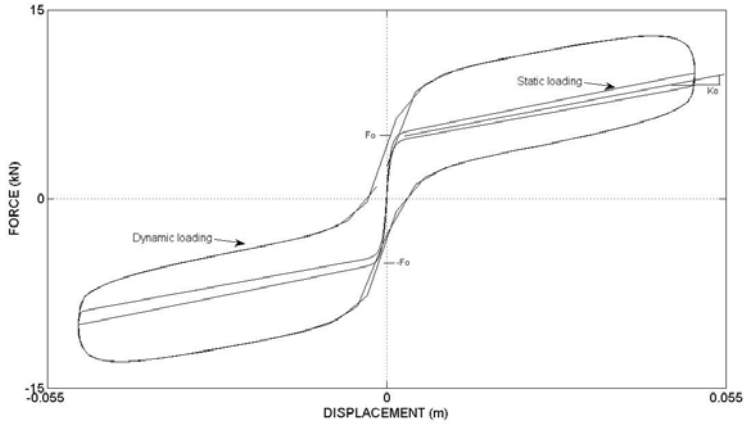

Figure (2-4) Force-Displacement Relationship of Fluid Restoring Force and Damping Device.

Each device performs like a fluid spring, with elastic linear component, contributing when the preload force is exceeded. A detailed explanation of the operation and the major components of the force output of the FRFD device is presented in the next two figures.

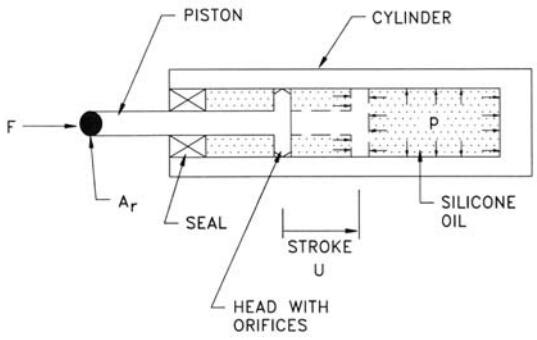

Figure (2-5) Principles of operation of Fluid Restoring Force and Damping Device (Tsopelas and Constantinou 1994).

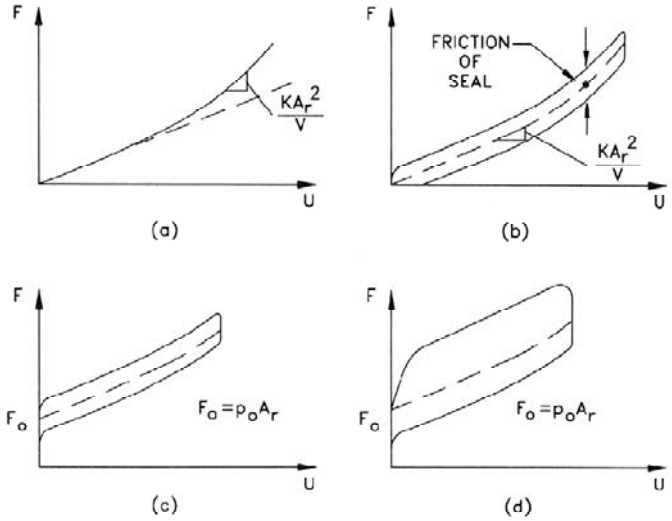

Figure (2-6) Components of Force in FRFDD (Tsopelas and Constantinou 1994).

Since the rod is moving into the hydraulic cylinder, filled with silicon oil, the volume of the fluid is reduced, equal to the volume of the stroke "u", times the rod area A_r. The overpressure that is developed for the certain rod displacement is $p = \frac{F}{A_r}$. The changed volume is determined as $\Delta V = A_r u$ and the overpressure is expressed differently as $p = K\frac{\Delta V}{V}$. Combining these two equations the Force induced in the device is given: $F = K\frac{A_r^2}{V}u$, where "K" is the fluid bulk modulus and "V" is the initial fluid volume.

In general the fluid bulk modulus "K" depends on overpressure "p", thus the force, as shown in Figure (2-6a) can be written more accurately, considering the volume "V" not to be constant but equal to $V_0 - A_r u$ as :

$$F = \int K(p_t)\frac{A_r^2}{V_0 - A_r u}du \qquad \textbf{(2-2)}$$

Where, "V_0" is the fluid volume at zero displacement and "u" the total stroke.

The different components comprising the total resisting force of the FRFD device, are presented in the Figure (2-6). The second component of the force of the device, Figure (2-6b) is the friction developed in the seals of device, forming a hysteretic loop independent from the rate of loading.

The third component is the preload force "F_0" proportional to the pressure "p_0" developed by pressurizing the internal fluid:

$$F_o = A_r p_o \quad \textbf{(2-3)}$$

The preload force must be exceeded for further fluid compression.

The last component of force is the viscous damping component developed when stroking occurs with velocity. Viscous damping is provided from the orifices on the piston head, during fluid flow through the chambers of the cylinder, Figure (2-6d). The level and nature of these forces are dependent on the shape and the area of the orifices and are always proportional to the velocity of stroking. For this particular device the viscous damping force is non-linear in nature and is given by the following expression:

$$F = c\dot{u}^a \quad \textbf{(2-4)}$$

Where "c" is the damping constant, and "a" is a parameter determining the behavior of the device against the velocity, where $0 < a \leq 1$ with typical values for this case to be around 0.2-0.3.

From Figure (2-6d) is observed that higher viscous force is obtained when the stroke increases than when the rod returns. Such a behavior could be desirable, since larger resisting force (higher damping) is needed when the stroke increases to reduce as much as possible the maximum displacements and smaller resisting force is needed when the device is returning to its initial position (accelerate the return).

3 Effective Isolation Systems

In order to evaluate that effect of the constant restoring force of an isolation system on the bridge responses one has to design/create a seismic isolation system which will provide similar isolation period and damping properties to the isolation system with the constant restoring force.

An isolation system consisting of sliding bearings and FRFDD is considered as the system which provides constant restoring force, and its response will be compared to another isolation system consisting of sliding bearings and linear visco-elastic devices. The first system, the one with the constant restoring force, was chosen to be the one, reported by Tsopelas and Constantinou (1994) since it is a well studied and reported system in the literature. The second system is the one which its linear stiffness and damping properties are derived in such a way that they will be equivalent to the properties provided by the system with the FRFDD.

One has to recognize that such a design (with effective linear stiffness and damping) will depend on the displacement amplitude the isolation system will be responding with. This chapter presents the procedures to derive the effective linear properties of the isolation system which its response will be compared to the isolation system with the FRFDD.

3.1 Effective Linear Viscous Damping

Consider a linear viscous element which undergoes a harmonic deformation $u = u_0 \sin(\omega t)$. The resulting viscous force in the element is $F_D = C \cdot u_0 \cdot \omega \cdot \cos(\omega t)$. An estimate of the energy dissipated per cycle of deformation (area under the F-u loop) can be evaluated from the following integral:

$$W_D = \oint F_D du = \oint C\dot{u}\, du = \int_0^{2\pi/\omega} C\dot{u}^2 dt = Cu_o^2\omega^2 \int_0^{2\pi/\omega} \cos^2(\omega t) dt = Cu_o^2\omega^2 \int_0^{2\pi} \cos^2(\omega t) d(\omega t) \quad \textbf{(3-1)}$$

Which results in :

$$W_D = \pi\, C\, u_o^2\, \omega \quad \textbf{(3-2)}$$

With the help of the above equation the effective damping constant of a restoring force and damping device (e.g. a fluid restoring force and damping device which exhibits a constant restoring force mechanism and a non-linear damping mechanism) is given by Equation (3-3).

It should be noted that it has been implied that a restoring force and damping device is (can be accurately modeled by) a linear visco-elastic device with stiffness K_{eff} and viscous constant C_{eff}.

$$C_{eff} = \frac{W_D}{\pi u_o^2 \omega} \quad \textbf{(3-3)}$$

One, using the critical value of the viscous constant $C_{cr} = {2K_{eff}}/{\omega}$, can obtain the performance index "ξ" which is given by the following expression:

$$\xi = \frac{C}{C_{cr}} = \frac{W_D}{2\pi u_o^2 K_{eff}} = \frac{W_D}{4\pi W_S} = \beta_{eff} \quad \textbf{(3-4)}$$

Where, W_D and W_S are the dissipated energy and the potential strain energy stored in the system (FRFDD) at displacement amplitude "u_0". The enclosed area of the force-displacement loop (half of it is depicted in Figure (3-1)) represents the dissipated energy W_D and the shaded area in the same figure represents the potential/strain energy W_S. The value of the performance index "ξ" coincides with (can be viewed as) the effective damping ratio β_{eff}, only if a mass is connected to the restoring force and damping device giving natural frequency of the dynamical system equal to "ω" (the excitation frequency). Therefore, the damping capacity of a restoring force and damping device can be approximated with an effective value β_{eff}, depicted by the above equation.

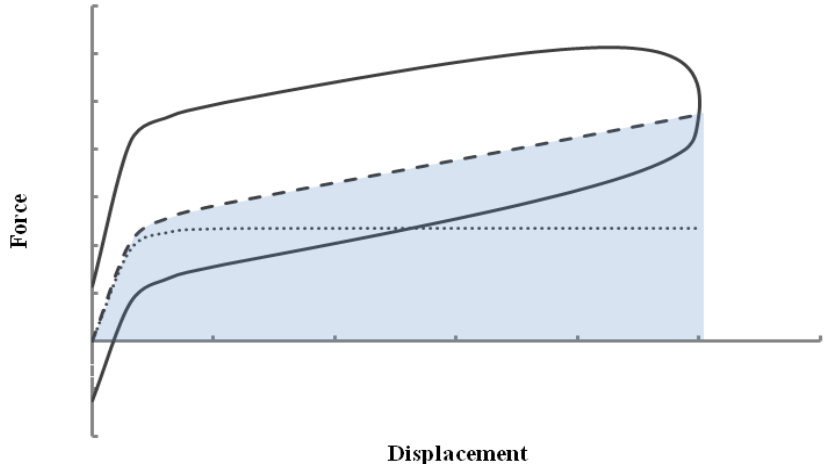

Figure (3-1) Typical force-displacement loop (continuous line), its corresponding potential/strain energy (shaded area) and constant restoring force (dotted line) of FRFDD.

Figure (3-2), plots the variation of the effective viscous damping ratio, evaluated from Equation (3-4) when a FRFDD was excited by a harmonic displacement of amplitude "u_0" and frequency "ω", with respect to the frequency and amplitude of loading.

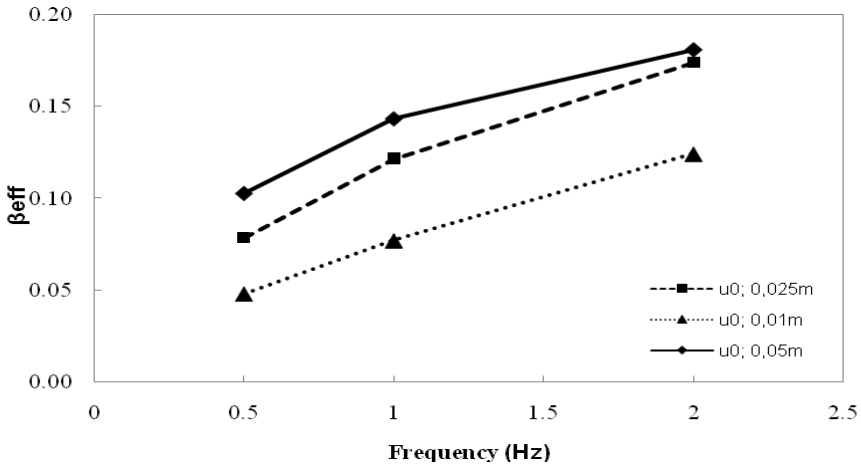

Figure (3-2) Effective damping ratio for FRFDD, for various amplitudes and frequencies of a harmonic loading.

It becomes evident from the Equation (3-4) above that the effective damping ratio β_{eff} , of a restoring force and damping device is a function of displacement because both W_D and W_S are direct functions of displacement. This creates a difficulty when an effective linear system (no dependence on displacement) is required to represent the behavior of an arbitrary restoring force and damping device. The representation is not unique and depends on the amplitude of displacement as depicted in Figure (3-2).

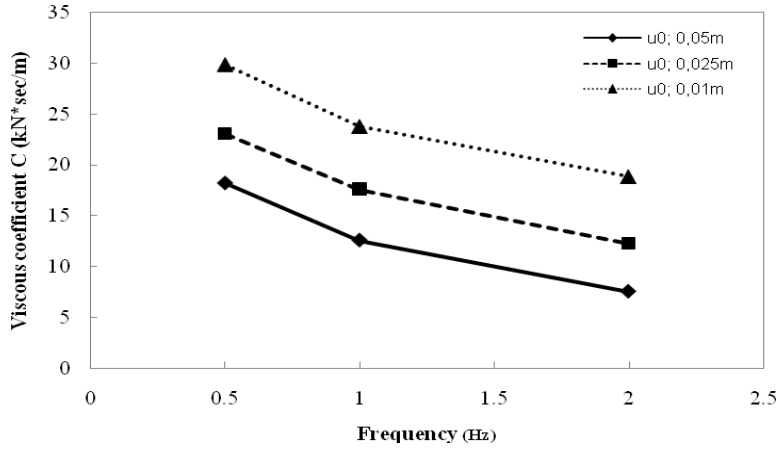

Figure (3-3) Effective viscous coefficient for FRFDD for different displacement amplitudes and frequencies of a harmonic loading.

This is the reason for using three different levels of displacement amplitude to create three effective linear visco-elastic systems to represent the behavior of the fluid restoring force and damping device (FRFDD). Figure (3-3), plots Equation (3-3), the effective viscous coefficient for various displacement amplitudes "u_0" and frequencies "ω" for a FRFDD.

3.2 Effective Linear Stiffness

There are two approaches in evaluating the effective linear stiffness of a restoring force and damping device.

- In the first approach K_{eff} is the ratio of the maximum developed resisting force at a specific displacement amplitude "u_0", as shown by the following equation.

$$K_{eff} = \frac{F_{R,\max}}{u_o} \quad \textbf{(3-5)}$$

- In the second approach, which is based on the potential strain energy stored in the device at displacement "u_0", K_{eff} is given by Equation (3-6).

$$K_{eff} = \frac{2W_S^{FRFDD}}{u_o^2} \quad \textbf{(3-6)}$$

Where $F_{R,max}$ is the peak restoring force of the restoring force and damping device. Equation (3-6) is derived by equating the potential energy of the effective linear spring with stiffness K_{eff} ($W_S^{eff} = \frac{1}{2} K_{eff}\, u_o^2$), to the potential strain energy of the FRFDD (see shaded area of Figure (3-1)) W_S^{FRFDD}.

Comparing the two ways to calculate the effective stiffness of a FRFDD we observe that the one based on equal potential strain energies (Equation (3-6)) results in higher stiffness than the one based on the ratio of maximum force over its corresponding displacement (Equation (3-5)) (see also Figure (3-1)).

The resulting effective visco-elastic system behavior is governed by Equation (3-7) which is graphically depicted in Figure (3-4).

$$F = K_{eff}\, u + C_{eff}\, \dot{u} \quad \textbf{(3-7)}$$

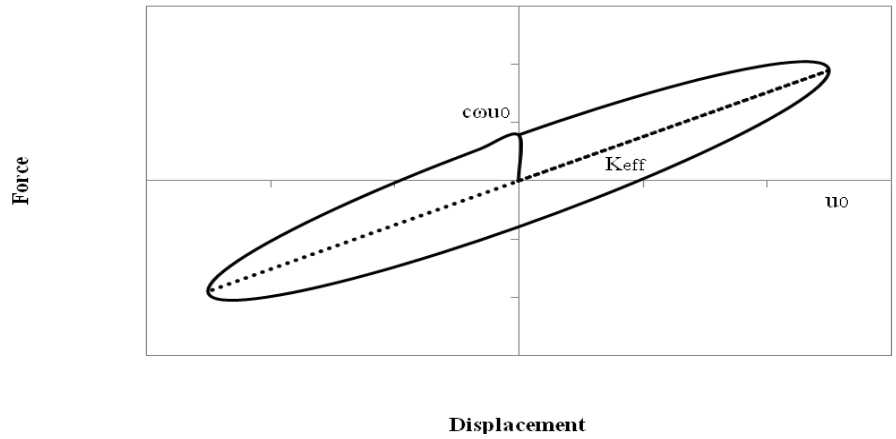

Figure (3-4) Force-displacement loop, for an effective linear visco-elastic device.

The response of a bridge model under near and far-fault seismic excitations is used to investigate the effect of constant restoring force in a seismic isolation system. For this task the response of a bridge model with FRFDD (which incorporates constant restoring force) and the response of a bridge model with an effective linear restoring force and damping device (visco-elastic device) are compared. Due to the aforementioned dependency of the stiffness and damping of a FRFDD on the displacements, three different effective systems corresponding to different levels of displacement are considered as were presented in Figure (3-2). It should be noted here that the displacement levels ($u_0 = 0{,}01 - 0{,}025 - 0{,}05\ m$) are chosen based on the experimental results presented by Tsopelas and Constantinou (1994).

However, for the extensive parametric analyses conducted in this study it was chosen only one set of values (amplitude $u_0 = 0.025\ m$ and frequency $f = 1\ Hz$) which the effective damping and stiffness were obtained and used in the analyses. As expected the comparison results from the parametric analyses (seismic excitations) will be conditionally valid since the isolation system with FRFDD and the ones with the effective stiffness and effective damping are equivalent only for oscillations with amplitude $0.025\ m$ and frequency $1\ Hz$, where under a seismic excitation oscillations occur at large number of frequencies and with various amplitudes.

The value of frequency $f = 1\ Hz$, was chosen because it is very close to the mean value of the predominant frequencies of the recorded near-field seismic excitations considered in this study. The value of the displacement amplitude $u_0 = 0.025\ m$, was chosen because it is a very close approximation of the expected isolation system response. It should also be noted that the results of the extensive experimental program by Tsopelas and Constantinou (1994) guided this choice even though the seismic events used in that program were mainly far-field excitations.

Based on the analysis of the effective stiffness presented above for $u_0 = 0.025\,m$ and $f = 1\,Hz$ there are two effective visco-elastic devices which can be obtained to be used in the parametric study in the present work. Both effective devices will have the same effective damping constant, however they will have different effective stiffness, one base on Equation (3-5) and the other based on Equation (3-6). For the rest of the study the first effective visco-elastic device will be referred as visco-elastic device (VE) and the second as stiff visco-elastic device (SVE). The following table presents the properties of the two effective visco-elastic devices representing the FRFDD considered in this study.

Table (3-1) Properties of the two effective visco-elastic devices.

	VE Visco-Elastic Device	**SVE** Stiff Visco-Elastic Device
C_{eff} (kN*sec/m)	17.6	17.6
K_{eff} (kN/m)	284.0	454.48

4 Analytical Model of Seismically Isolated Bridge

4.1 Bridge Model

The analytical model of the bridge structure considered, takes into account the pier flexibility, the pier top rotation, and the characteristics of the restoring force/damping devices and sliding bearings.

The model consists of five (5) degrees of freedom (DOFs) in the longitudinal direction, as depicted in the Figure (4-1). Those are the deck displacement with respect to the table "u_d", the pier displacements "u_{p1}" and "u_{p2}", and the pier rotations "φ_{p1}" and "φ_{p2}".

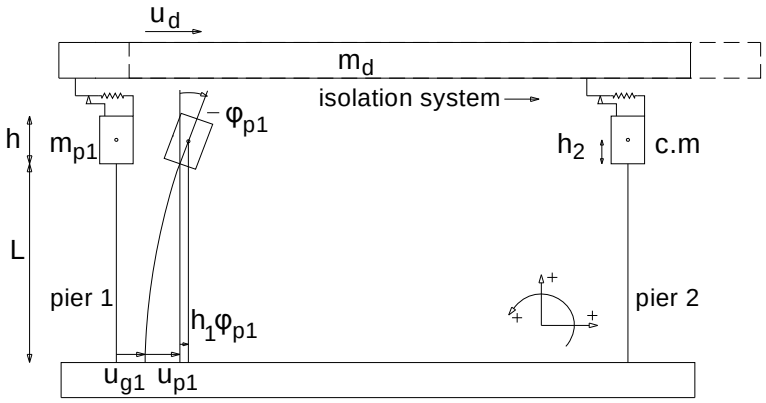

Figure (4-1) Longitudinal direction model of isolated bridge.

Each pier is represented by a beam element fixed on the seismic simulator, and a lumped mass at its top. The lumped mass is considered as a rigid block with height "h", mass "m_p" and mass moment of inertia about the center of mass "I_p". The center of mass is located at distance "h_i" from the bottom of the block. The properties of the pier determining the dynamic response, are assumed the pier length "L_i" , moment of inertia "I_i" and the modulus of elasticity "E_i". The deck is considered as a rigid block articulated to the pier tops (no transfer of moment is considered). In reality, there is transfer of moment due to the rotational stiffness of the supporting disc of the sliding bearings. The transferred moments and forces are depicted in the free-body diagram Figure (4-2).

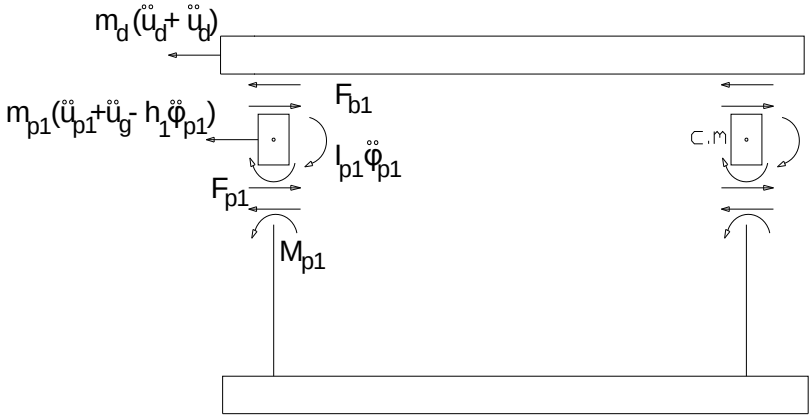

Figure (4-2) Free body diagram of bridge model.

The equations of motion are derived considering dynamic equilibrium of the deck and piers translational degrees of freedom and of the piers in the rotational degrees of freedom. The resulting system of differential equations is:

$$m_d(\ddot{u}_d + \ddot{u}_g) + F_{b1} + F_{b2} = 0 \quad \textbf{(4-1)}$$

$$m_{p1}(\ddot{u}_{p1} + \ddot{u}_g - h_1\ddot{\varphi}_{p1}) + F_{p1} - F_{b1} = 0 \quad \textbf{(4-2)}$$

$$m_{p2}(\ddot{u}_{p2} + \ddot{u}_g - h_2\ddot{\varphi}_{p2}) + F_{p2} - F_{b2} = 0 \quad \textbf{(4-3)}$$

$$I_{p1}\ddot{\varphi}_{p1} + M_{p1} + F_{p1}h_1 + F_{b1}(h - h_1) = 0 \quad \textbf{(4-4)}$$

$$I_{p2}\ddot{\varphi}_{p2} + M_{p2} + F_{p2}h_2 + F_{b2}(h - h_2) = 0 \quad \textbf{(4-5)}$$

Where, "$\ddot{u}_g$" is the horizontal, ground (table) acceleration, "F_{b1} , F_{b2}" are the lateral forces developed by the isolation system, "F_{pi}" are the lateral forces of the piers and "M_{pi}" are the bending moments of the piers. The linear elastic resisting forces of the piers, could be evaluated as function of pier displacement and rotation, as expressed, in matrix form in the Equation (4-6). Additional the second part of equation, describes the damping forces provided from the piers.

$$\begin{Bmatrix} F_{pi} \\ M_{pi} \end{Bmatrix} = E_i I_i \begin{bmatrix} \frac{12}{L_i^3} & \frac{6}{L_i^2} \\ \frac{6}{L_i^2} & \frac{4}{L_i} \end{bmatrix} \begin{Bmatrix} u_{pi} \\ \varphi_{pi} \end{Bmatrix} + \begin{bmatrix} C_{pi}^1 & 0 \\ 0 & C_{pi}^2 \end{bmatrix} \begin{Bmatrix} \dot{u}_{pi} \\ \dot{\varphi}_{pi} \end{Bmatrix} \quad \textbf{(4-6)}$$

4.2 Isolation System Model

The isolation system has two components a) the sliding bearings and b) the component which provides restoring force and damping which could be i) fluid restoring force/damping devices or ii) visco-elastic devices. The force of the isolation system is expressed by Equation (4-7) as follows:

$$F_{bi} = \mu_i \dot{u}_{bi} w_i z_i + F_{ti} \quad \textbf{(4-7)}$$

Where "μ_i" is the coefficient of friction of the sliding bearing "i", "w_i" the deck normal load carried from bearing "i", and "F_{ti}" is the force from the restoring force/damping device at pier "i". It should be noted that variable "u_{bi}", sliding bearing displacement, is given from the following equation:

$$u_{bi} = u_d - u_{pi} + h\varphi_{pi} \quad \textbf{(4-8)}$$

Furthermore, variable "z_i" captures the hysteretic nature of friction in the sliding bearing (the yield state of the sliding surface). Variable "z" satisfies the following equation, also known as Bouc-Wen hysteretic model (Tsopelas and Constantinou 1994).

$$y_i \dot{z}_i + \gamma |\dot{u}_{bi}| z_i |z_i| + \beta \dot{u}_{bi} z_i^2 - \dot{u}_{bi} = 0 \quad \textbf{(4-9)}$$

Where "y_i" expresses the yield displacement of the sliding surfaces, ($y_i = 0{,}25\ mm$) and "β, γ"are parameters satisfying the condition, $\beta + \gamma = 1$.

4.3 Analytical model of the Fluid Restoring Force/Damping Device

Four different components contribute to the total resisting force of the fluid restoring force/damping device, as it discussed in a previous section. This device presents some stiffness and significant damping capacity. For the aforementioned behavior are responsible the preload force, the restoring force, the friction force at the seal and the fluid damping force. For each component mathematical expressions have been proposed by Tsopelas and Constantinou (1994).

The preload term can be expressed as follows:

$$F_p = F_0[1 - \exp(-\delta |u_{bi}|)] sgn(u_{bi}) \quad \textbf{(4-10)}$$

Where, "F_0" is a preload force due to fluid pressurization. An alternative and simpler expression, without introducing much error, for the preload force could be $F_0 \cdot sgn(u_{bi})$. In reality, however, the stiffness of the preload force of the device is not infinitely large at zero displacement, rather dependents on the velocity of motion of the piston rod. This behavior is

accounted for in Equation (4-10) by the exponential term for the preload, in which "δ" is a function of velocity as shown in the following equation:

$$\delta = \delta_0 \exp(-\delta_1 |\dot{u}_{bi}|) \quad \textbf{(4-11)}$$

From the force-displacement relationship, it can be observed that the slope dF_p/du_{bi}, at zero displacement is equal to $F_0\delta$. In the present model the device displacement coincides with the sliding bearing displacement, "u_{bi}".

The device restoring (spring) force is expressed with the following equation:

$$F_s = K_0 u_{bi} \quad \textbf{(4-12)}$$

Where, "K_0" is the stiffness of the device, which is due to the fluid compressibility.

The component of friction of the seal, influence the behavior of the device reducing the restoring force at the return of the rod. The hysteretic behavior of the friction is expressed from the following equation:

$$F_f = [F_{min} + \zeta K_0 |u_{bi}|] z_t \quad \textbf{(4-13)}$$

Where, "F_{min}" is the seal friction at zero displacement and "z_t"is a variable governed by an equation similar to Bouc-Wen model, providing a hysteretic behavior to friction force. Increasing stroking and therefore increasing internal pressure in the device, results to increased friction in the seal, as is expressed with the additional term to "F_{min}".

The flow of the oil in the device chambers (orificing), during stroking, is responsible for the energy dissipation capability of the device. The design of the device used in this study is such that the damping capacity is higher when the stroke increases and lower when the stroke of the device decreases. Mathematical expressions to accurately capture this behavior and the form of damping (non-linear viscous) these devices give, have been proposed by Tsopelas and Constantinou (1994). In the present study a simpler expression is utilized also proposed by Tsopelas and Constantinou (1994) and is given by the following equation:

$$F_d = \begin{cases} F_{max1}[1 - \exp(-\varepsilon_1 |\dot{u}_{bi}|] & when\ u_{bi}\dot{u}_{bi} > 0 \\ F_{max2}[1 - \exp(-\varepsilon_2 |\dot{u}_{bi}|] & when\ u_{bi}\dot{u}_{bi} < 0 \end{cases} \quad \textbf{(4-14)}$$

It should be noted that this expression was found to be appropriate for velocities up to 0,5 m/sec, while tend to predict constant damping forces at large velocities, which seems to be incorrect. The several variables which were not discussed are constant parameters adjusting the properties of the device.

5 Seismic Excitations

The bridge model considered in this study was analyzed for near and far-fault type of seismic motions. The characteristics of these excitations are presented in detail.

5.1 Near- field ground motions

Earthquake ground motions could be classified as near-field (fault) and far-field and their destructive potential in a certain location, depends on event's magnitude, source characteristics, distance and direction from the rupture location and local soil conditions. Far-field motions are characterized from high frequency signal and sharp acceleration records while near-fault motions result to large ground displacements, from $0.5\ m$ to more than $1\ m$, with distinct pulses in their velocity and displacement records. Near-fault motions and their effect on seismically-isolated structures, long-span bridges and flexible buildings have gained considerable attention from earthquake engineering researchers.

First Housner and Trifunac (1967) identified, from the 1966 Parkfield, California earthquake, the coherent long period pulses in velocity and displacement time histories, dissociating this record from a typical far-field signal. Then such the existence of these pulses are verified from a representative data set of recorded ground motions worldwide, Bertero et al. (1978) observed the severe implications on flexible structures, when after the 1994 Northridge California earthquake this scientific area was accepted from the majority of engineers.

Near-fault motions are the result of stress waves moving in the same direction as the fault ruptures, thereby being crowded together to produce a long-duration pulse. Although the large collected records from stations located near the causative fault, these intense pulses are not distinguished in the majority of the records. Effects as directivity and fling are often responsible for the pulse generation furthermore the relative position of the station that recorded the motion with respect to the direction of propagation of the rupture front on the fault plain is employed with the pulse existence (Mavroeidis and Papageorgiou, 2004)

5.1.1 Directivity effect

Directivity effect is related to the direction of the rupture front and it is distinguished as forward and backward directivity. Forward directivity observed when the site is away from the epicenter (it can be near the fault) and the rapture front propagates toward the site, where the station is located. Backward directivity occurs when the site is near the epicenter and the rapture propagates away from it. The velocity pulse is characterized by a positive and

negative swing (reversing pulse), caused by the constructive interference of SH waves, generated from the parts of the rapture, which are being activated in an earthquake. The finite time that the rapture occurs is responsible for this effect. Another feature of directivity effect is the under-predicted incoming pulse from the attenuation-relation models when the rupture propagates toward to the site, while for the reverse case more conservative pulse would be predicted. In addition with the far-field records, where the strong horizontal component seems to be random, in directivity effect the strong components is constantly appeared in the strike-normal direction, for strike-slip and also for dip-slip faults. It is expected, from definition that the coherent pulse perpendicular to the strike to be larger.

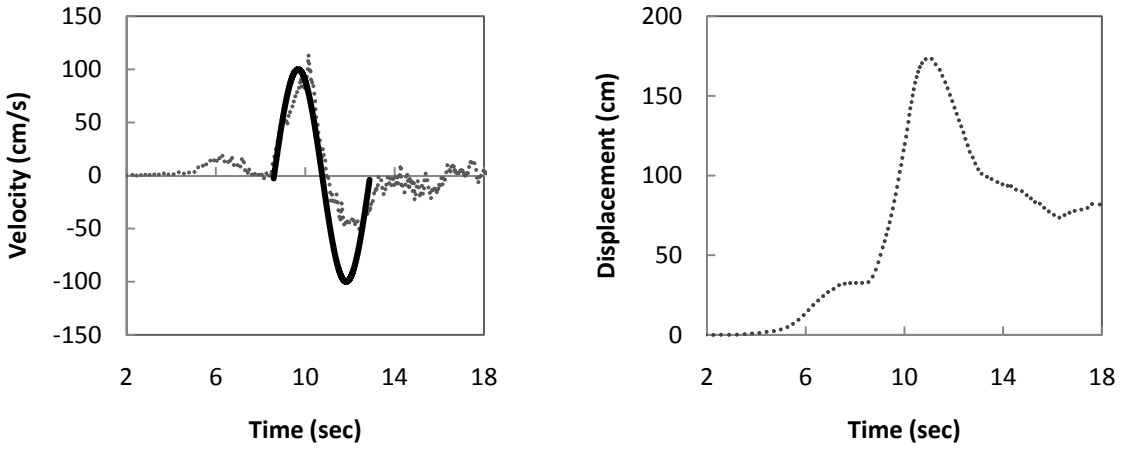

Figure (5-1) Velocity and displacement time histories from Landers (1992), California earthquake with the coherent reversing pulse.

5.1.2 Permanent Displacement (Fling) Effect

Fling is related to the permanent tectonic deformation at a site, which is located near the fault with distance mindless from the epicenter. In ground-displacement record, a permanent offset of the ground is identified as fling effect. The velocity time history plot is characterized by a one-sided velocity pulse, which in the strike-slip faults, is associated with the fault-parallel component. Fling for the strike-slip and dip-slip faults, is associated with the fault-parallel and fault-normal component, respectively.

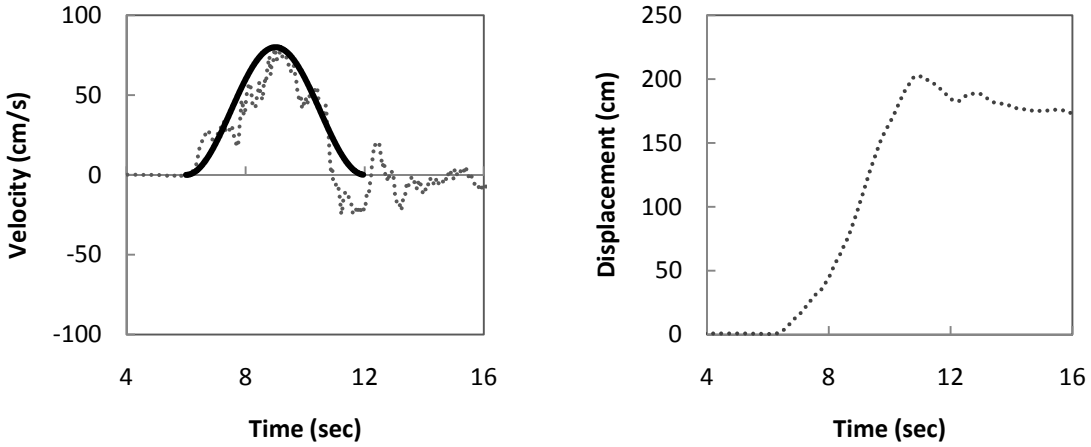

Figure (5-2) Velocity and displacement time histories from Izmit (1999) Turkey earthquake with the coherent one-sided pulse.

In the analysis were used 41 near-field seismic excitations, provided from the study of Mavroeidis et al. (2004). To satisfy the similitude requirements of the scaled bridge model the time step of the recorded ground motions was divided by 2. These motions are the horizontal components of 20 earthquakes. The following table presents these motions.

Table (5-1) Near-field motions used in Analysis

Year	Earthquake	Station	Component	Effect
1966	Parkfield, CA, U.S.A.	C02	SN	Forward Directivity
1971	San Fernando, CA, U.S.A	PCD	SN	
1976	Gazli, U.S.S.R.	KAR	Rad	
1977	Bucharest, Romania	BRI	SN	
1978	Tabas, Iran	TAB	Tran	Forward Directivity
1979	Coyote Lake, CA, U.S.A.	GA6	SN	
1979	Imperial Valley, CA, U.S.A.	E04	SN	
		E05	SN	
		E06	SN	
		E07	SN	
		EMO	SN	
1980	Mexicali Valley, Mexico	VCT	SN	
1984	Morgan Hill, CA, U.S.A.	HAL	SN	

1986	Palm Springs, CA, U.S.A.	NPS	SN	Forward Directivity
		DSP	SN	
1987	Whitter Narrows, CA, U.S.A.	DOW	SN	
		NWK	SN	
1987	Superstition Hills, CA, U.S.A.	PTS	SN	
		ELK	SN	
1989	Loma Prieta, CA, U.S.A.	LGP	SN	
		STG	SN	
1991	Sierra Madre, CA, U.S.A.	COG	Rad	
1992	Erzincan, Turkey	ERZ	SN	
1992	Landers, CA, U.S.A.	LUC	SN	Forward Directivity
1994	Northridge, CA, USA	JFA	SN	
		RRS	SN	
		SCG	SN	
		SCH	SN	
		NWS	SN	
1995	Aigion, Greece	AEG	Long	
		AEG	Tran	
1999	Izmit, Turkey	ARC	SN	
		SKR	SP	Permanent Disp.
		YPT	SP	
		GBZ	SN	Forward Dir.
		GBZ	SP	Permanent Disp.
1999	Chi-Chi, Taiwan	TCU052	SN	
		TCU068	SN	
		TCU075	SN	Forward Directivity
		TCU076	SN	
		TCU129	SN	

5.2 Far-Field Seismic Excitations

In the analysis were also used 20 scaled far field seismic excitations, provided from the study of Tsopelas et al. (1997). These motions are the horizontal components of the ten earthquakes shown in the following table.

Table (5-2) Far-field motions used in Analysis.

Year	Earthquake	Station	Component	Scale Factor
1949	Washington	325 (USGS)	N04W, N86E	2,74
1954	Eureka	022 (USGS)	N11W, N79E	1,74
1971	San Fernando	241 (USGS)	N00W, S90W	1,96
1971	San Fernando	458 (USGS)	S00W, S90W	2,22
1989	Loma Prieta	Gilroy 2 (CDMG)	90, 0	1,46
1989	Loma Prieta	Hollister (CDMG)	90, 0	1,07
1992	Landers	Yermo (CDMG)	360, 270	1,28
1992	Landers	Joshua (CDMG)	90, 0	1,48
1994	Northdridge	Moorpark (CDMG)	180, 90	2,61
1994	Northdridge	Century (CDMG)	90, 360	2,27

The earthquakes were selected to have magnitude larger than 6.5, epicentral distance between 10 and 20 km and site conditions of soft rock to stiff soil. The scaling performed in order to provide a balance contribution to the average response spectrum and preserves the frequency content.

6 Discussion of Analytical Results and Interpretation of the Response

The maximum responses of the bridge model excited by near and far-field seismic motions are presented in this chapter. The near-field seismic excitations consist of two suites, one with *forward directivity effect* and one with *permanent displacement effect*.

The comparisons between the behavior of the isolation system with FRFDD and the equivalent visco-elastic systems, aim to identify the effects of the constant restoring force present by in the FRFD device, on the responses of the isolated bridge. As was discussed previously constant restoring force may cause high velocities at the isolation system interface which in turn introduce high accelerations and possibly shear forces in the piers.

In figures depicting displacements amplitudes there is a red line representing the displacement level which was used to calibrate the two visco-elastic equivalent systems. This is to indicate the level of displacement amplitude where the three systems are equivalent in terms of the restoring force and the damping capacity.

Two sets of analyses are completed one for the sliding bearings with coefficient of friction at large velocities of sliding $f_{max} = 0.14$ (normal) and one were the coefficient of friction is $f_{max} = 0.068$ (low coefficient of friction). This parametric investigation was required in order to clarify the origin of the high acceleration and pier shear responses on the pier. It is expected that when the frictional forces are reduced then the influence of the constant restoring force mechanism within an isolation system is increasing.

6.1 Response to Near-Fault Ground Motions for Equivalent Systems Calibrated at $f = 1\ Hz$ and $u_0 = 0.025\ m$

The maximum responses of the bridge model excited with the suite of near-field seismic motions with *forward directivity effect* are presented in Figure (6-1), for systems with sliding bearings with normal friction ($f_{max} = 0.14$), and in Figure (6-2) for systems with low friction ($f_{max} = 0.068$). For all the near-field seismic motions PGV was used as a ground intensity measure. The effective visco-elastic properties of the seismic isolation systems with VE devices and SVE devices were calibrated for a harmonic loading with frequency $f = 1\ Hz$ and amplitude $u_0 = 0.025\ m$.

Concentrating on the isolation system displacements in Figure (6-1) it is observed that for the seismic excitations causing displacements in the vicinity of the $25\ mm$ the three systems (FRFDD, VED, and SVED) are equivalent. It is expected that in addition to the isolation

system displacements the other responses would have been similar for the three systems. However that is not the case, starting at the isolation system velocities the system with FRFDD experience higher values compared to the VED and SVED. The differences are more pronounced for the pier responses, where the presence of the constant restoring force mechanism in the isolation system results in larger values especially for the pier accelerations which are more than double of the values experienced from the VED and the SVED systems. Similar observations are made in Figure (6-2) for the isolation systems with sliding bearings with low friction ($f_{max} = 0.068$).

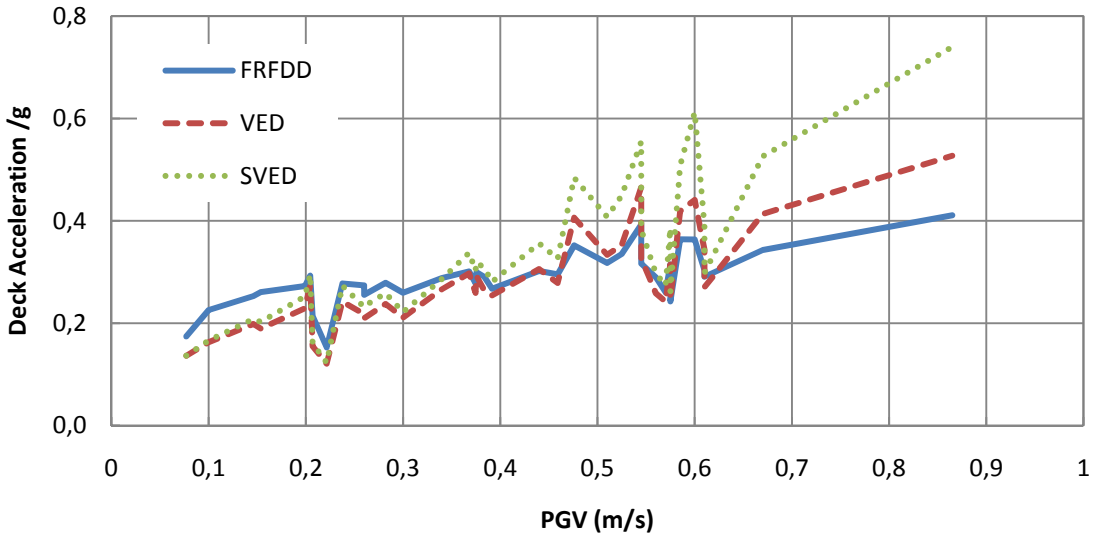

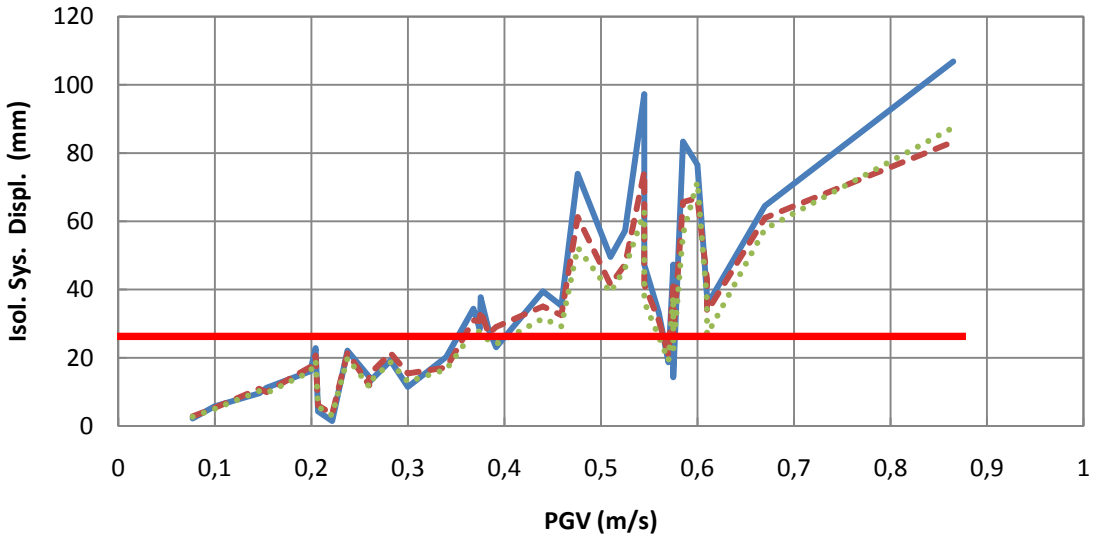

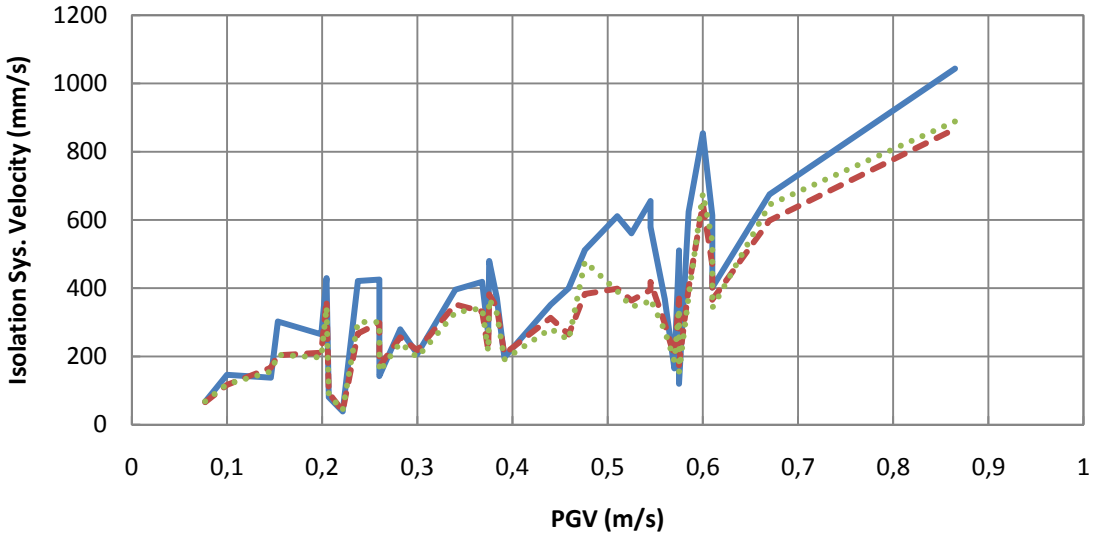

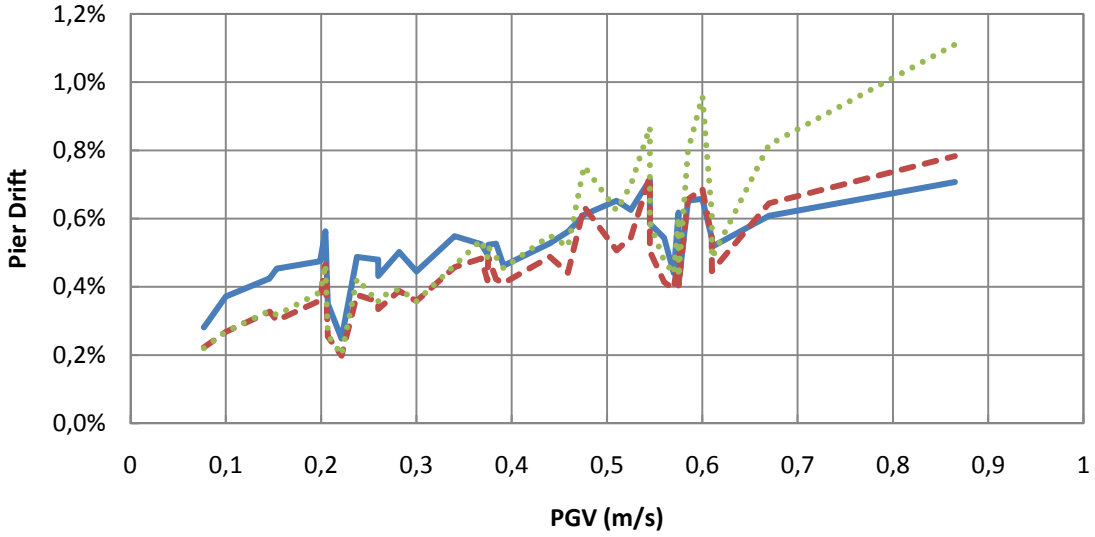

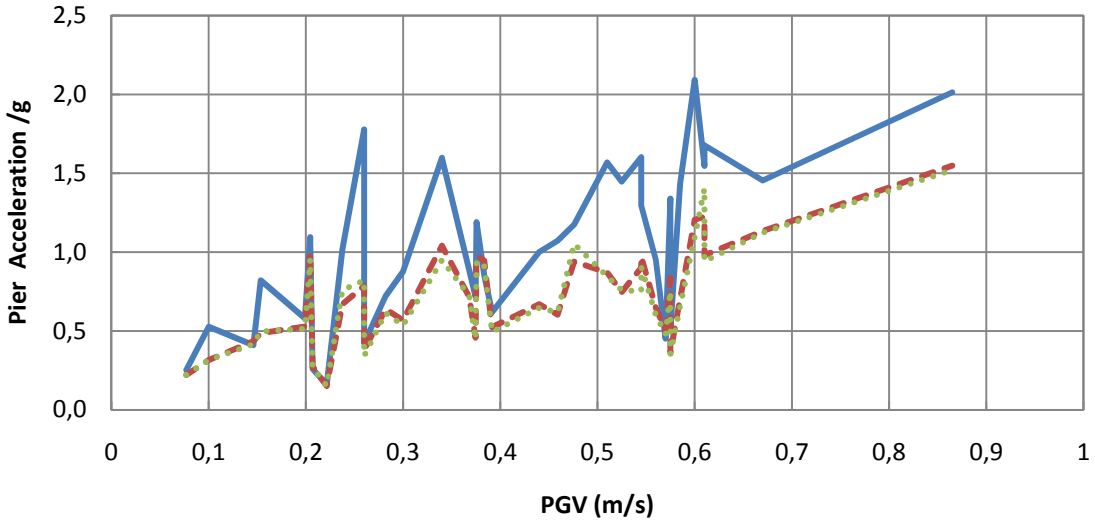

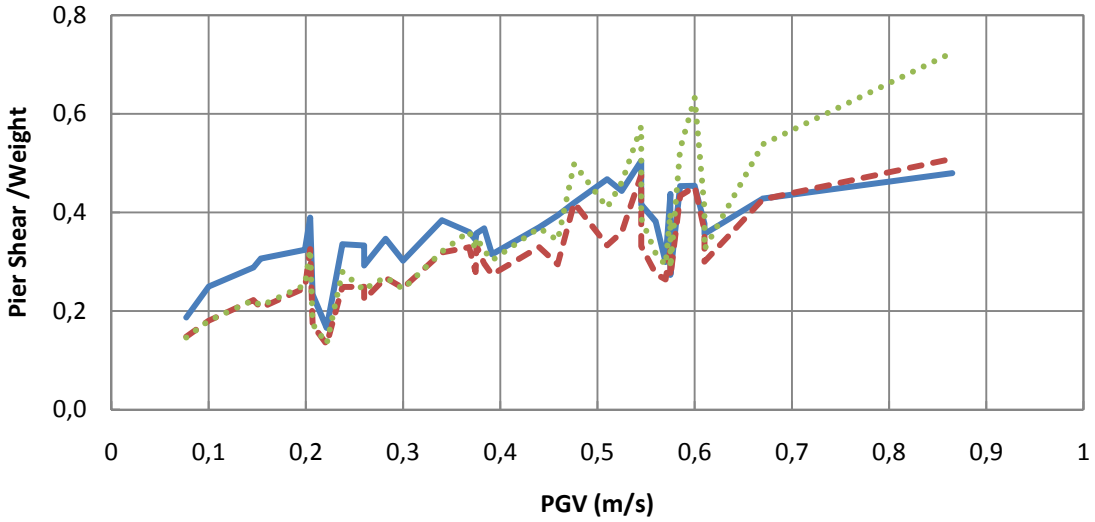

Figure (6-1) Response in near-field ground motions with forward directivity effect, as function of PGV. Sliding bearings with normal friction ($f_{max} = 0.14$).

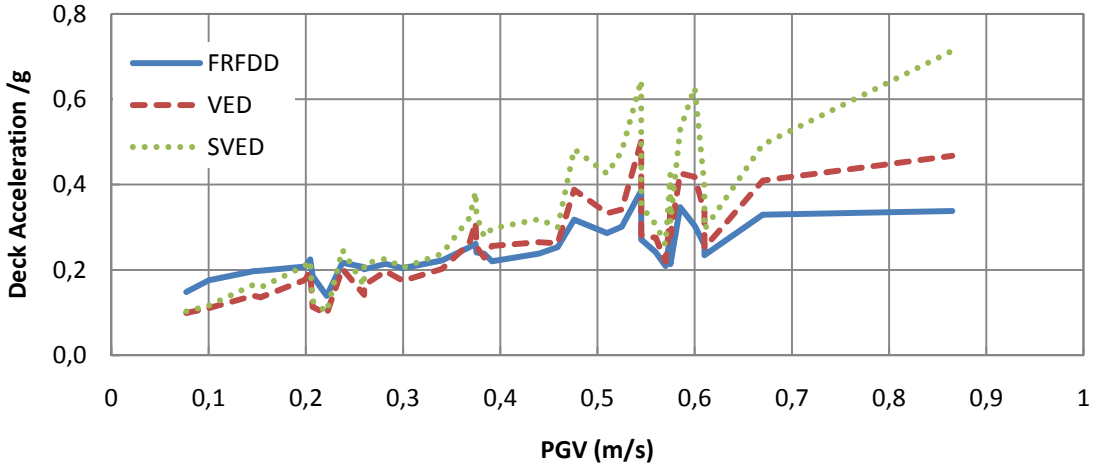

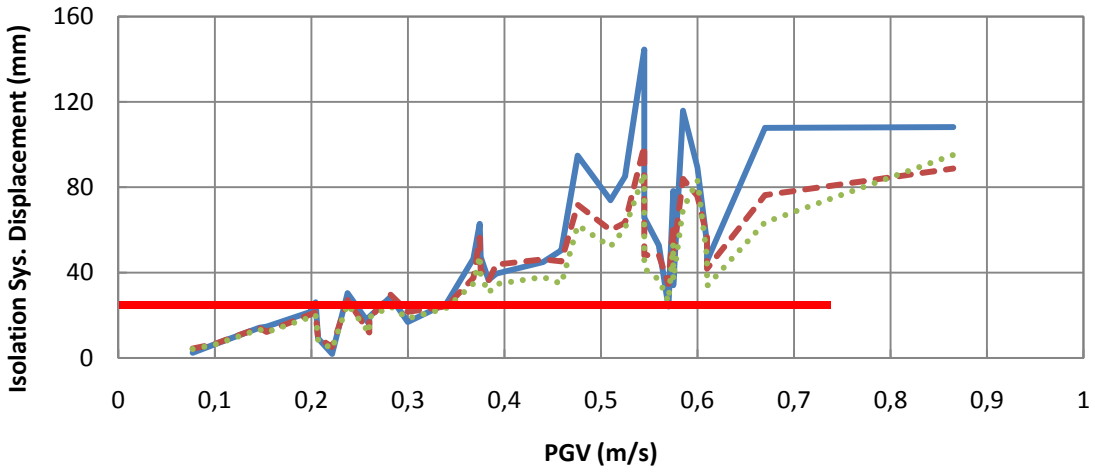

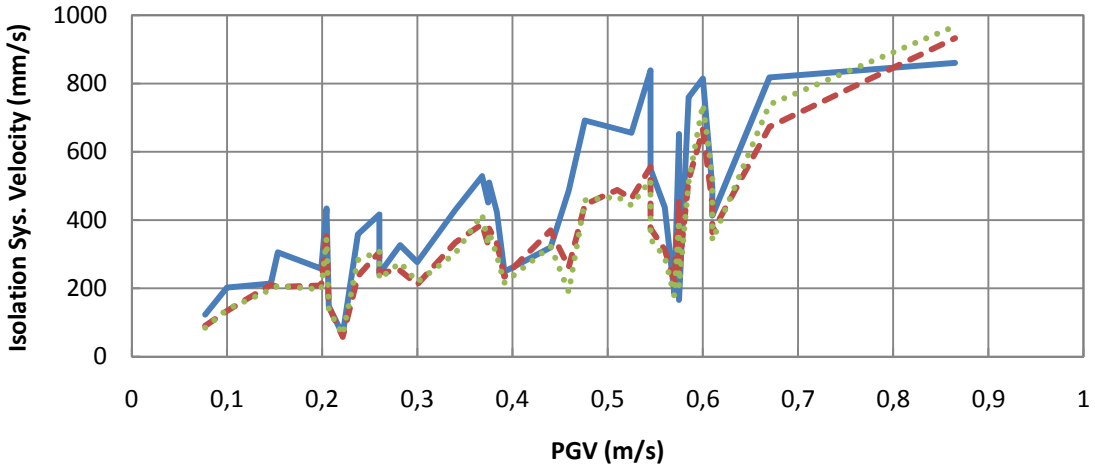

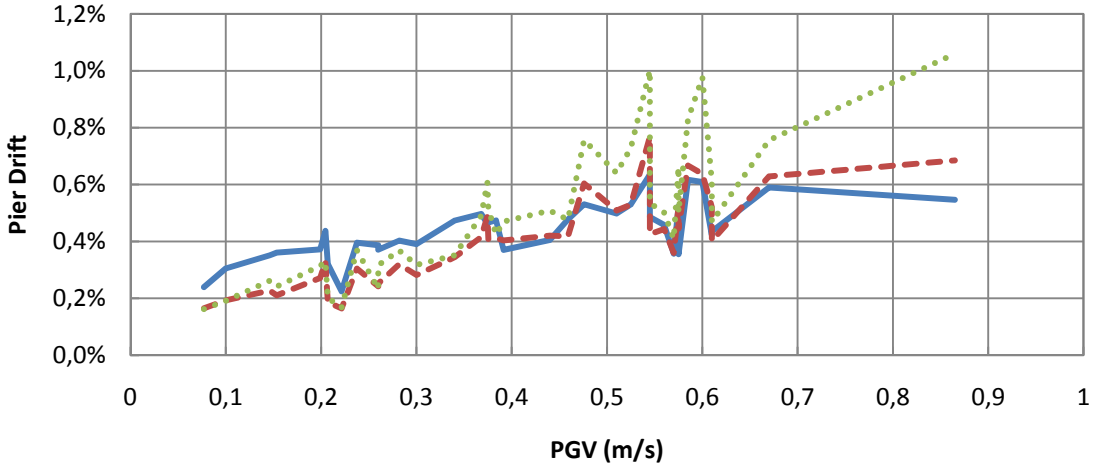

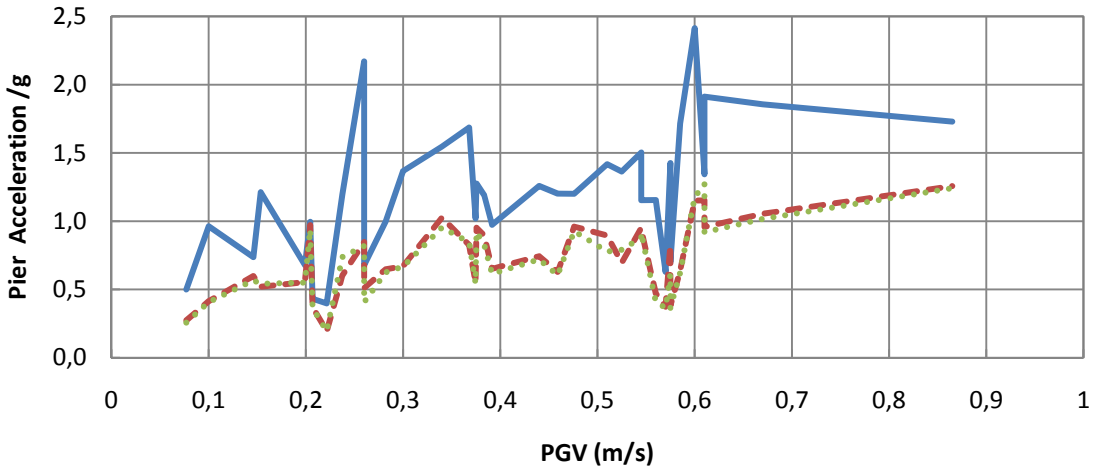

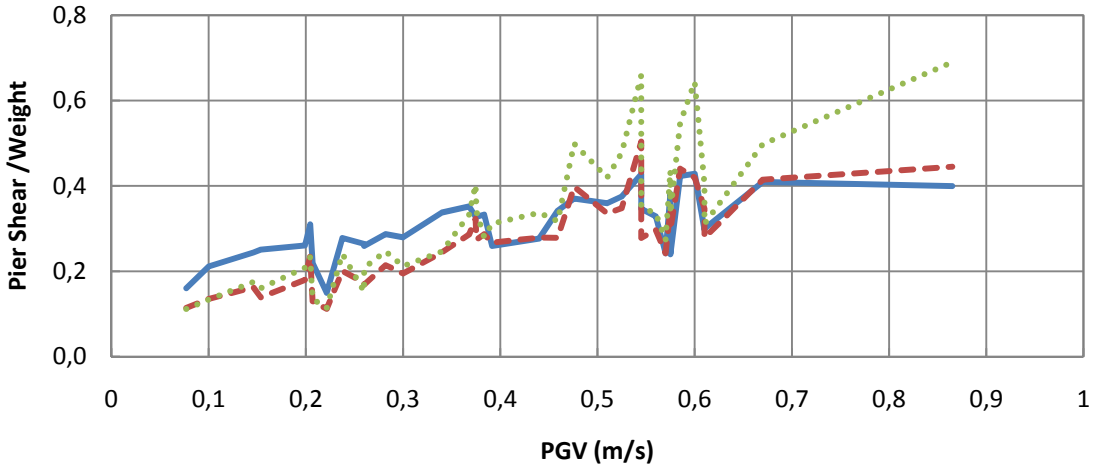

Figure (6-2) Response in near-field ground motions with forward directivity effect, as function of PGV. Sliding bearings with low friction ($f_{max} = 0.068$).

Figure (6-3) presents the responses for the near-field seismic motions with *permanent displacement effect*. The suite of these near field seismic excitations is not large (only 4 seismic excitations). It is observed that for the seismic excitations causing displacements in the vicinity of the $25\,mm$ (only two seismic motions from this suite resulted in isolation system displacement around $25\,mm$) the pier responses are much higher for the system with the FRFDD.

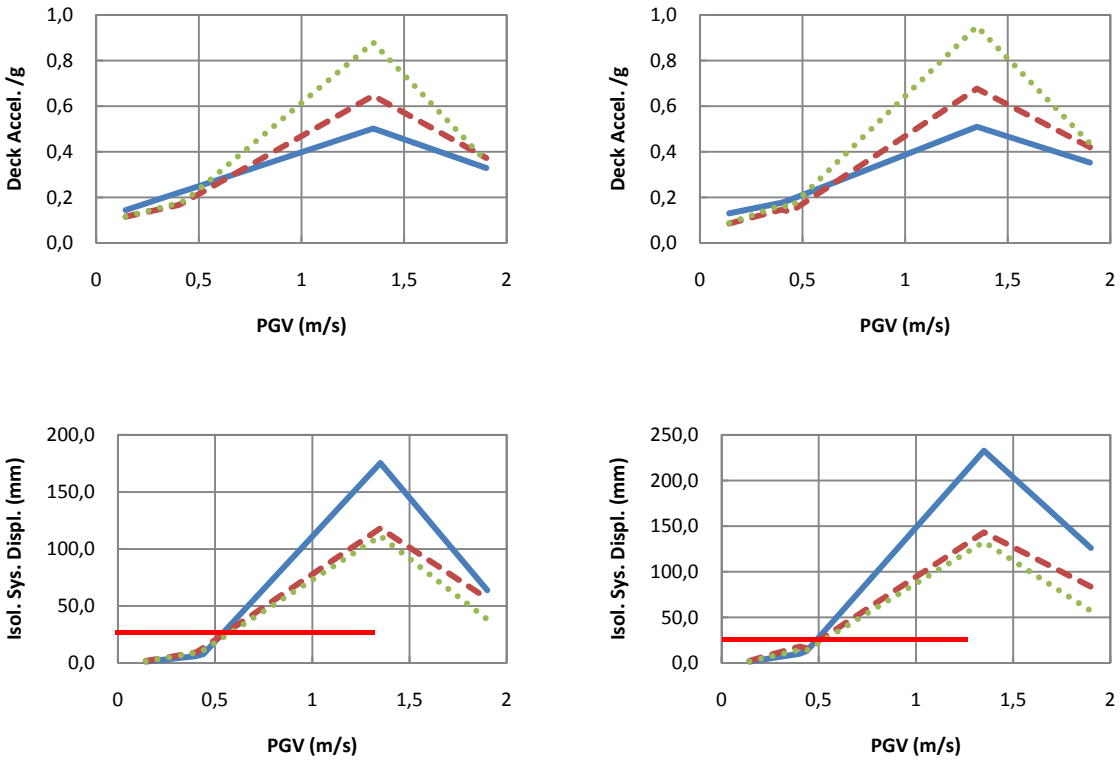

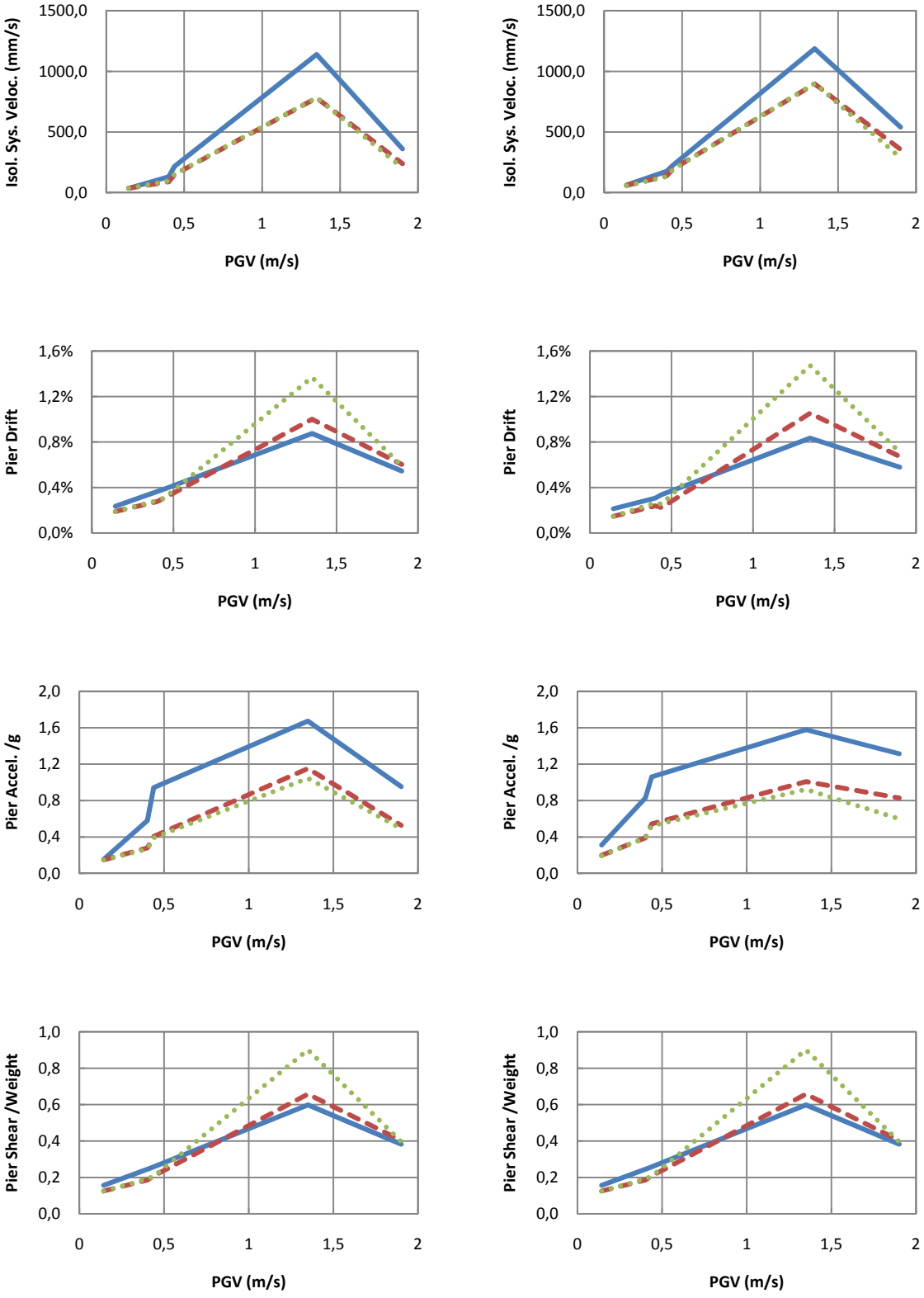

Figure (6-3) Response in near-field ground motions with permanent displacement effect, as function of PGV. Left column sliding bearings with normal friction, right column sliding bearings with low friction.

6.2 Response to Near-Fault Ground Motions for Equivalent Systems Calibrated at $f = 1\ Hz$ and $u_0 = 0.012\ m$

The results presented in this section are for the equivalent visco-elastic systems (VE and SVE) properties to have been calibrated for harmonic loading with frequency $f = 1\ Hz$ and amplitude $u_0 = 0.012\ m$. The maximum responses of the bridge model excited with the suite of near-field seismic motions with *forward directivity effect* are presented in Figure (6-4). Figure (6-5) presents the responses for the near field seismic motions with *permanent displacement effect*. The same observations made in the previous section are made in these figures also. That is, in spite of the similar isolation system displacements the response in the bridge substructure appears higher for the system with the constant restoring force mechanism than the systems with the effective visco-elastic properties.

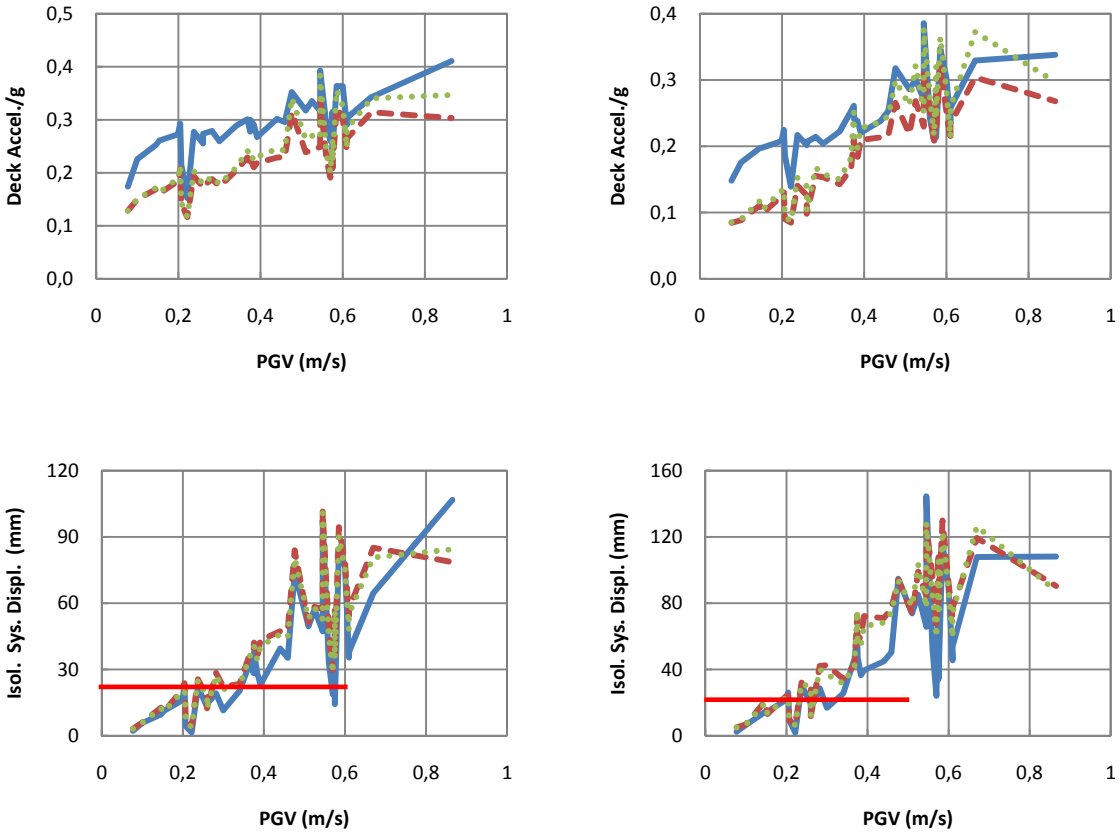

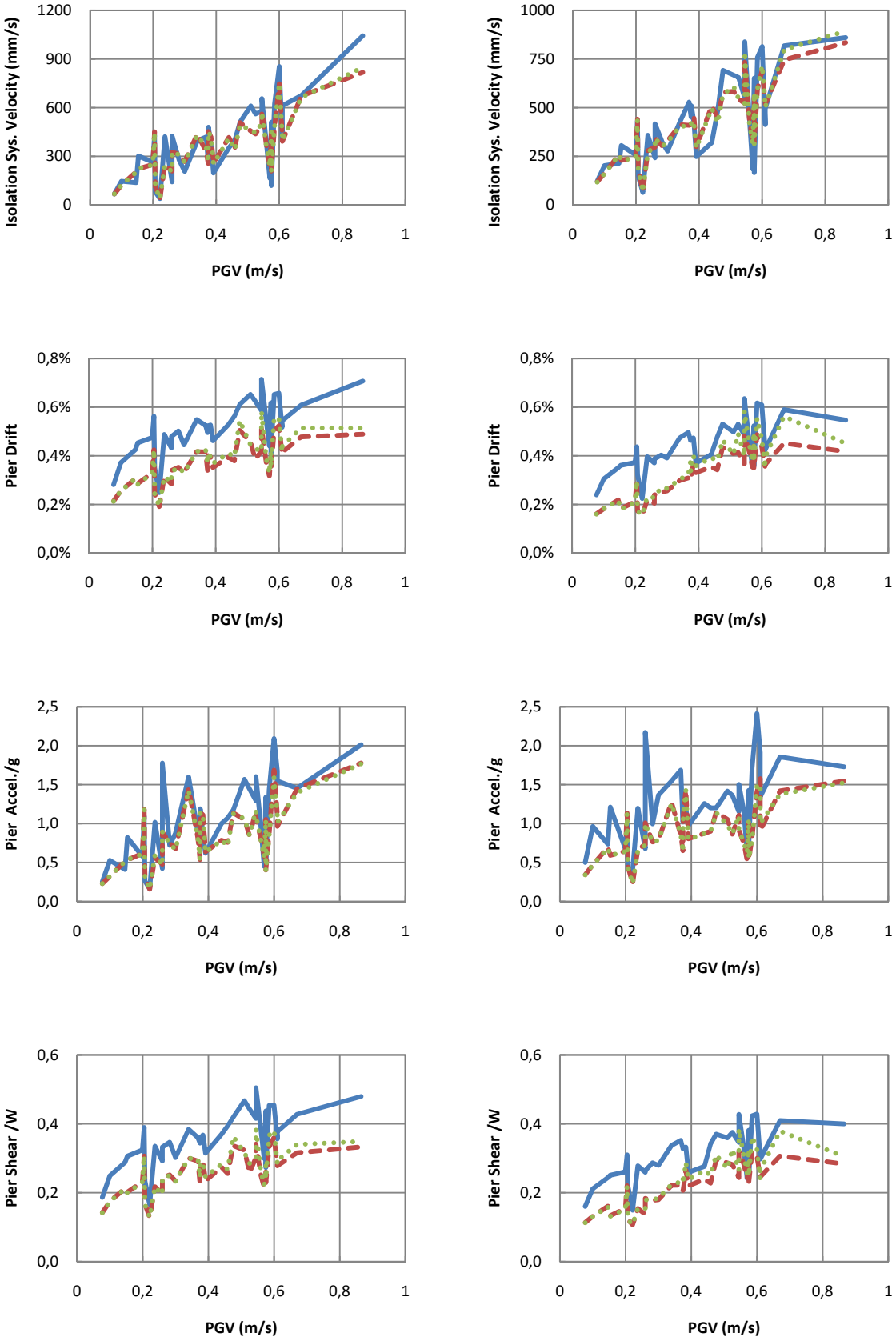

Figure (6-4) Response in near-field ground motions with forward directivity effect, as function of PGV. Left column sliding bearings with normal friction, right column sliding bearings with low friction.

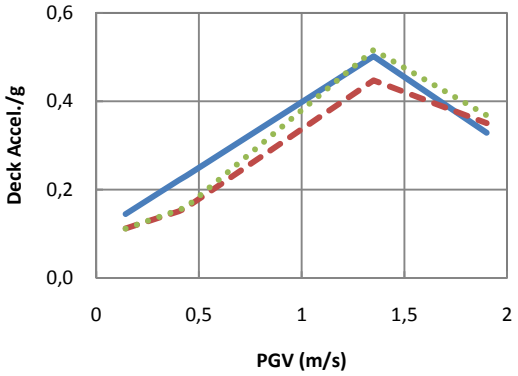

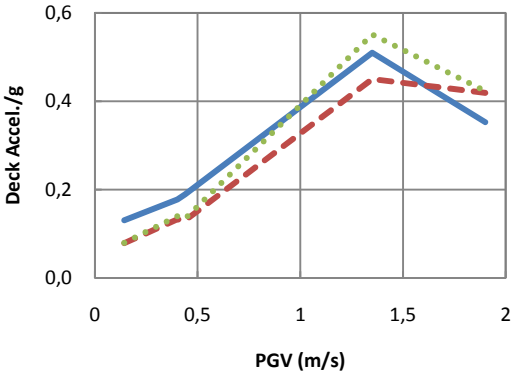

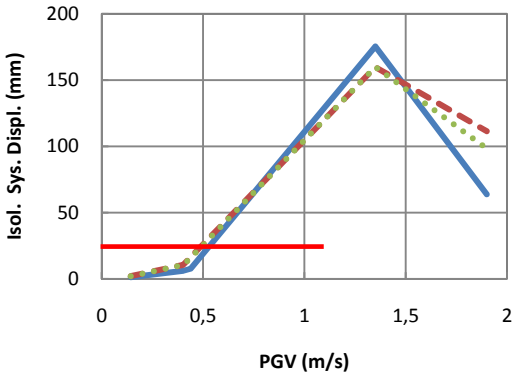

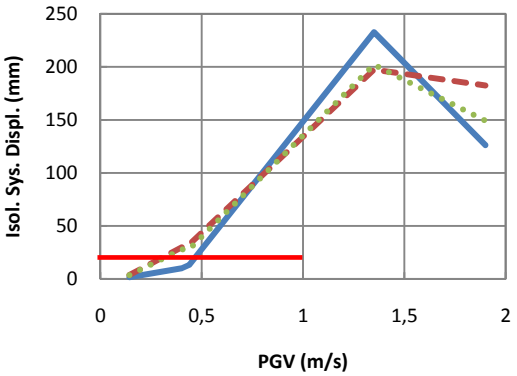

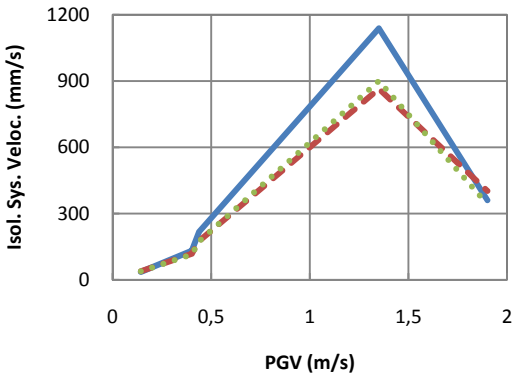

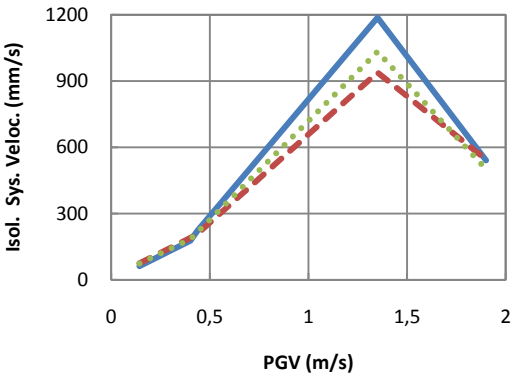

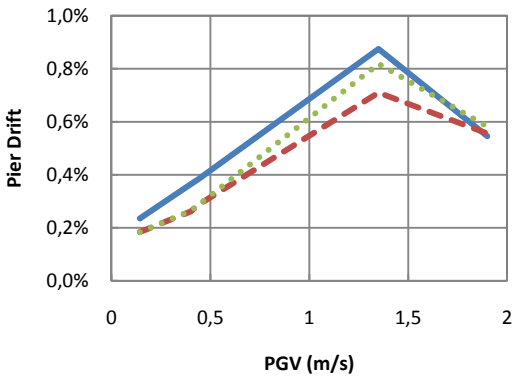

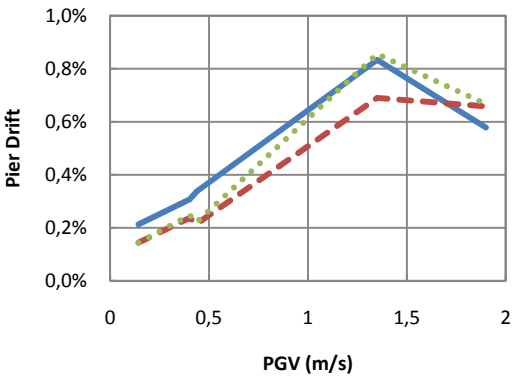

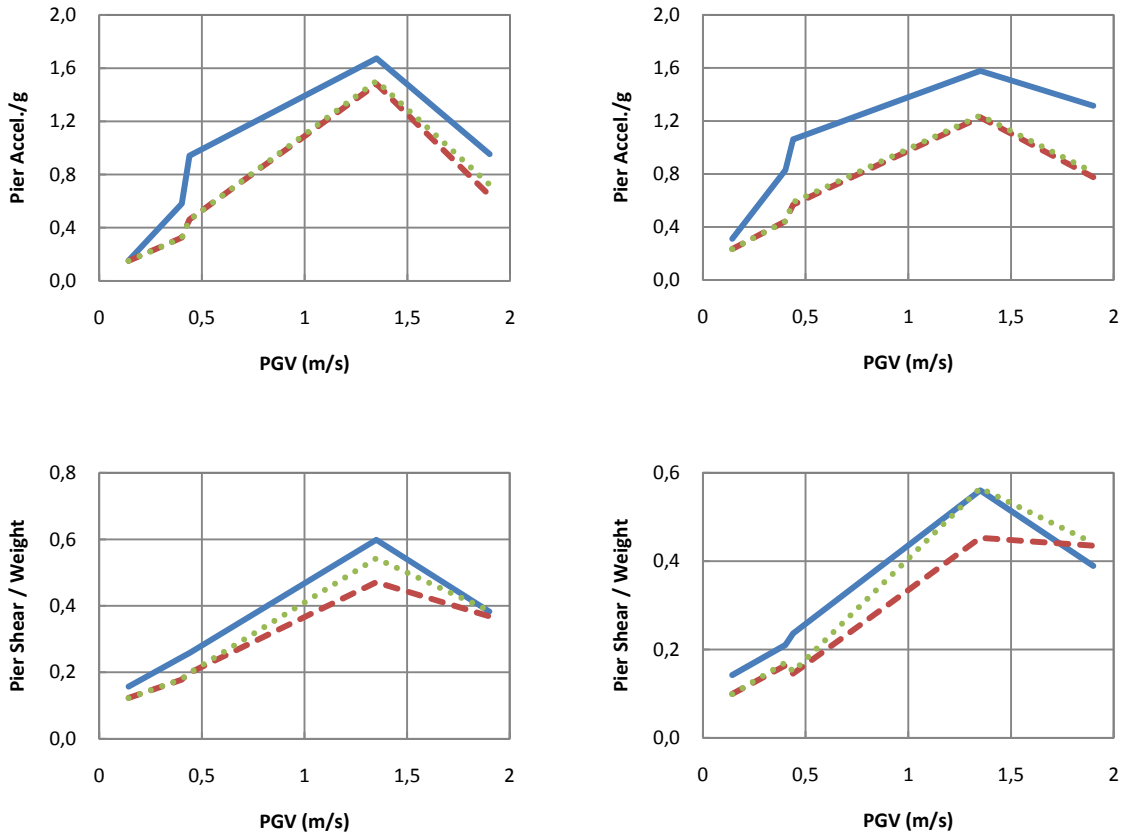

Figure (6-5) Response in near-field ground motions with permanent displacement effect, as function of PGV. Left column sliding bearings with normal friction, right column sliding bearings with low friction. FRFDD continuous line, VED dashed line, SVED dotted line.

6.3 Response to Far-Field Ground Motions for Equivalent Systems Calibrated at $f = 1\ Hz$ and $u_0 = 0.025\ m$

The maximum responses of the bridge model excited with the suite of far-field seismic motions are presented in Figure (6-6). For these seismic excitations the PGA (peak ground acceleration) was used as a ground intensity measure. The effective visco-elastic properties of the seismic isolation systems with VE devices and SVE devices were calculated for a harmonic loading with frequency $f = 1\ Hz$ and amplitude $u_0 = 0.025\ m$.

From Figure (6-6) the maximum isolation system displacement experienced by the FRFDD is slightly higher than the other two equivalent visco-elastic systems for all the seismic motions. This indicates that the effective systems are representing the FRFDD quite well. Observing the isolation system velocities it appears that the velocities for the FRFDD are consistently higher than the two equivalent visco-elastic systems. As was explained in previous chapters this is rather expected due to the nature of the constant restoring force. In turn these large

velocities at the isolation system interface cause large pier drifts, shears and accelerations. The same behavior is observed for the both the normal and low friction sliding bearings.

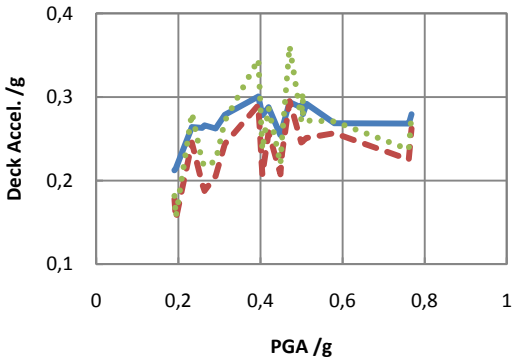

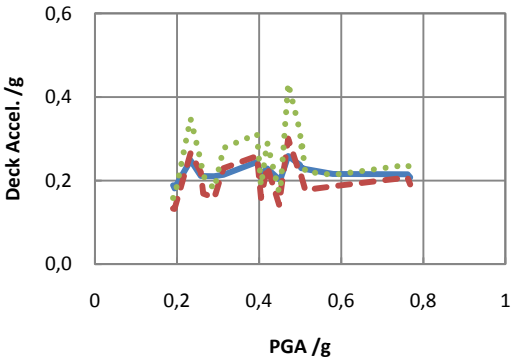

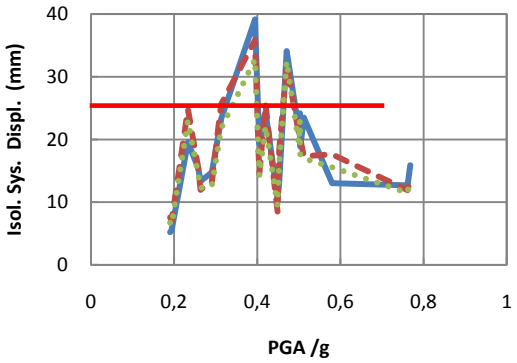

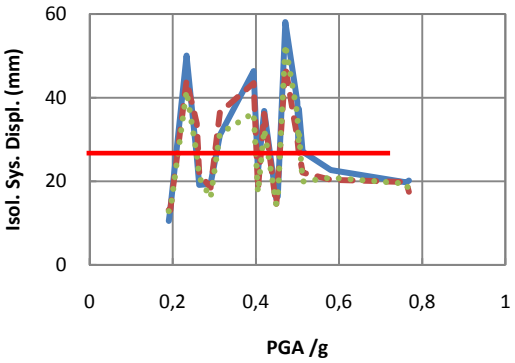

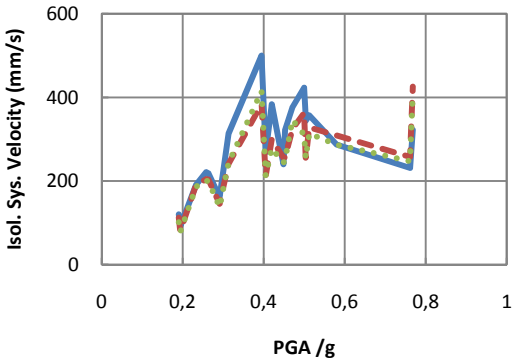

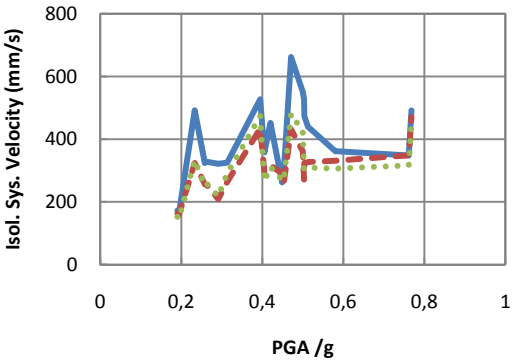

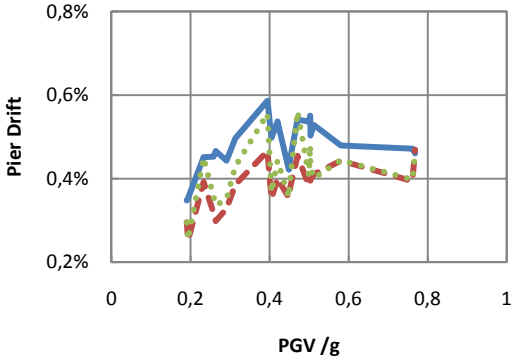

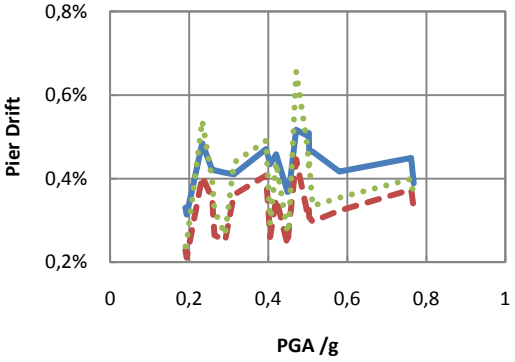

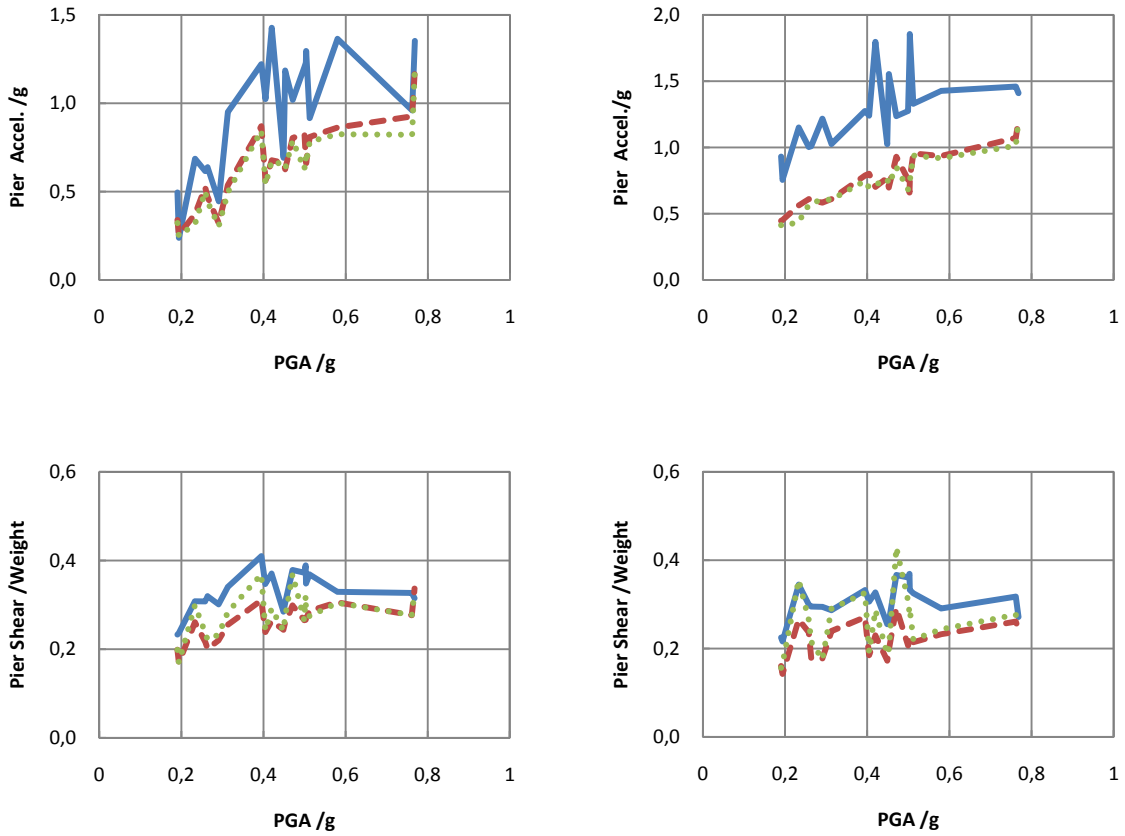

Figure (6-6) Response in far-field ground motions, as function of PGA. Left column sliding bearings with normal friction, right column sliding bearings with low friction. FRFDD continuous line, VED dashed line, SVED dotted line.

Looking at all the figures it becomes also clear that even when the isolation system displacements are much larger than the level of displacement used for the calibration of the effective systems the pier responses are also large. This actually is counterintuitive since the isolation system forces are smaller for the FRFDD than the effective systems and someone expects that the forces and accelerations in the substructure, the pier, would be smaller for the FRFDD system compared to the VE and the SVE systems. This behavior is because of the nature of the constant restoring force mechanism of the FRFDD which results in high velocities at the isolation interface which in turn impose high accelerations and accordingly high shear forces in the piers.

All the presented results in this section support the analysis of the influence of the constant restoring force mechanism in an isolation system on the response parameters of a bridge structure which was presented earlier in this study. Accordingly the use of constant restoring force mechanism in seismic isolations systems, despite their effectiveness in keeping large displacement due to near-fault excitations in check, has to be done accepting that higher velocities might cause larger shear forces in the bridge piers.

A detailed presentation with time histories and loops of bridge responses is presented in the Appendix of this work for all the near-field seismic excitations as well as all the parameters varied in the study, frictional coefficient of sliding bearings and damping systems (FRFDD, VE and SVE).

7 References

Pekcan, G., Mander, J. B., and Chen, S. S. (1995). “The seismic response of a 1:3 scale R.C. structure with elastomeric spring dampers.” Earthquake Spectra, Earthquake Engineering Research Institute, 11(2), 249–267.

Tsopelas, P., Constantinou, M.C. "NCEER-TAISEI Corporation Research Program on Sliding Seismic Isolation Systems for Bridges-Experimental and Analytical Study of Systems Consisting of Sliding Bearings and Fluid Restoring Force/Damping Devices." Report No. NCEER 94-0014. Nat. Ctr. for Earthquake Engrg. Res., State Univ. of New York, Buffalo, NY., (1994).

Christopoulos, C., Tremblay, R., Kim, H.-J., and Lacerte, M. (2008). “Self-centering energy dissipative (SCED) bracing system for the seismic resistance of structures: Development and validation.” J. Struct. Eng., 134(1), 96–107.

Tsopelas, P., Constantinou, M. C., Kircher, C. A. and Whittaker, A. S. "Evaluation of a Simplified Methods of Analysis for Yielding Structures with Energy Dissipation Systems." Report No. NCEER 97-0012. Nat. Ctr. for Earthquake Engrg. Res., State Univ. of New York, Buffalo, NY., (1997)

Mavroeidis, G. P. and A. S. Papageorgiou. (2003) “A Mathematical Representation of Near-Fault Ground Motions” Bulletin of the Seismological Society of America, Vol. 93, No. 3, pp. 1099–1131,

Mavroeidis, G. P., Dong, G. and Papageorgiou,A.S. (2004) “Near-fault ground motions, and the response of elastic and inelastic single-degree-of-freedom (SDOF) systems” Earthquake Engng Struct. Dyn. 33:1023–1049 (DOI: 10.1002/eqe.391)

Housner, G. W., and M. D. Trifunac (1967). Analysis of accelerograms – Parkfield earthquake, Bulletin of the Seismological Society of America, 57, 1193-1220.

Bertero, V. V., S. A. Mahin, and R. A. Herrera (1978). Aseismic design implications of near-fault San Fernando earthquake records, Earthquake Engineering and Structural Dynamics, 6, 31-42.

8 APPENDIX in response for near-filed earthquakes

This appendix contains the detailed resuts in a graphical form of the parametric analyses of this study.

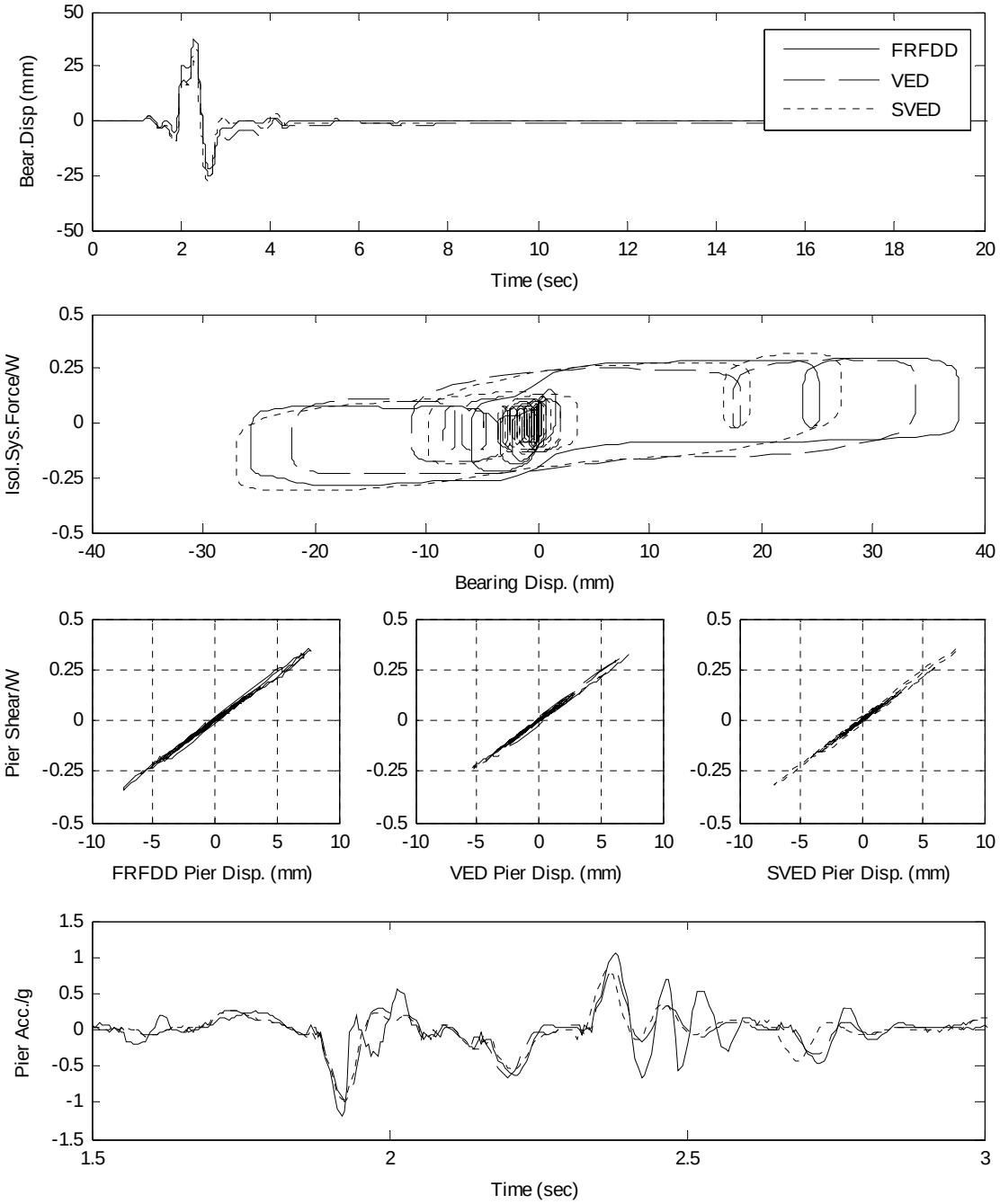

Figure (8-1) Comparison in response for isolation systems with FRFDD, VED, SVED subjected to 1966 Parkfield USA, earthquake, station C02.

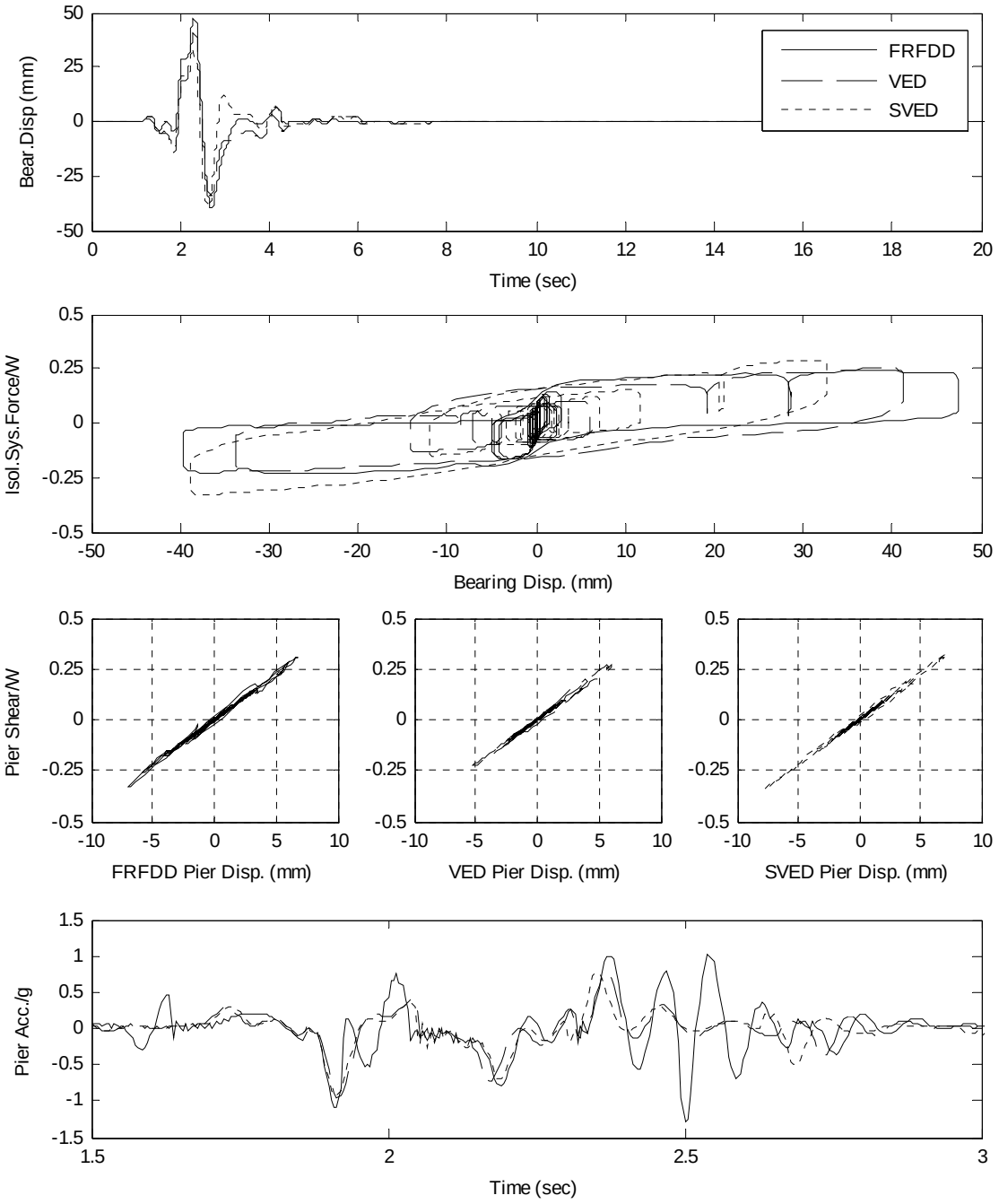

Figure (8-2) Comparison in response for isolation systems with FRFDD, VED, SVED subjected to 1966 Parkfield USA, earthquake, station C02. Sliding bearings with low friction.

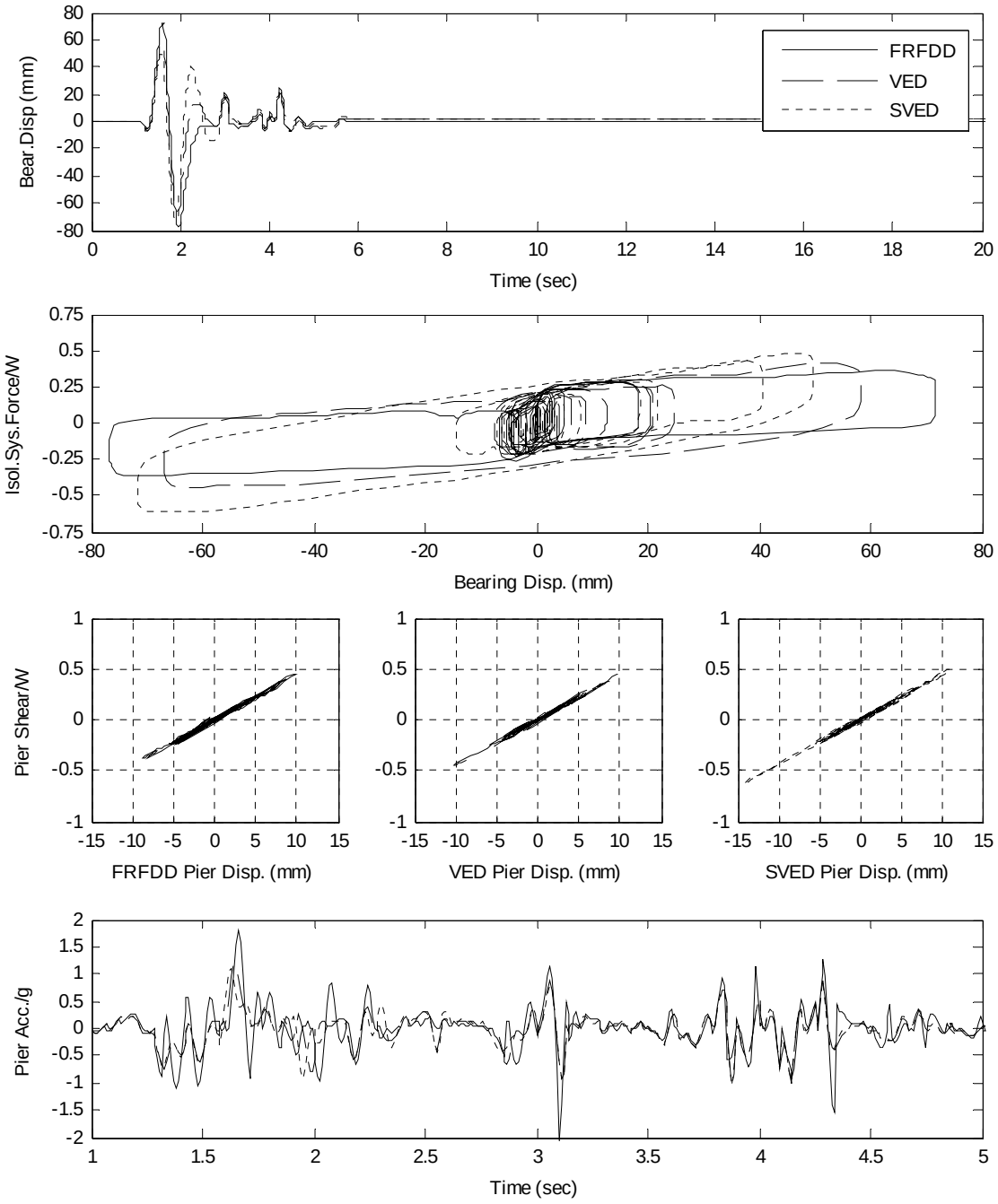

Figure (8-3) Comparison in response for isolation systems with FRFDD, VED, SVED subjected to 1971 San Fernando USA earthquake, station PCD.

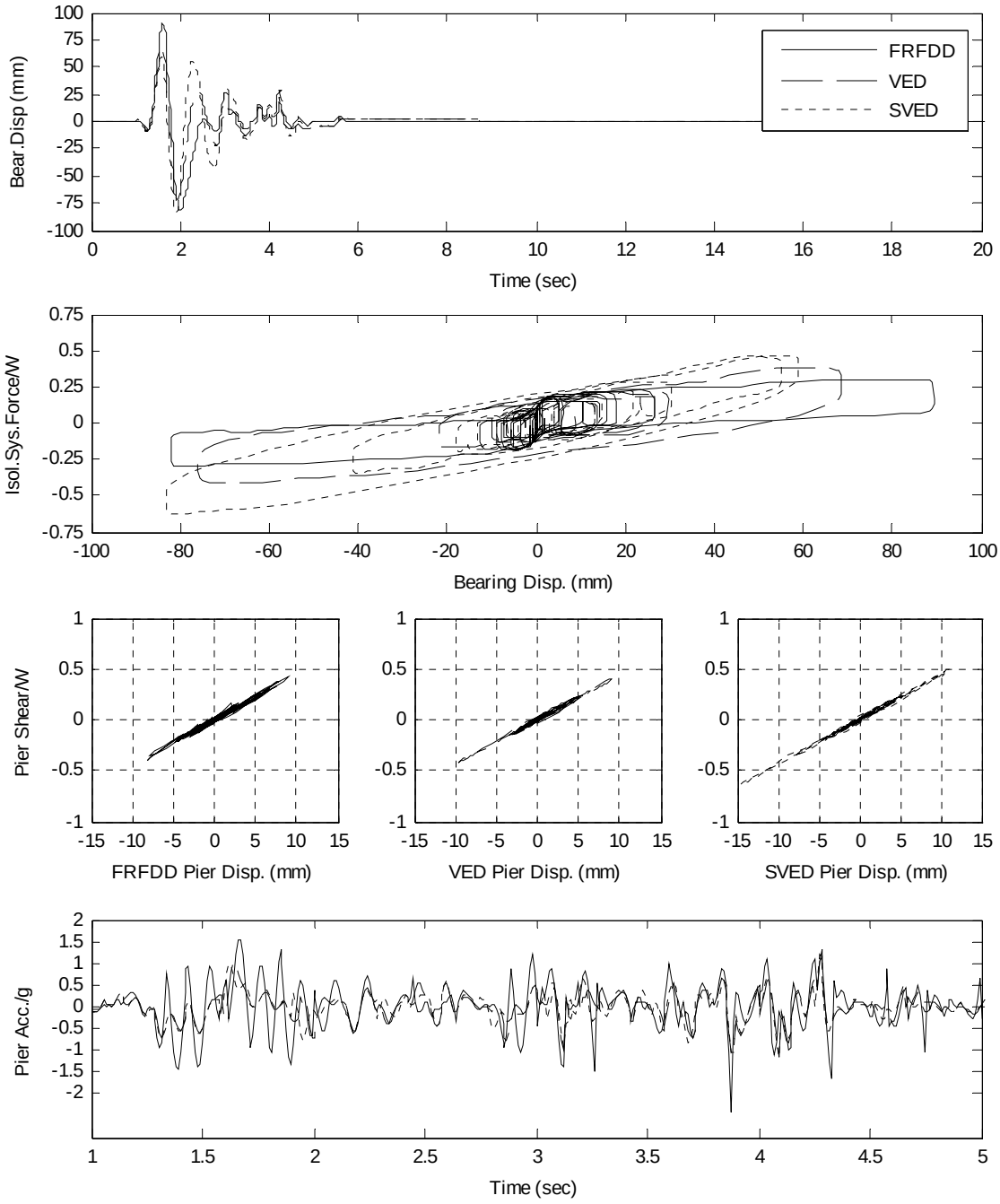

Figure (8-4) Comparison in response for isolation systems with FRFDD, VED, SVED subjected to 1971 San Fernando USA earthquake, station PCD. Sliding bearings with low friction.

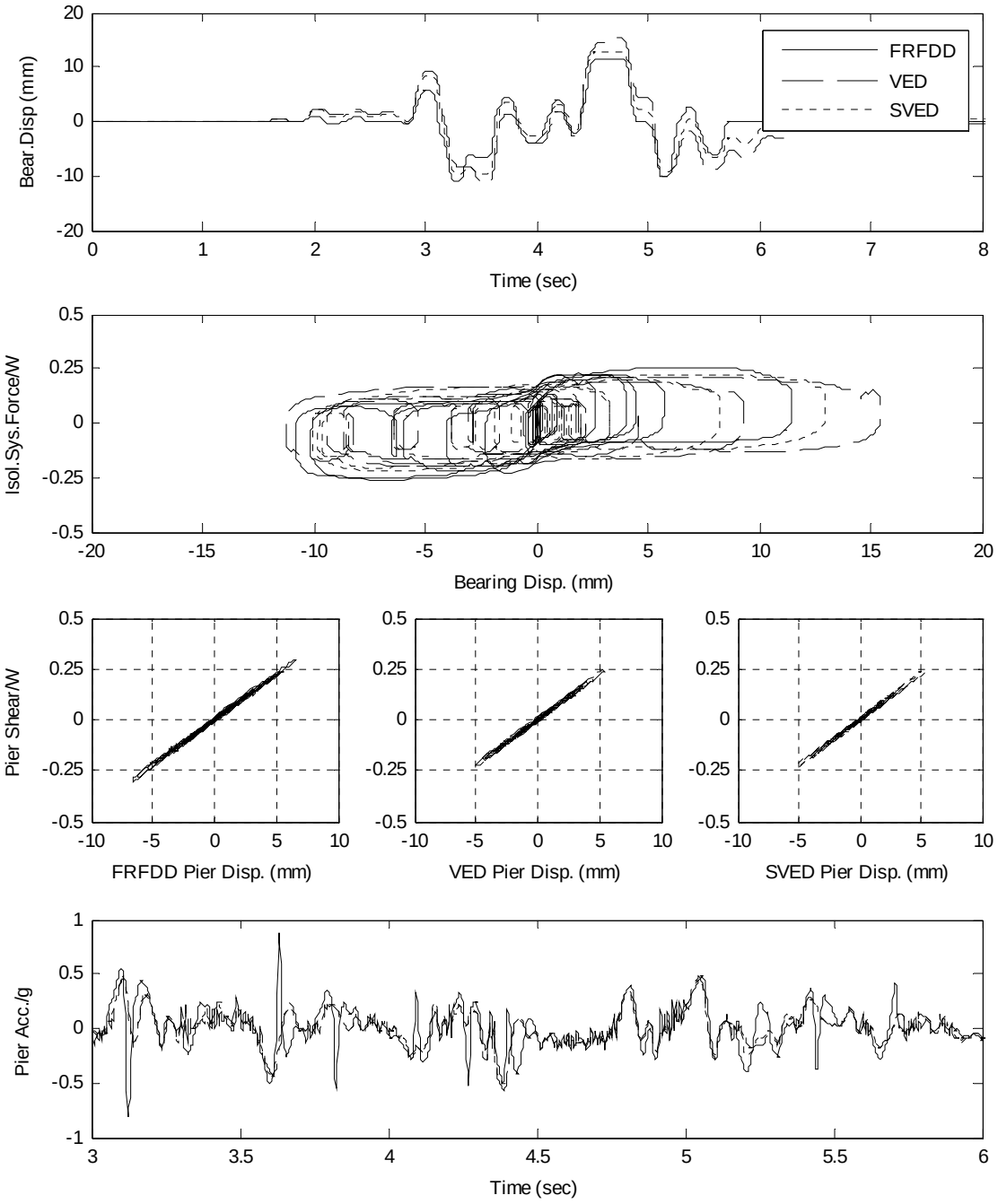

Figure (8-5) Comparison in response for isolation systems with FRFDD, VED, SVED subjected to 1976 Gazli USSR, station KAR.

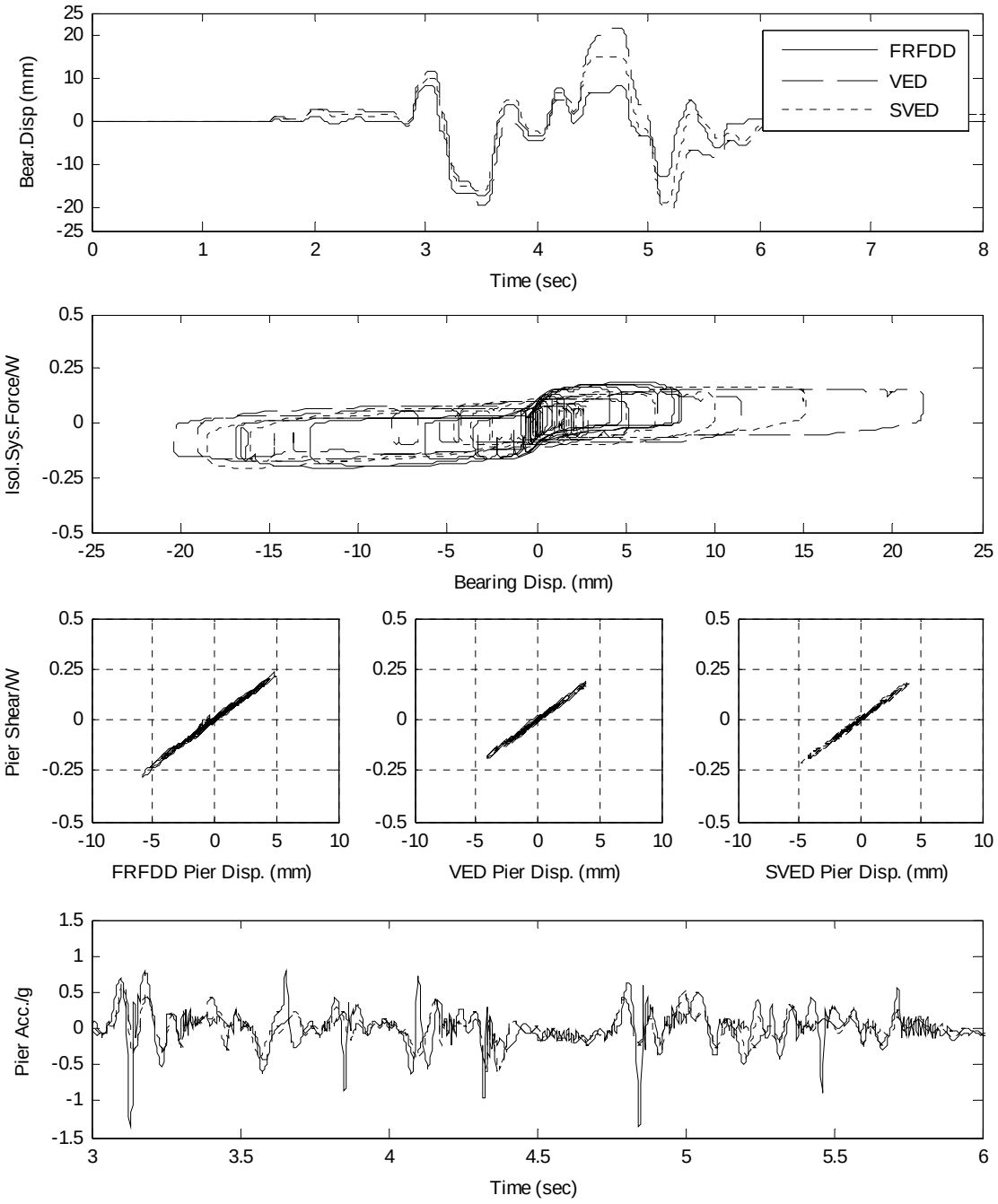

Figure (8-6) Comparison in response for isolation systems with FRFDD, VED, SVED subjected to 1976 Gazli USSR, station KAR. Sliding bearings with low friction.

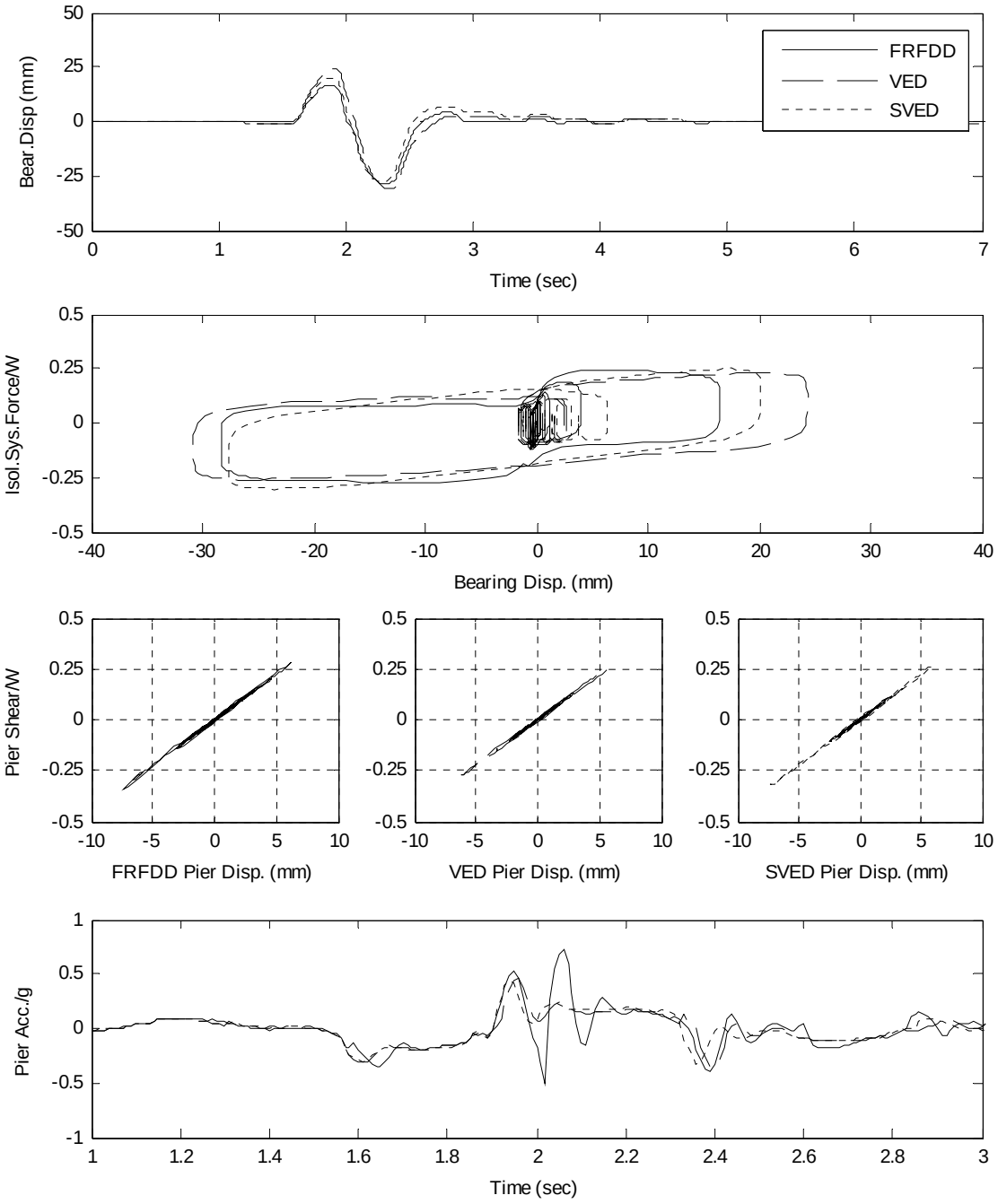

Figure (8-7) Comparison in response for isolation systems with FRFDD, VED, SVED subjected to 1977 Bucharest Romania earthquake, station BRI.

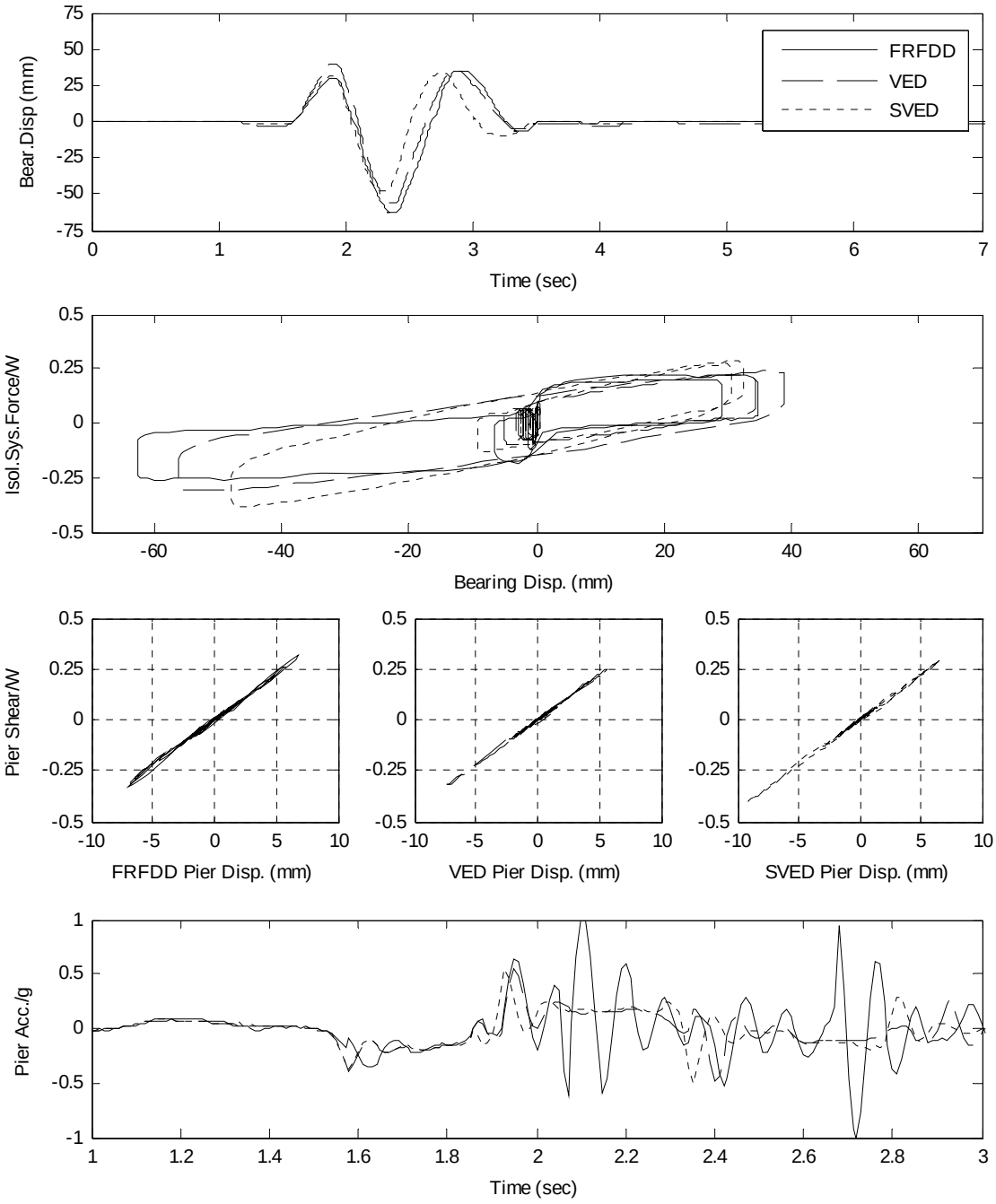

Figure (8-8) Comparison in response for isolation systems with FRFDD, VED, SVED subjected to 1977 Bucharest Romania earthquake, station BRI. Sliding bearings with low friction.

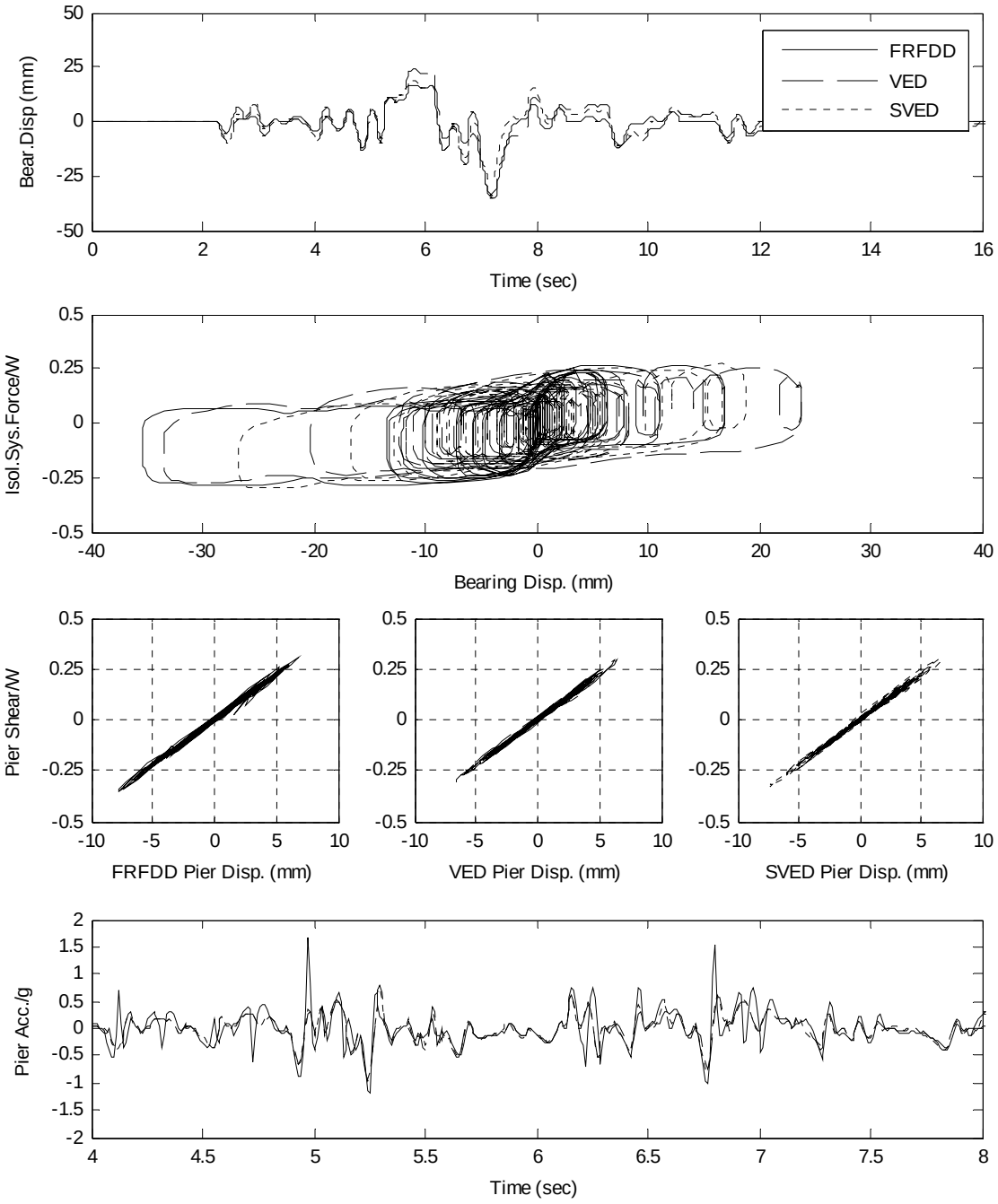

Figure (8-9) Comparison in response for isolation systems with FRFDD, VED, SVED subjected to 1978 Tabas Iran earthquake, station TAB.

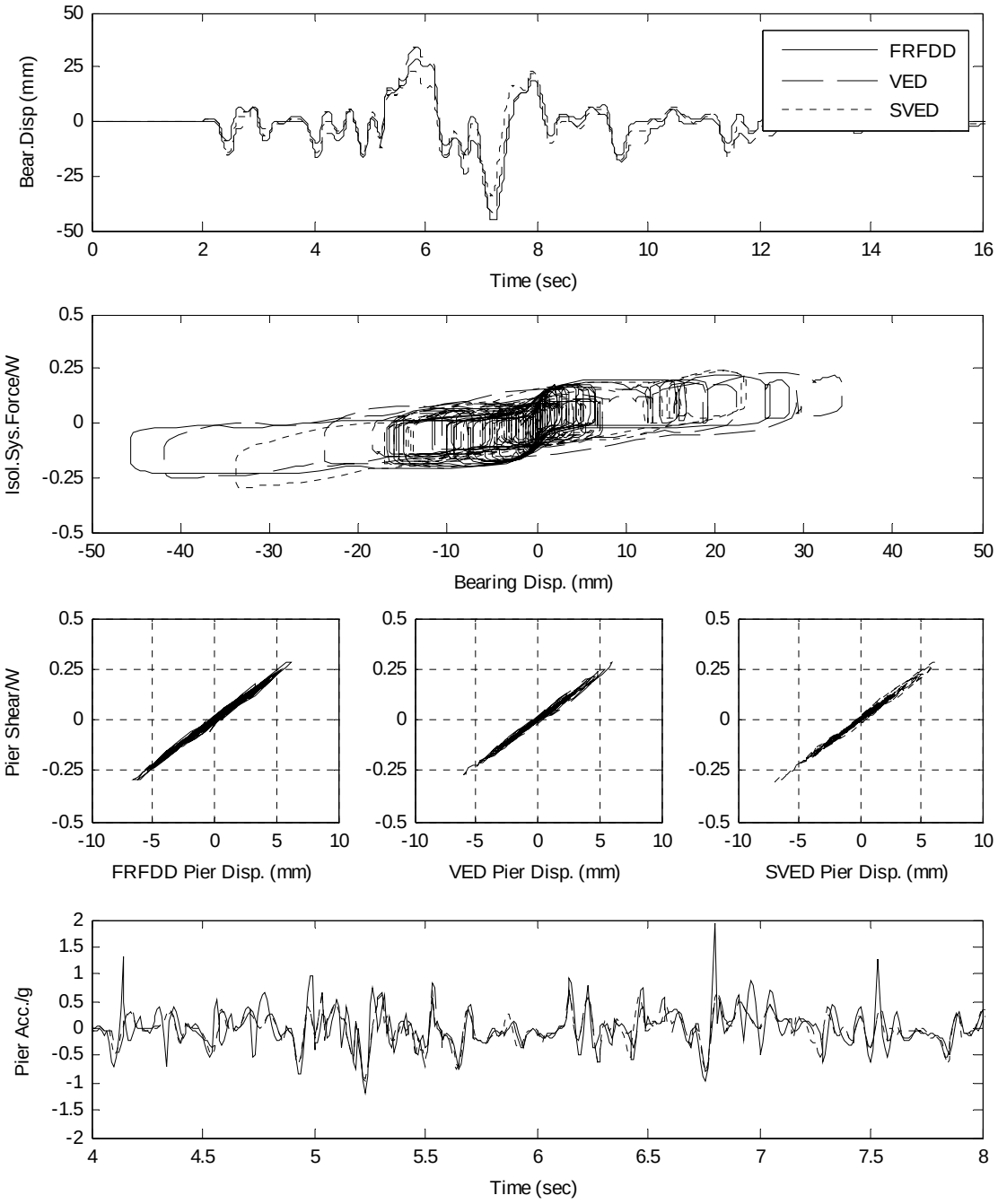

Figure (8-10) Comparison in response for isolation systems with FRFDD, VED, SVED subjected to 1978 Tabas Iran earthquake, station TAB. Sliding bearings with low friction.

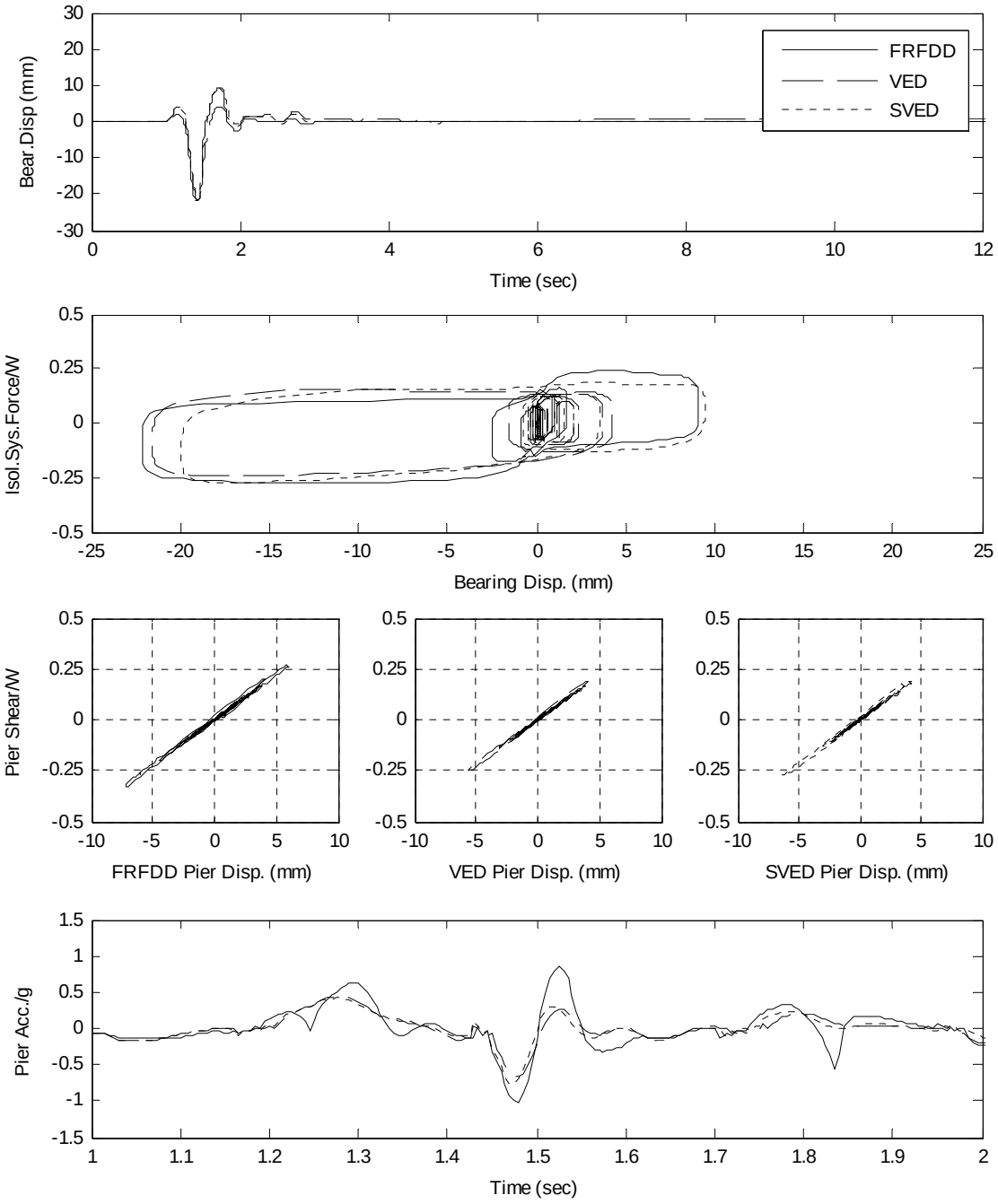

Figure (8-11) Comparison in response for isolation systems with FRFDD, VED, SVED subjected to 1979 Coyote Lake USA earthquake, station GA6.

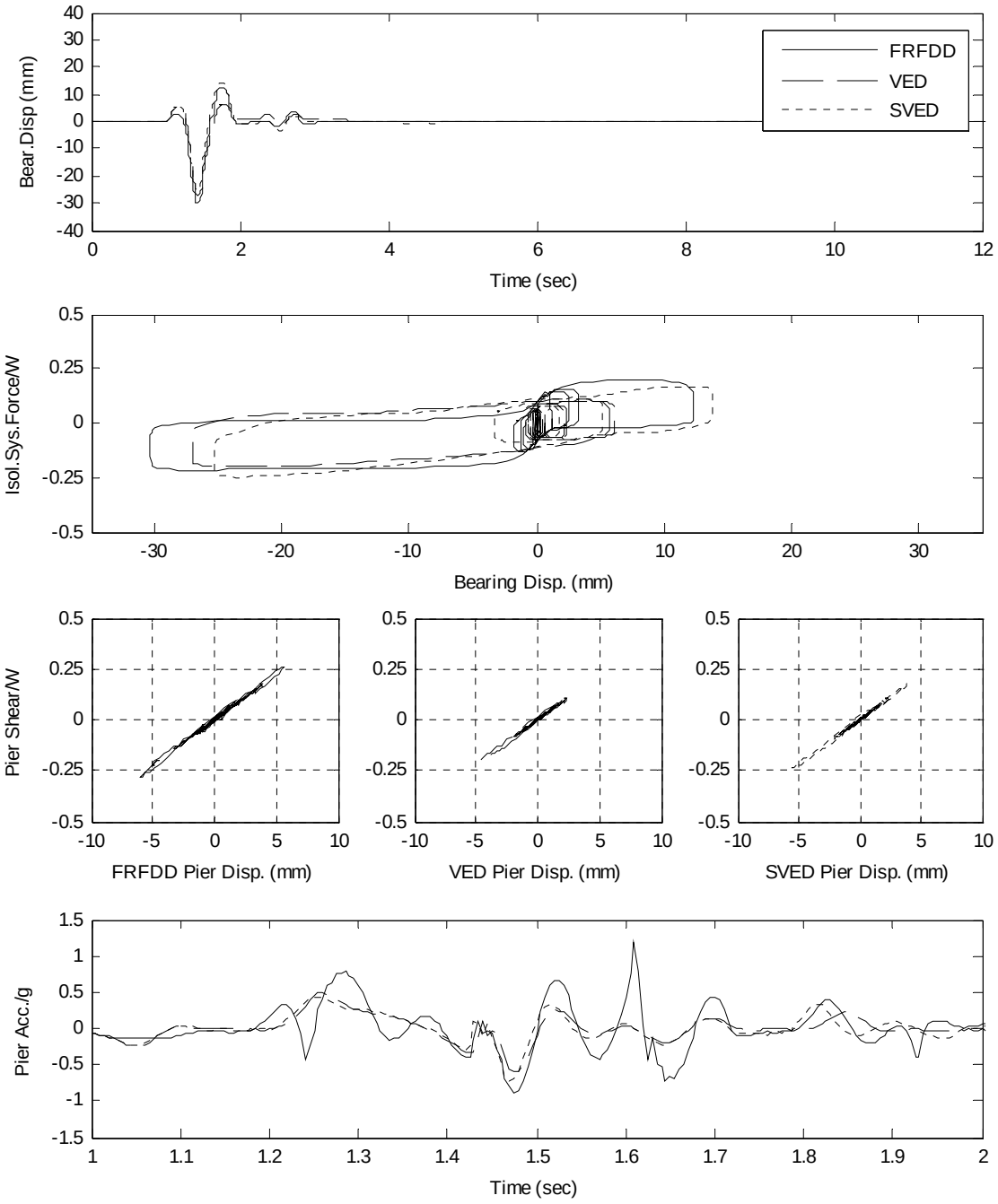

Figure (8-12) Comparison in response for isolation systems with FRFDD, VED, SVED subjected to 1979 Coyote Lake USA earthquake, station GA6. Sliding bearings with low friction.

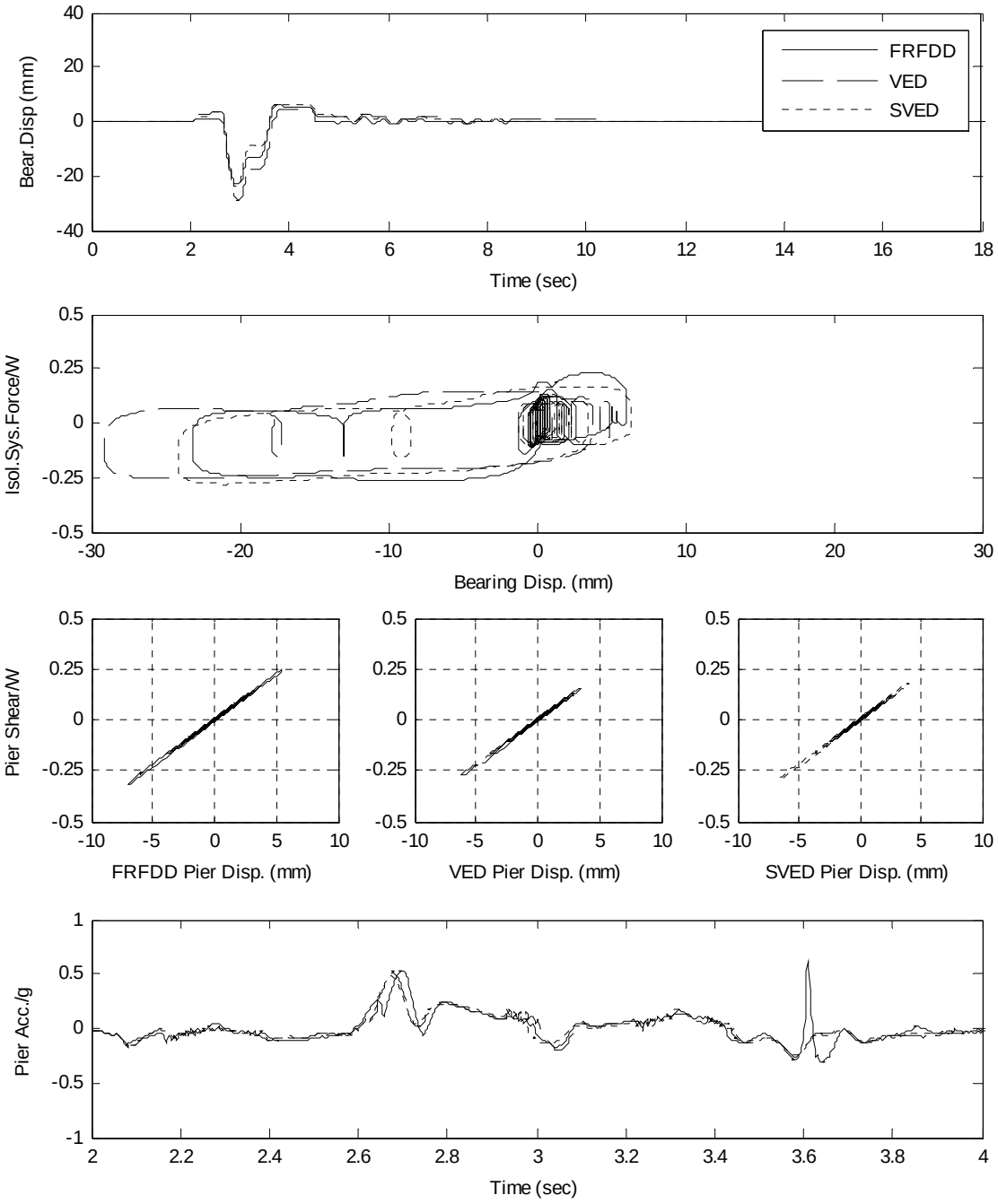

Figure (8-13) Comparison in response for isolation systems with FRFDD, VED, SVED subjected to 1979 Imperial Valley USA earthquake, station E04.

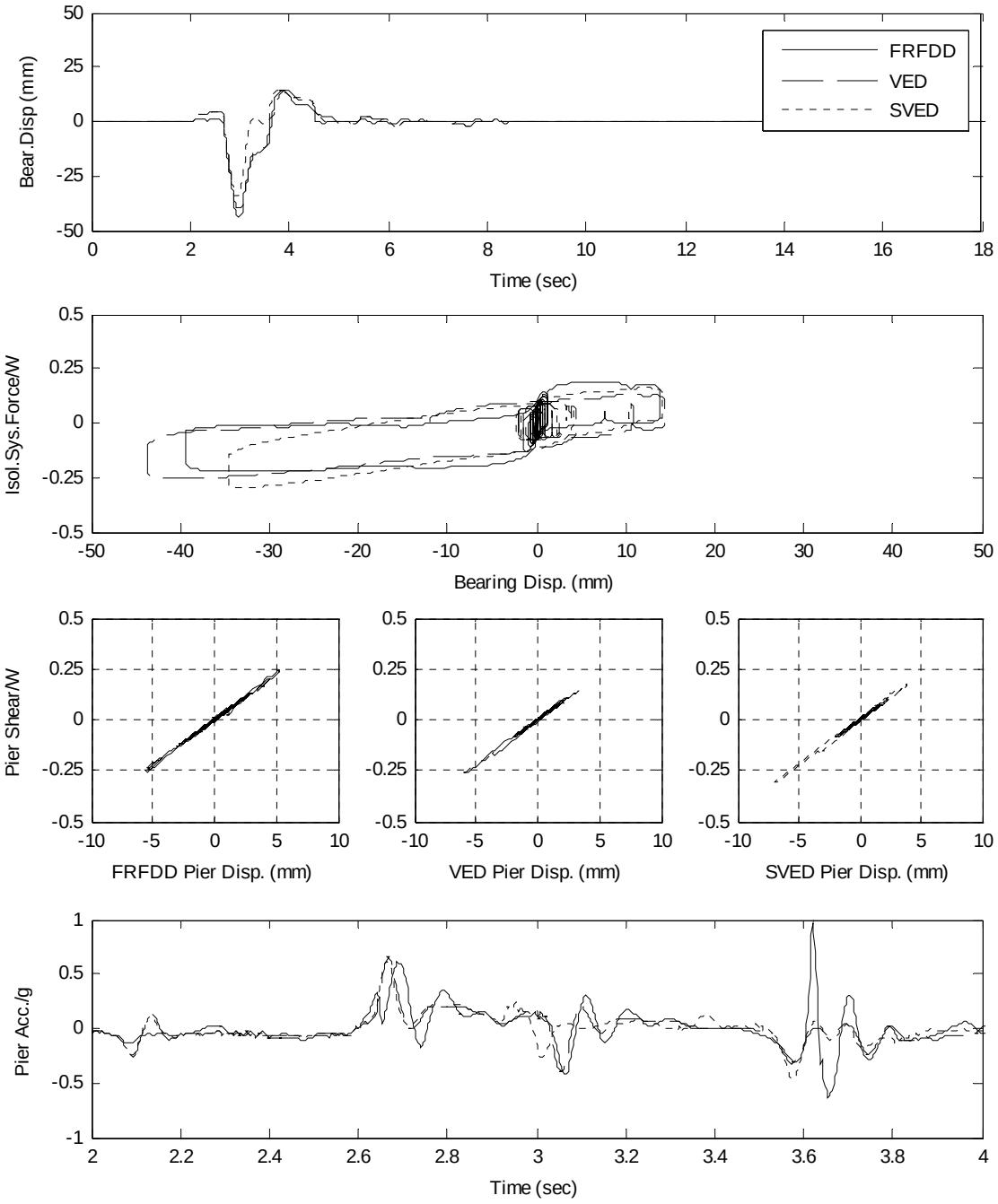

Figure (8-14) Comparison in response for isolation systems with FRFDD, VED, SVED subjected to 1979 Imperial Valley USA earthquake, station E04. Sliding bearings with low friction.

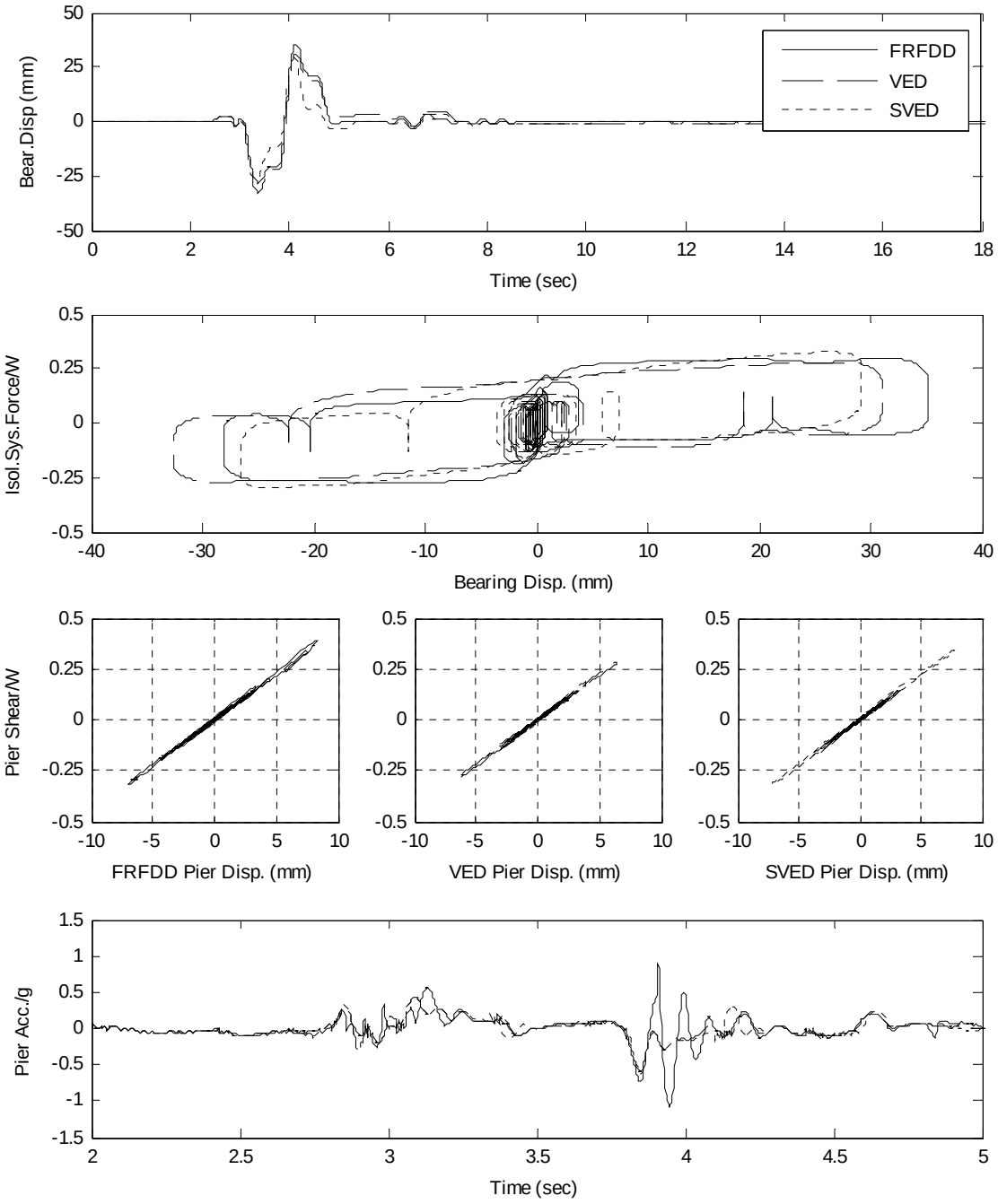

Figure (8-15) Comparison in response for isolation systems with FRFDD, VED, SVED subjected to 1979 Imperial Valley USA earthquake, station E05.

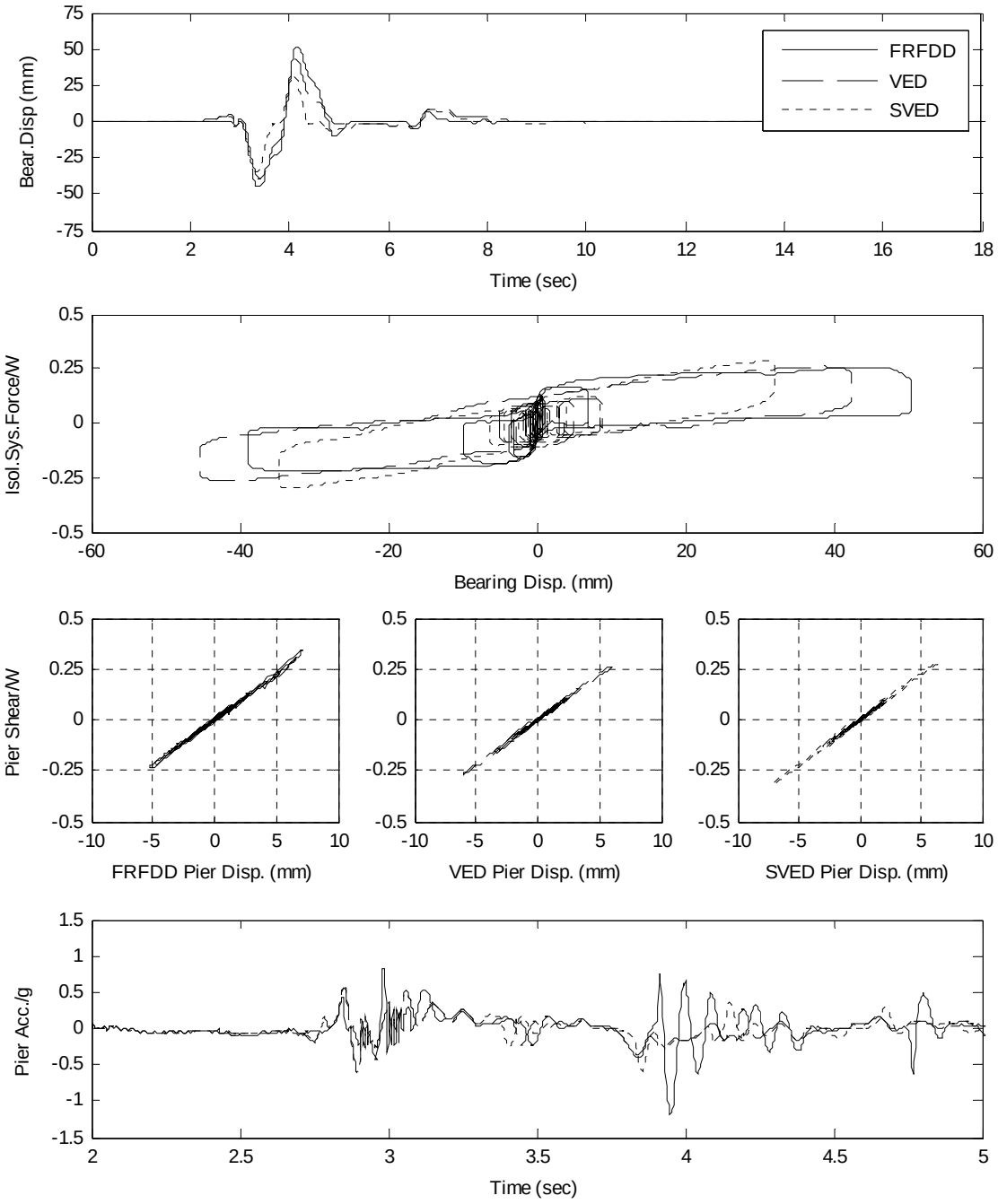

Figure (8-16) Comparison in response for isolation systems with FRFDD, VED, SVED subjected to 1979 Imperial Valley USA earthquake, station E05. Sliding bearings with low friction.

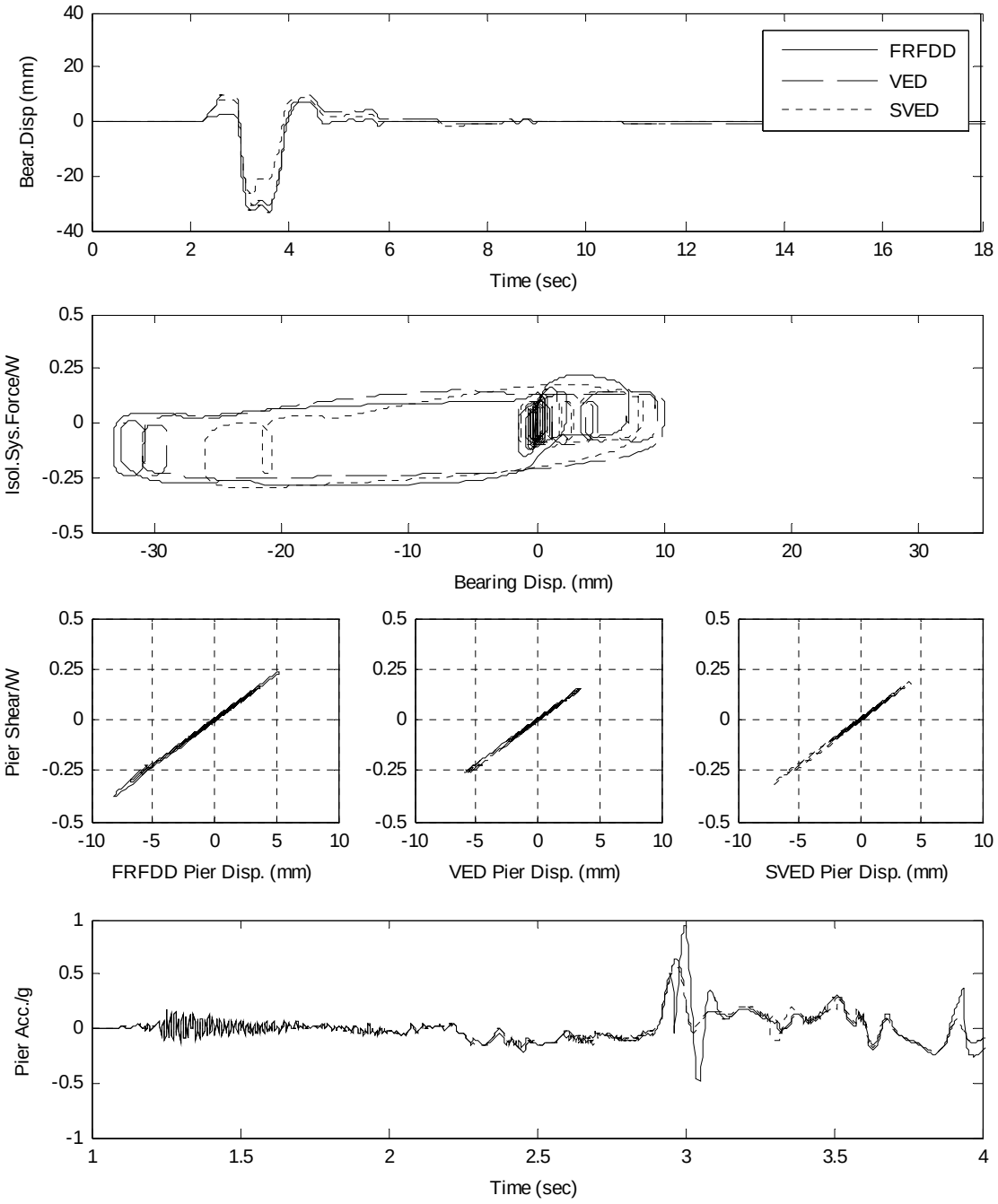

Figure (8-17) Comparison in response for isolation systems with FRFDD, VED, SVED subjected to 1979 Imperial Valley USA earthquake, station E06.

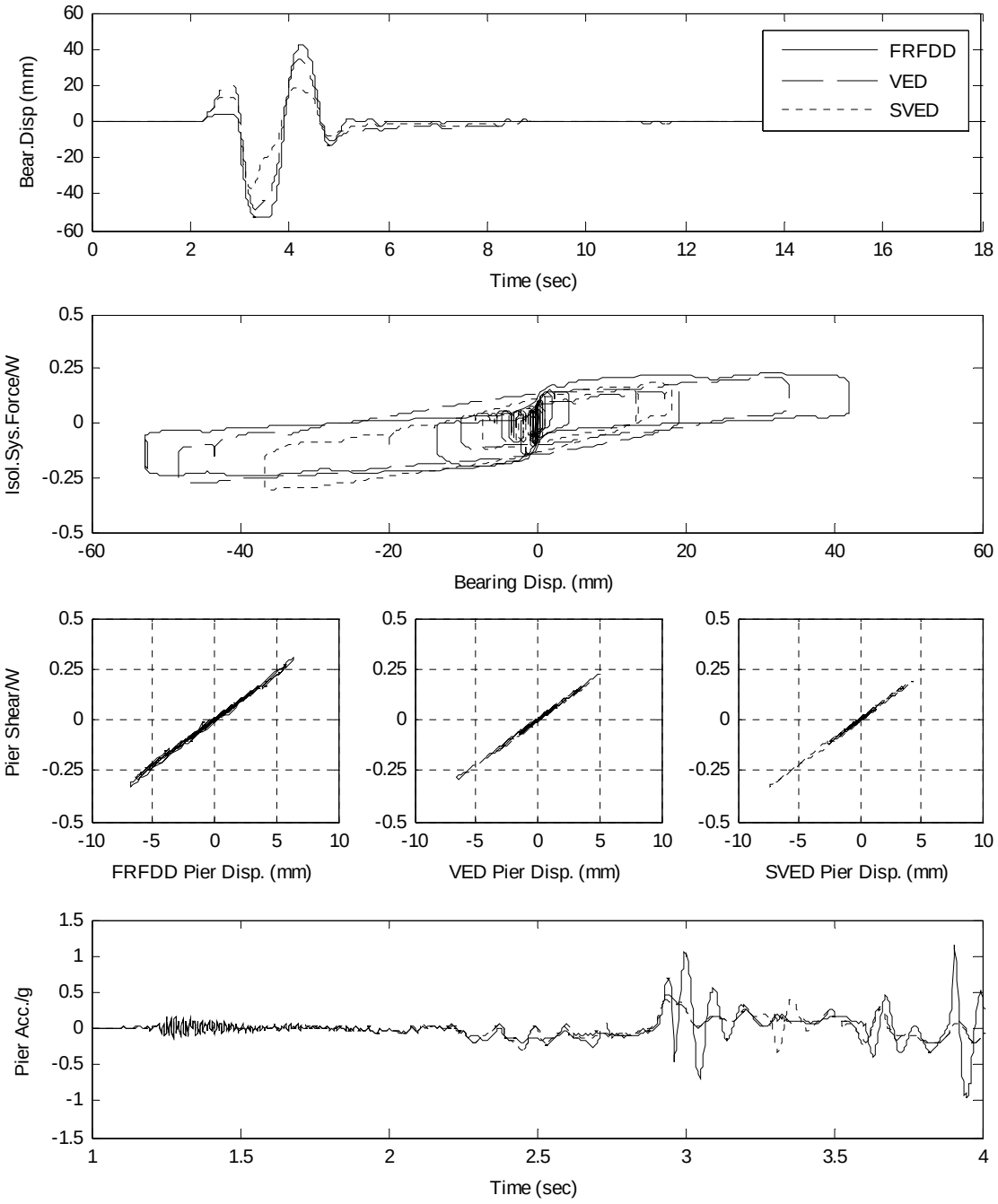

Figure (8-18) Comparison in response for isolation systems with FRFDD, VED, SVED subjected to 1979 Imperial Valley USA earthquake, station E06. Sliding bearings with low friction.

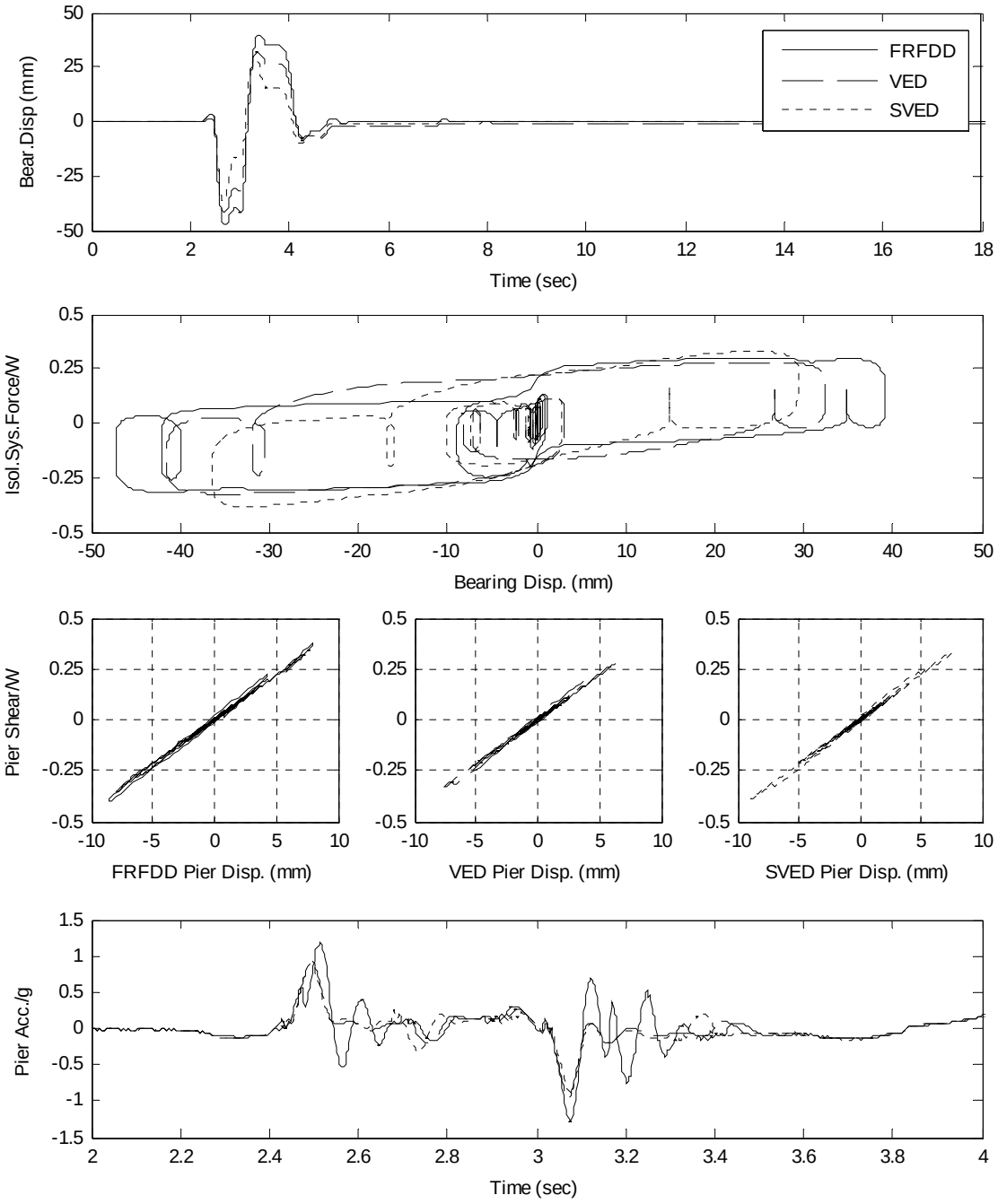

Figure (8-19) Comparison in response for isolation systems with FRFDD, VED, SVED subjected to 1979 Imperial Valley USA earthquake, station E07.

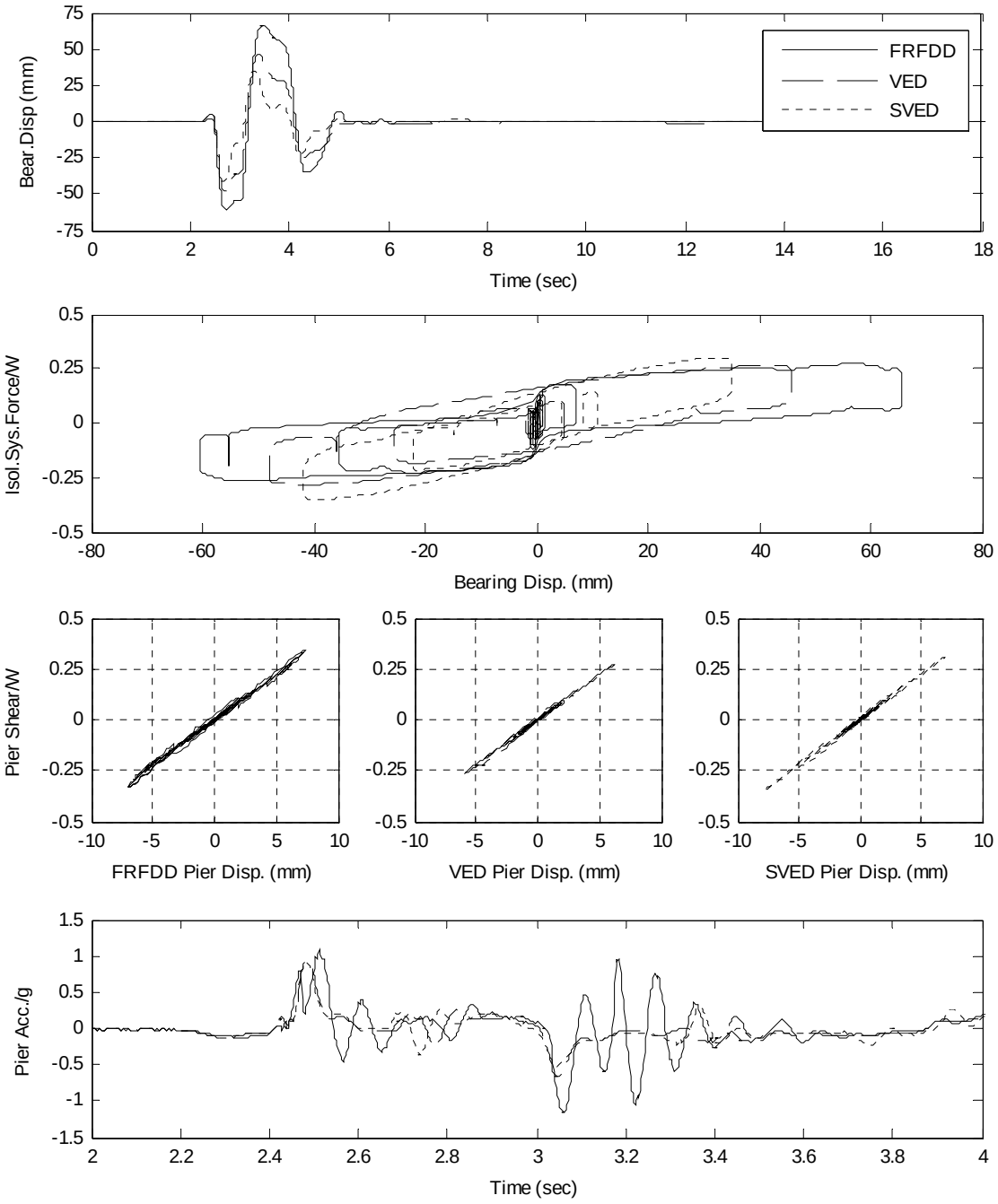

Figure (8-20) Comparison in response for isolation systems with FRFDD, VED, SVED subjected to 1979 Imperial Valley USA earthquake, station E07. Sliding bearings with low friction.

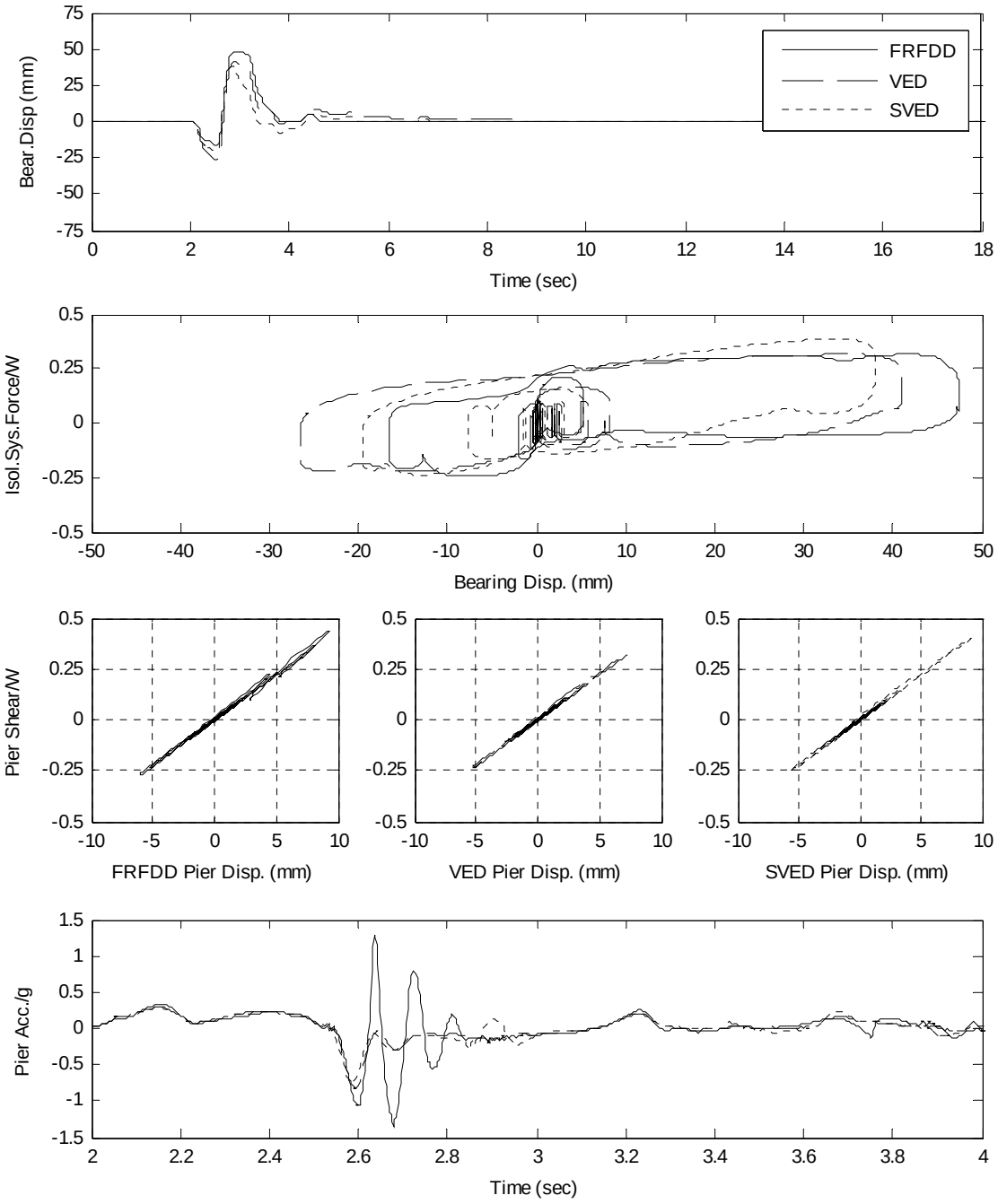

Figure (8-21) Comparison in response for isolation systems with FRFDD, VED, SVED subjected to 1979 Imperial Valley USA earthquake, station EMO.

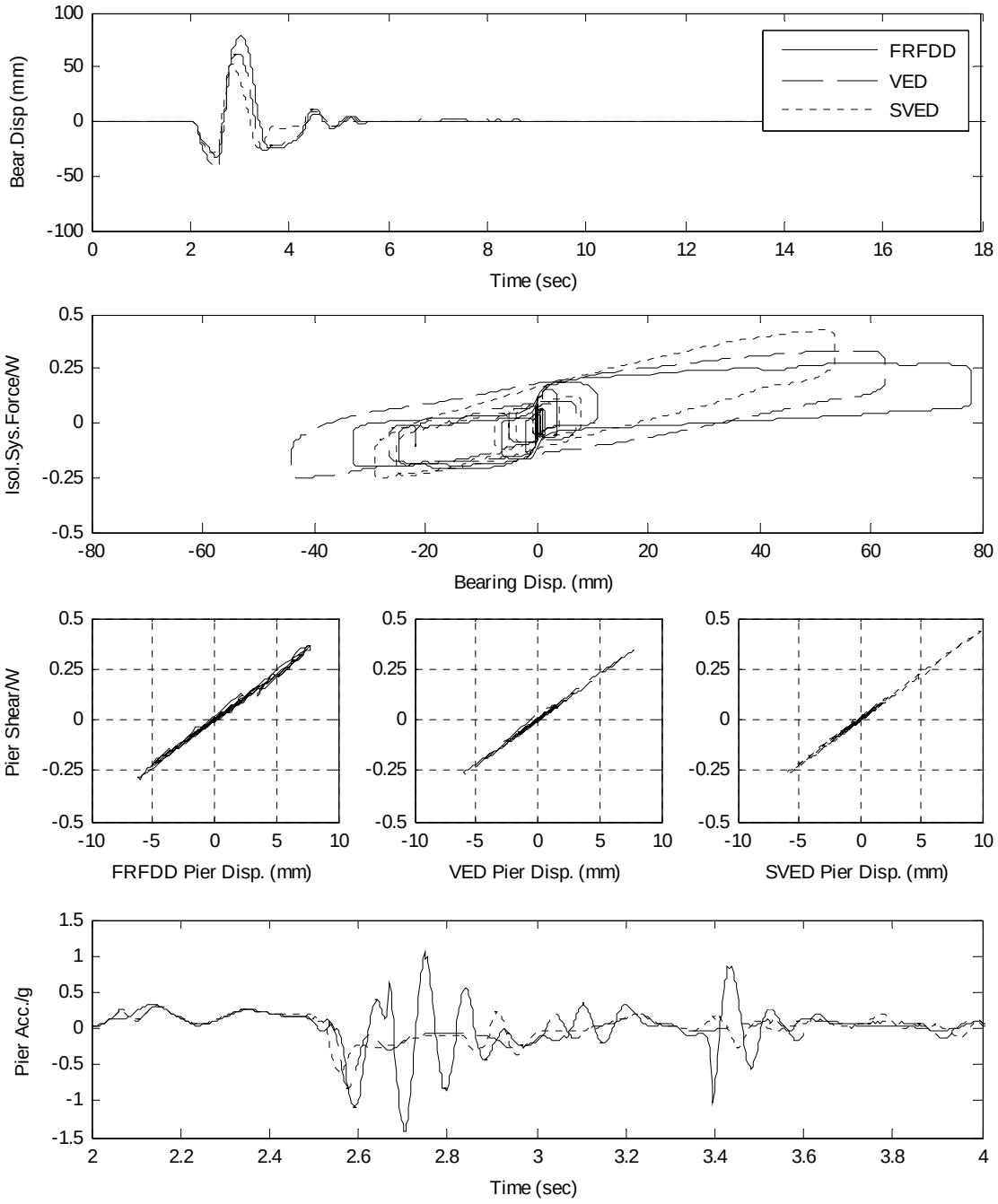

Figure (8-22) Comparison in response for isolation systems with FRFDD, VED, SVED subjected to 1979 Imperial Valley USA earthquake, station EMO. Sliding bearings with low friction.

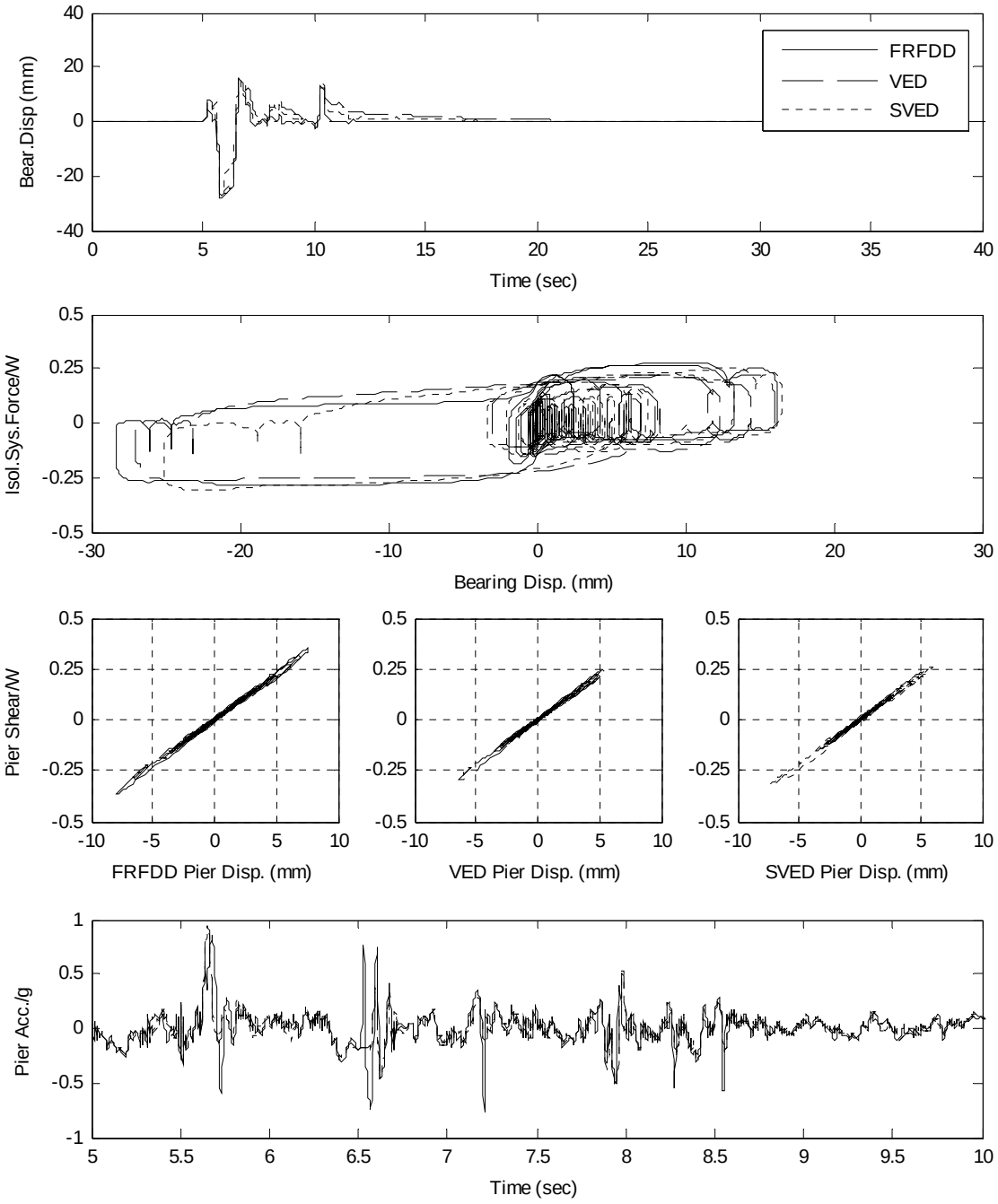

Figure (8-23) Comparison in response for isolation systems with FRFDD, VED, SVED subjected to 1980 Mexicali Valley Mexico, station VCT.

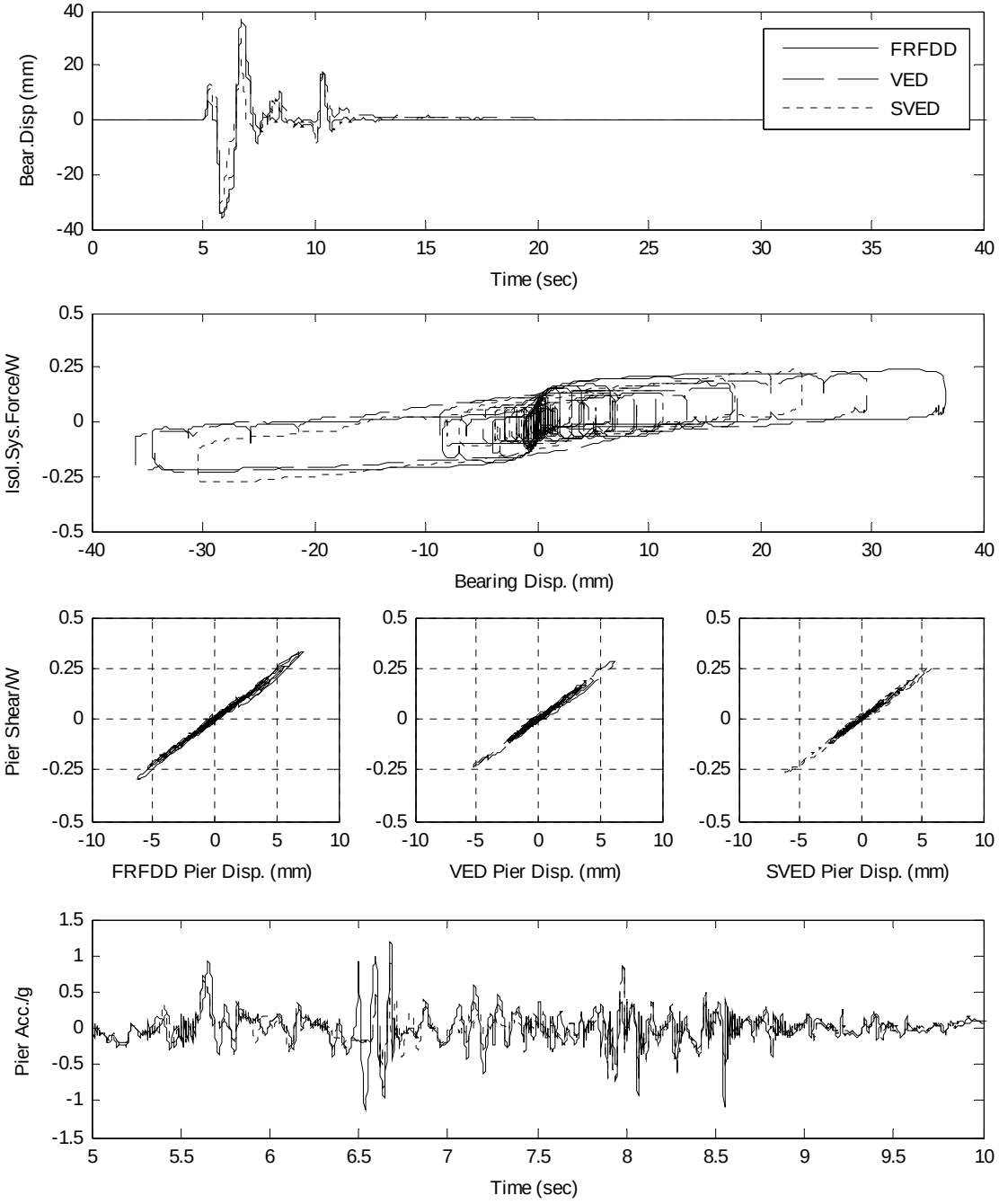

Figure (8-24) Comparison in response for isolation systems with FRFDD, VED, SVED subjected to 1980 Mexicali Valley Mexico, station VCT. Sliding bearings with low friction.

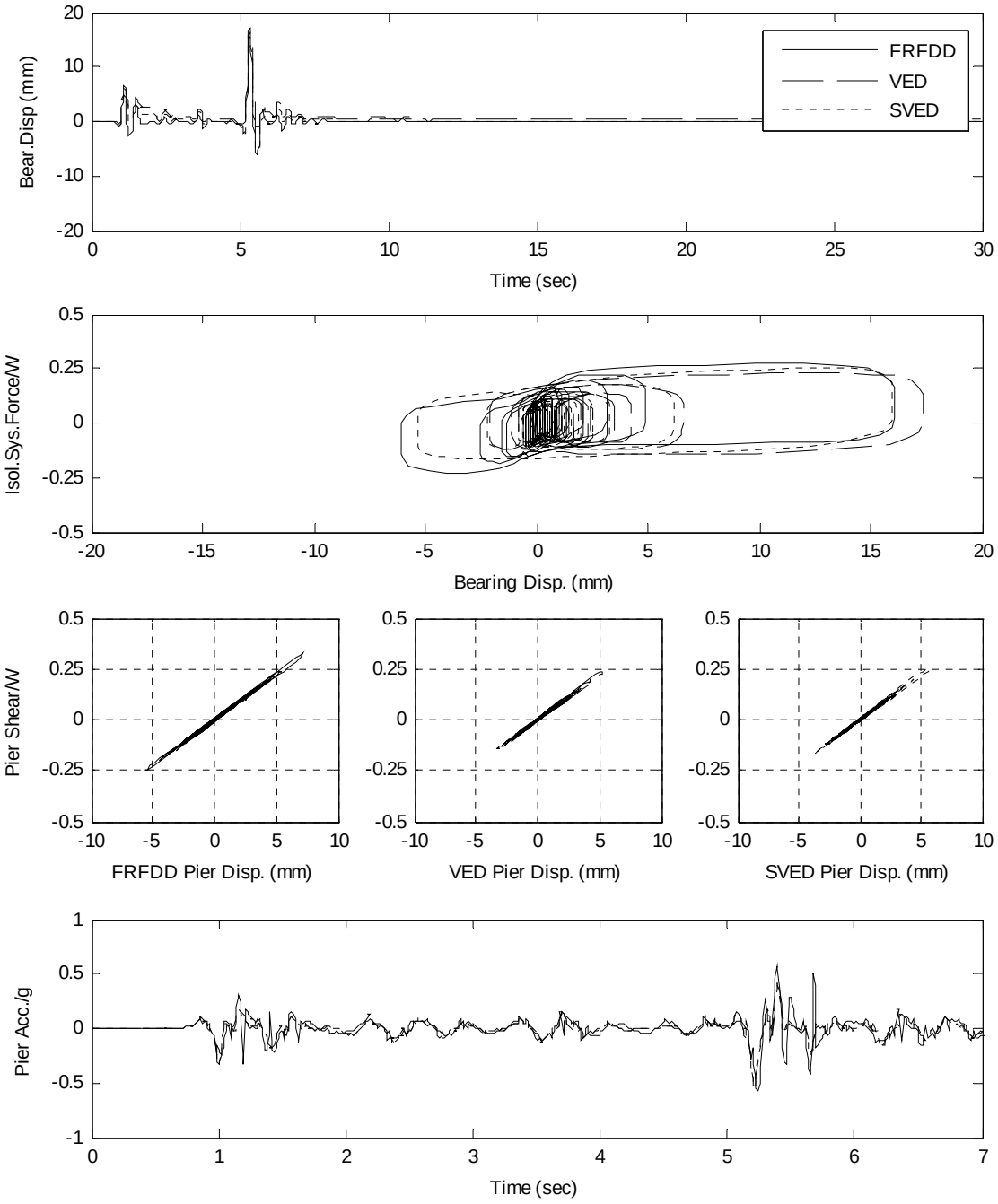

Figure (8-25) Comparison in response for isolation systems with FRFDD, VED, SVED subjected to 1984 Morgan Hill USA earthquake, station HAL.

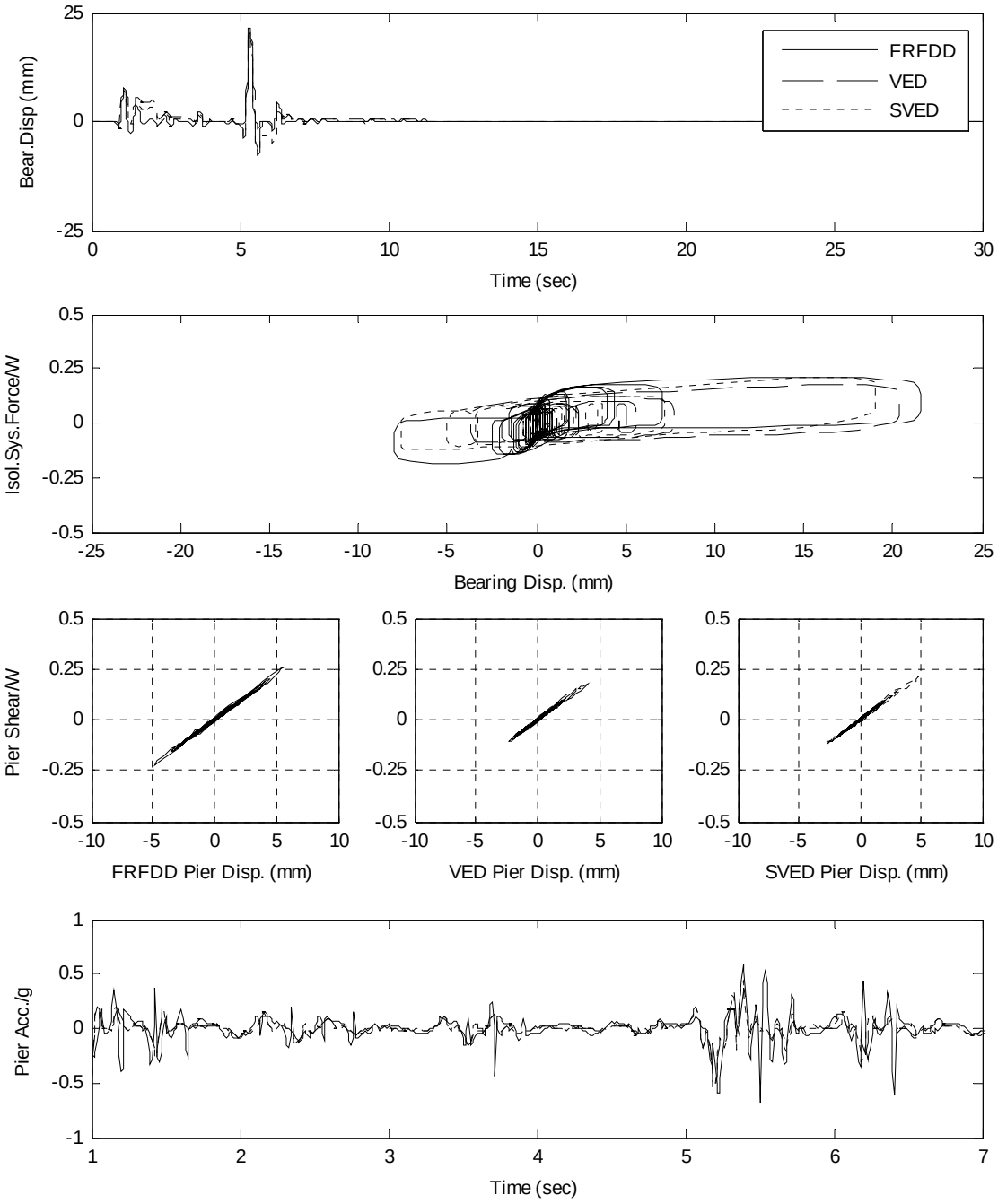

Figure (8-26) Comparison in response for isolation systems with FRFDD, VED, SVED subjected to 1984 Morgan Hill USA earthquake, station HAL. Sliding bearings with low friction.

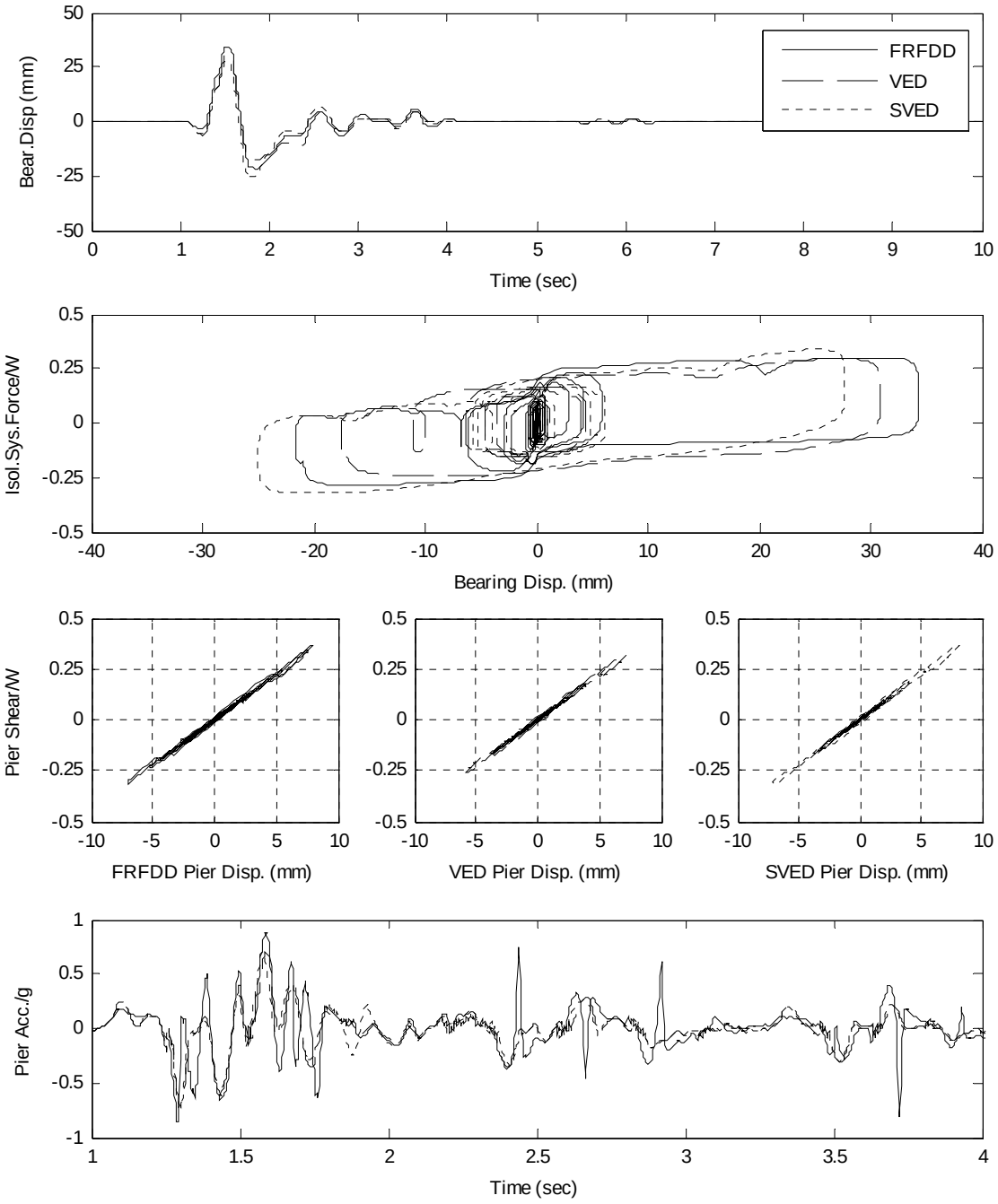

Figure (8-27) Comparison in response for isolation systems with FRFDD, VED, SVED subjected to 1986 Palm Springs USA earthquake, station NPS.

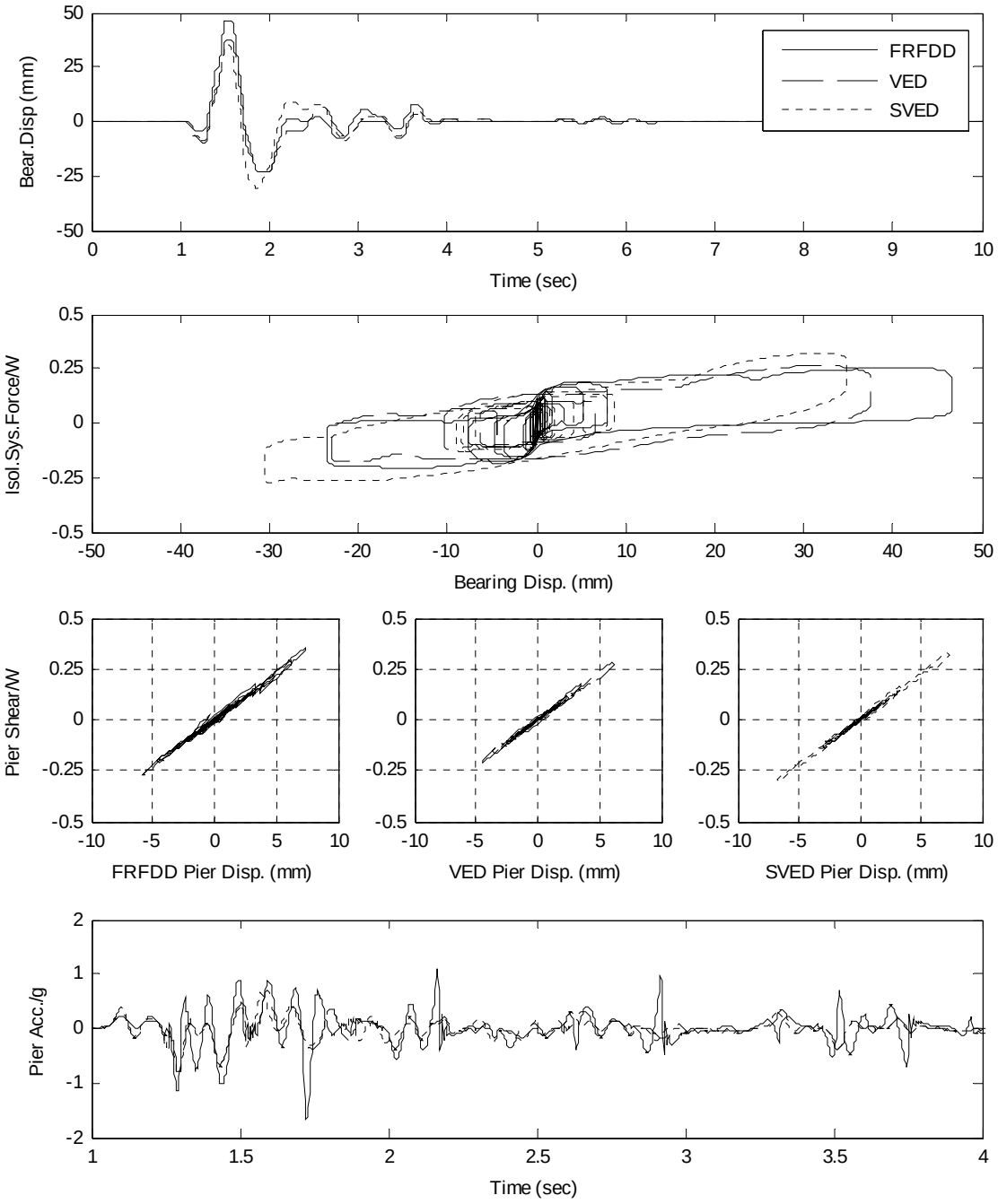

Figure (8-28) Comparison in response for isolation systems with FRFDD, VED, SVED subjected to 1986 Palm Springs USA earthquake, station NPS. Sliding bearings with low friction.

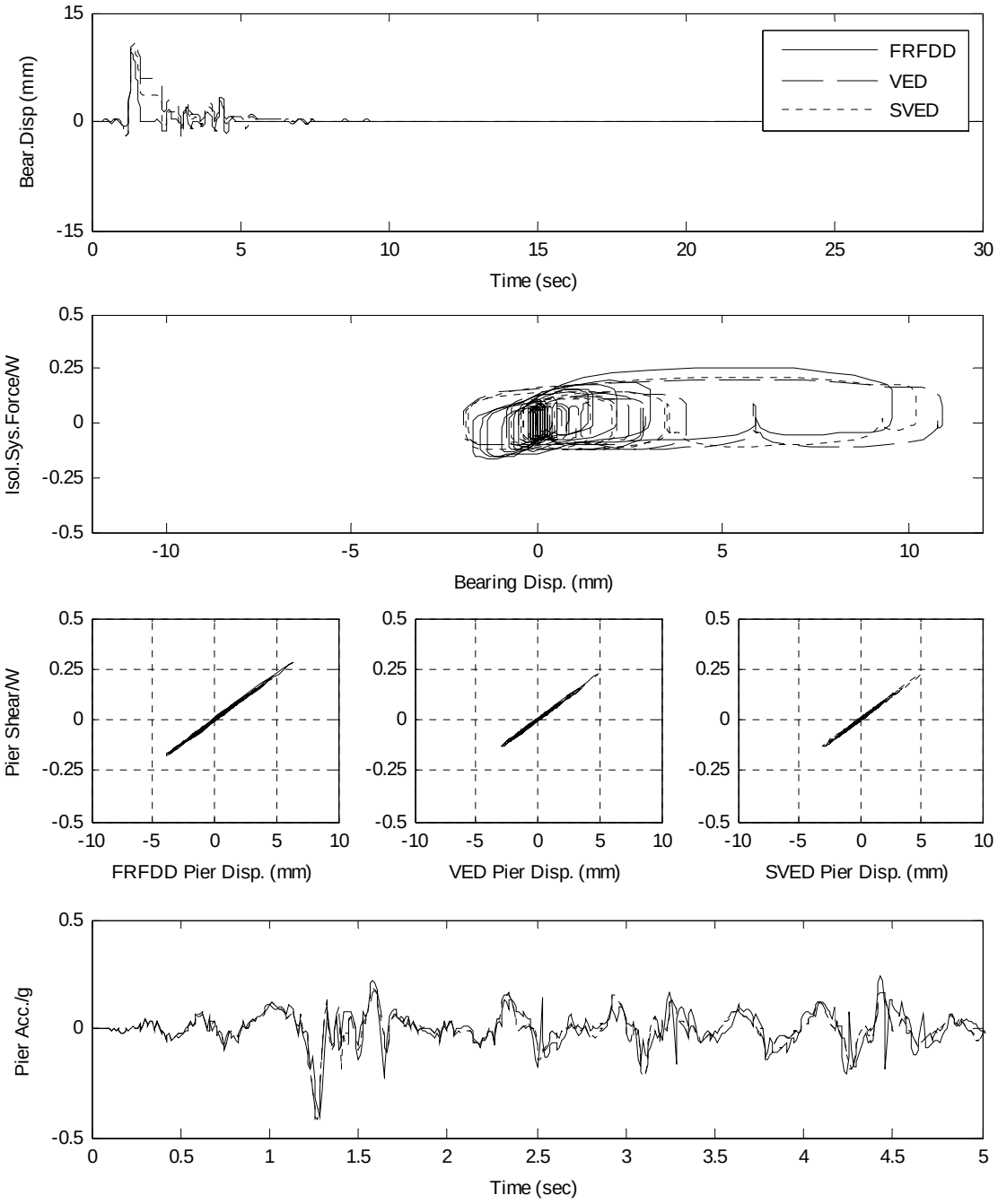

Figure (8-29) Comparison in response for isolation systems with FRFDD, VED, SVED subjected to 1986 Palm Springs USA earthquake, station DSP.

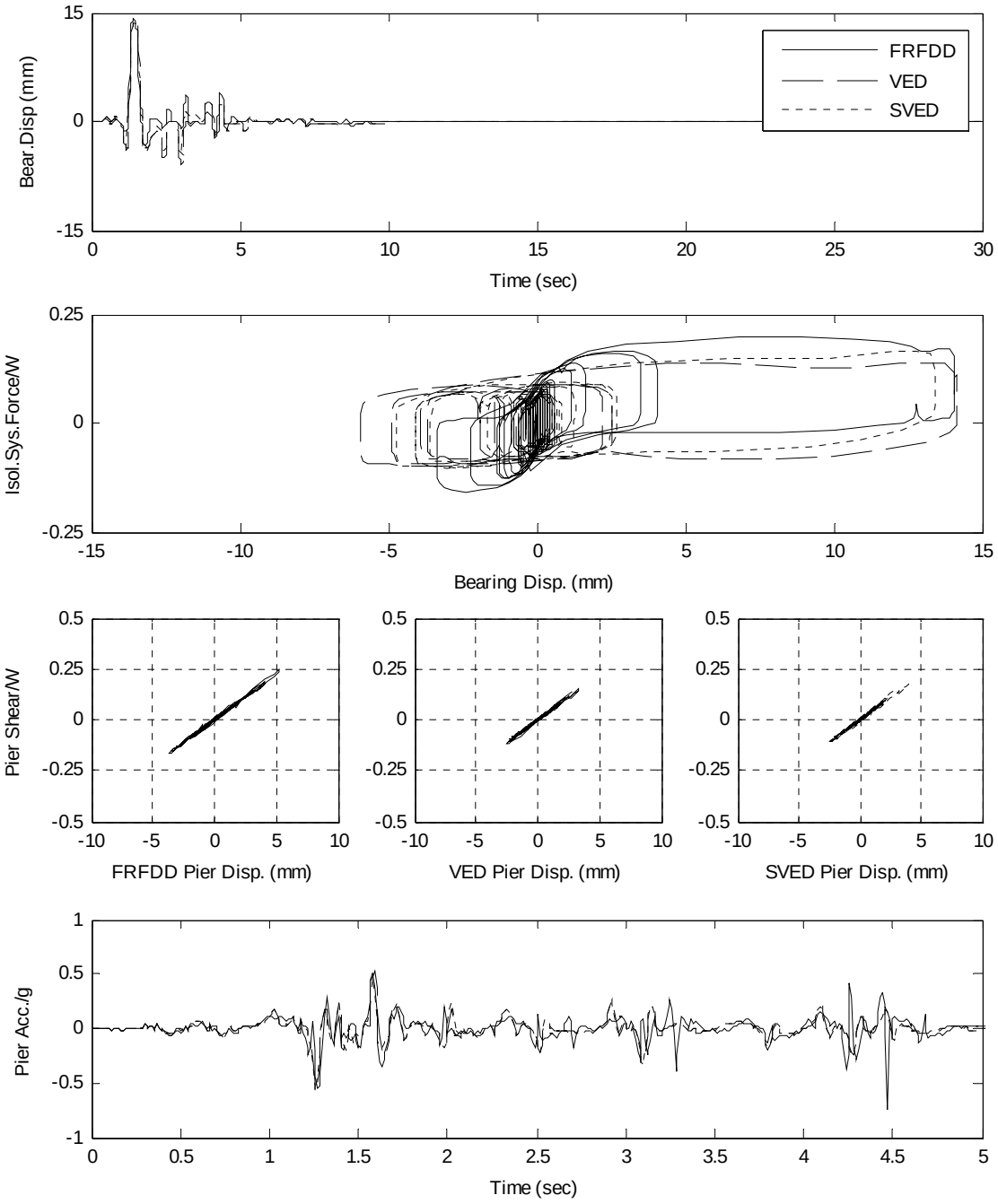

Figure (8-30) Comparison in response for isolation systems with FRFDD, VED, SVED subjected to 1986 Palm Springs USA earthquake, station DSP. Sliding bearings with low friction.

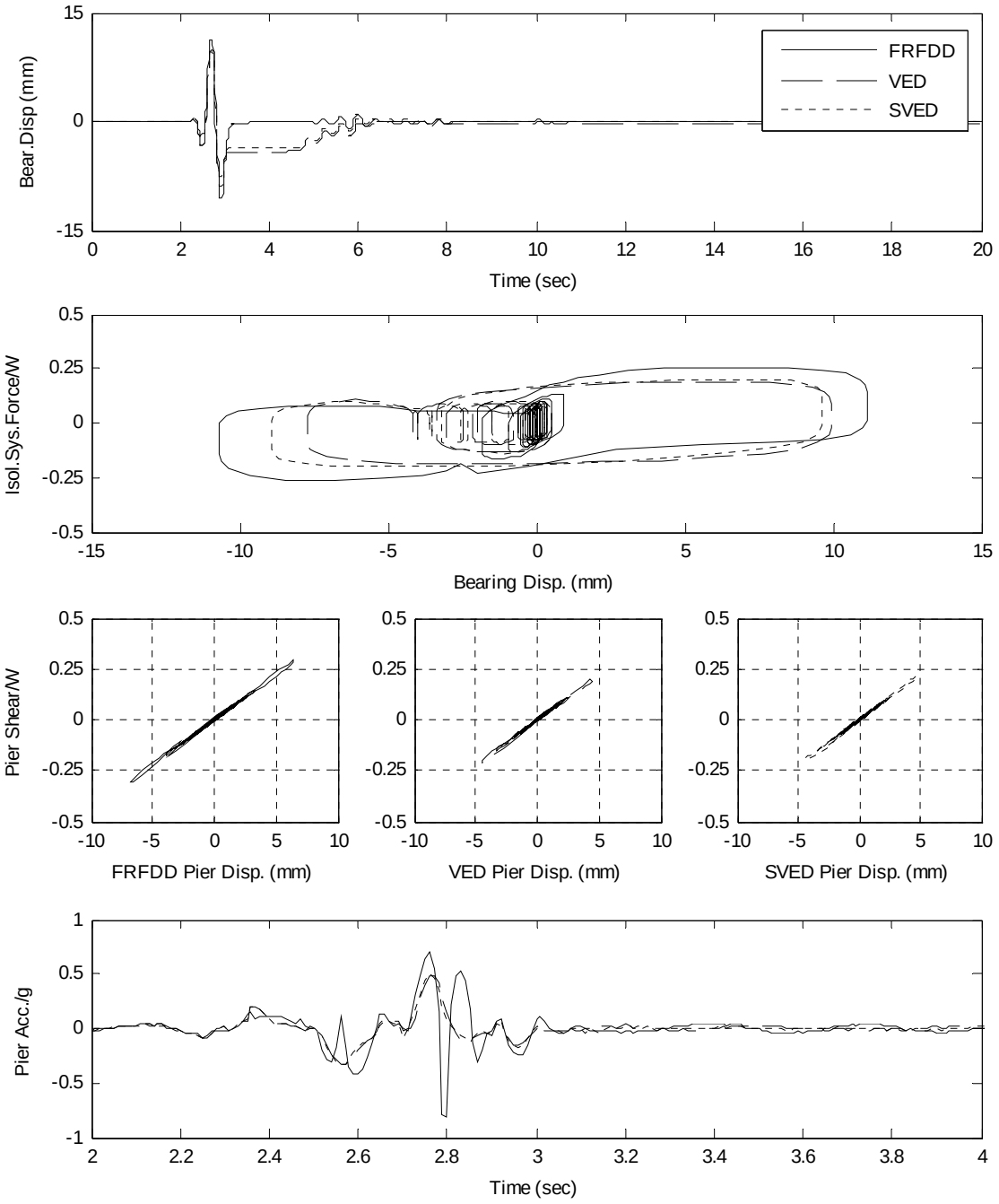

Figure (8-31) Comparison in response for isolation systems with FRFDD, VED, SVED subjected to 1987 Whittier Narrows USA earthquake, station DOW.

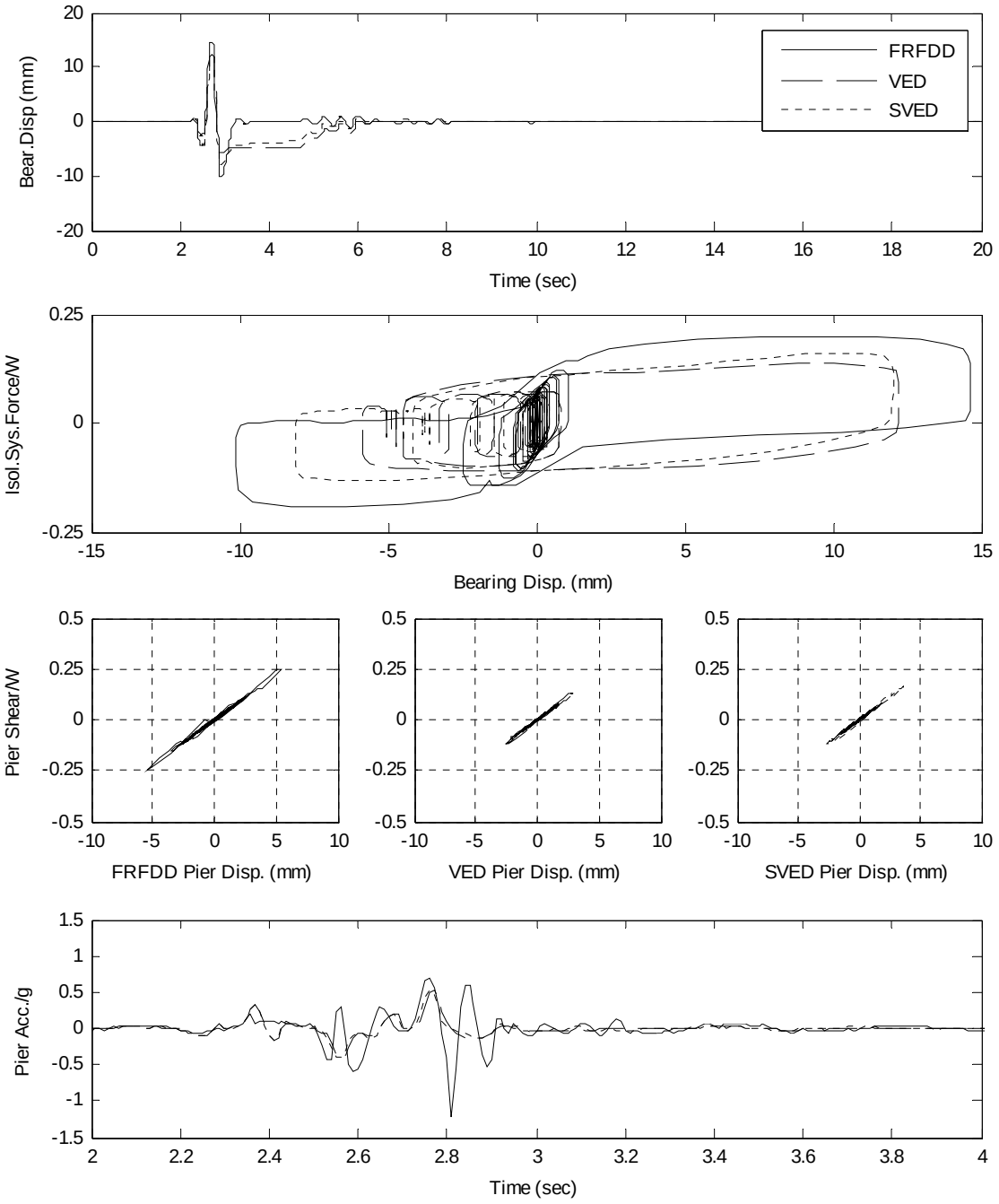

Figure (8-32) Comparison in response for isolation systems with FRFDD, VED, SVED subjected to 1987 Whittier Narrows USA earthquake, station DOW. Sliding bearings with low friction.

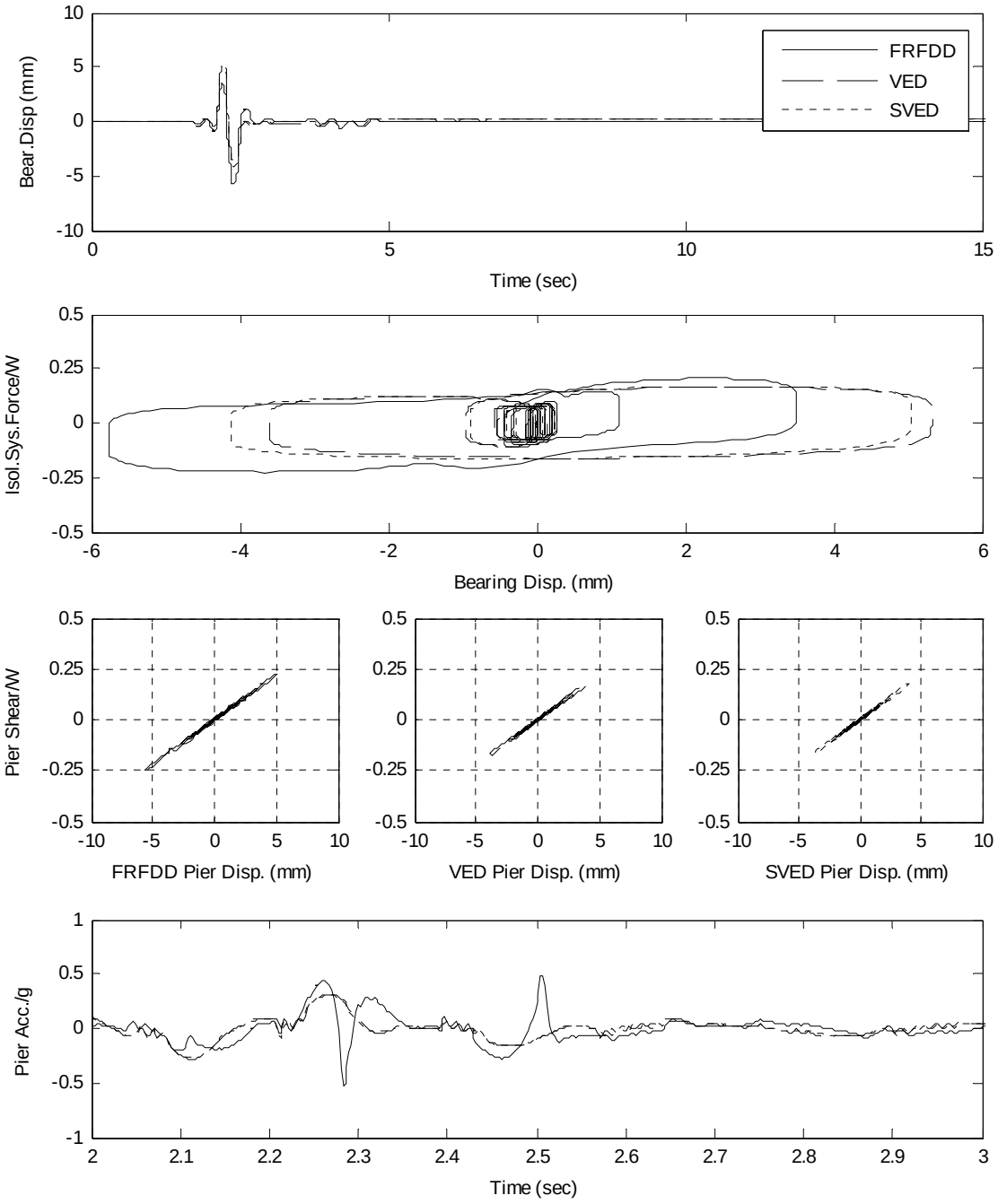

Figure (8-33)) Comparison in response for isolation systems with FRFDD, VED, SVED subjected to 1987 Whittier Narrows USA earthquake, station NWK.

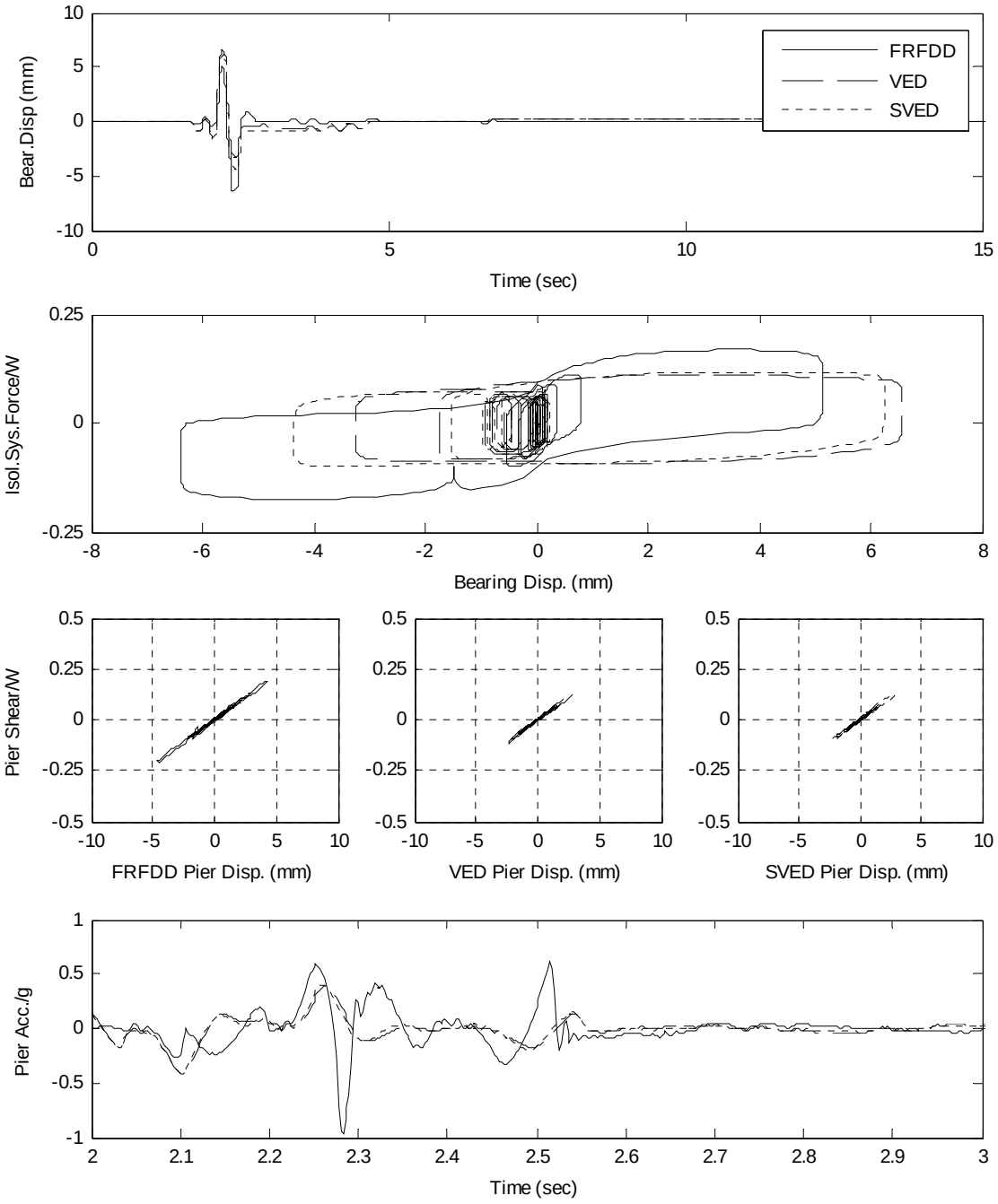

Figure (8-34) Comparison in response for isolation systems with FRFDD, VED, SVED subjected to 1987 Whittier Narrows USA earthquake, station NWK. Sliding bearing with low friction.

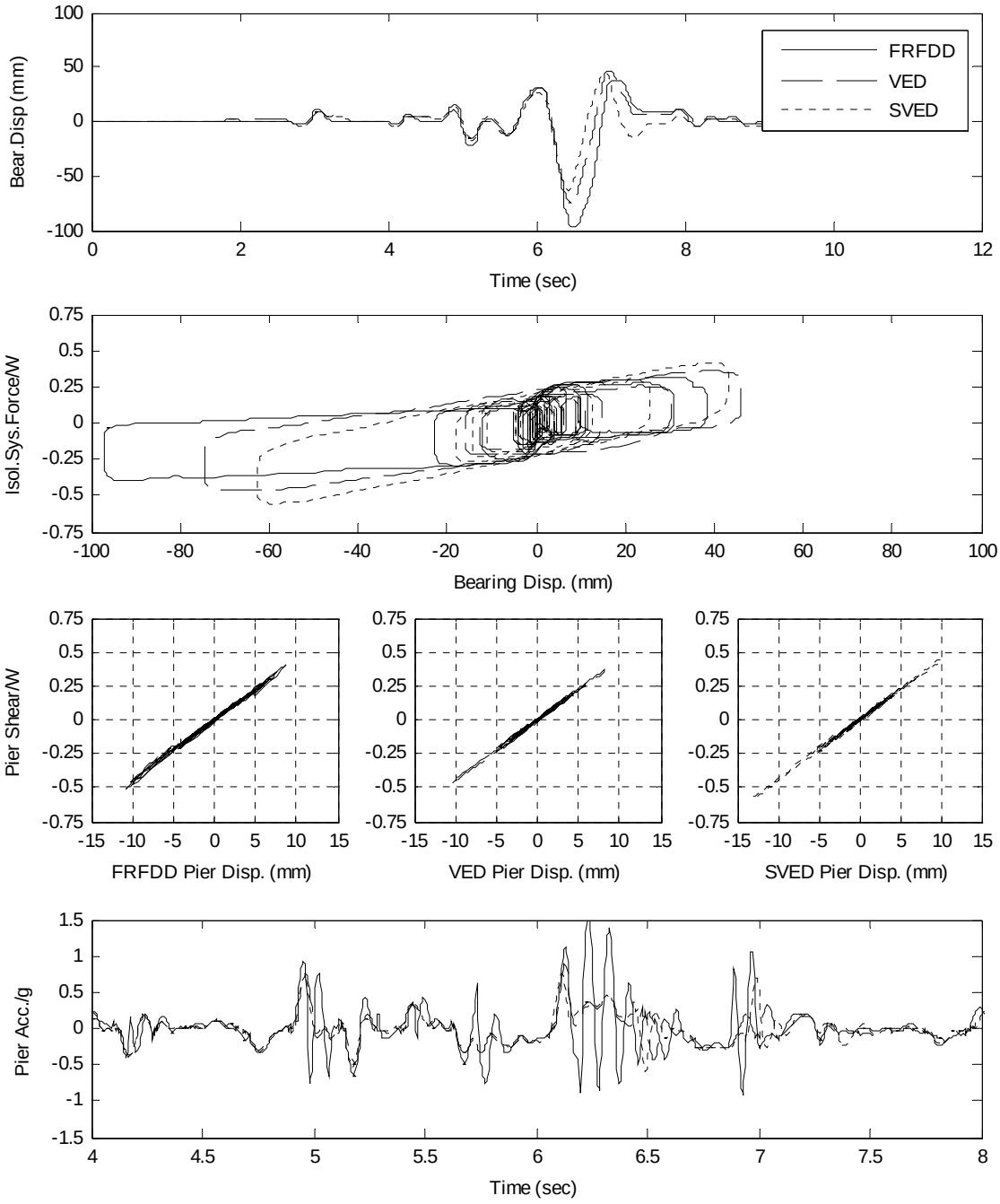

Figure (8-35) Comparison in response for isolation systems with FRFDD, VED, SVED subjected to 1987 Superstition Hills USA earthquake, station PTS.

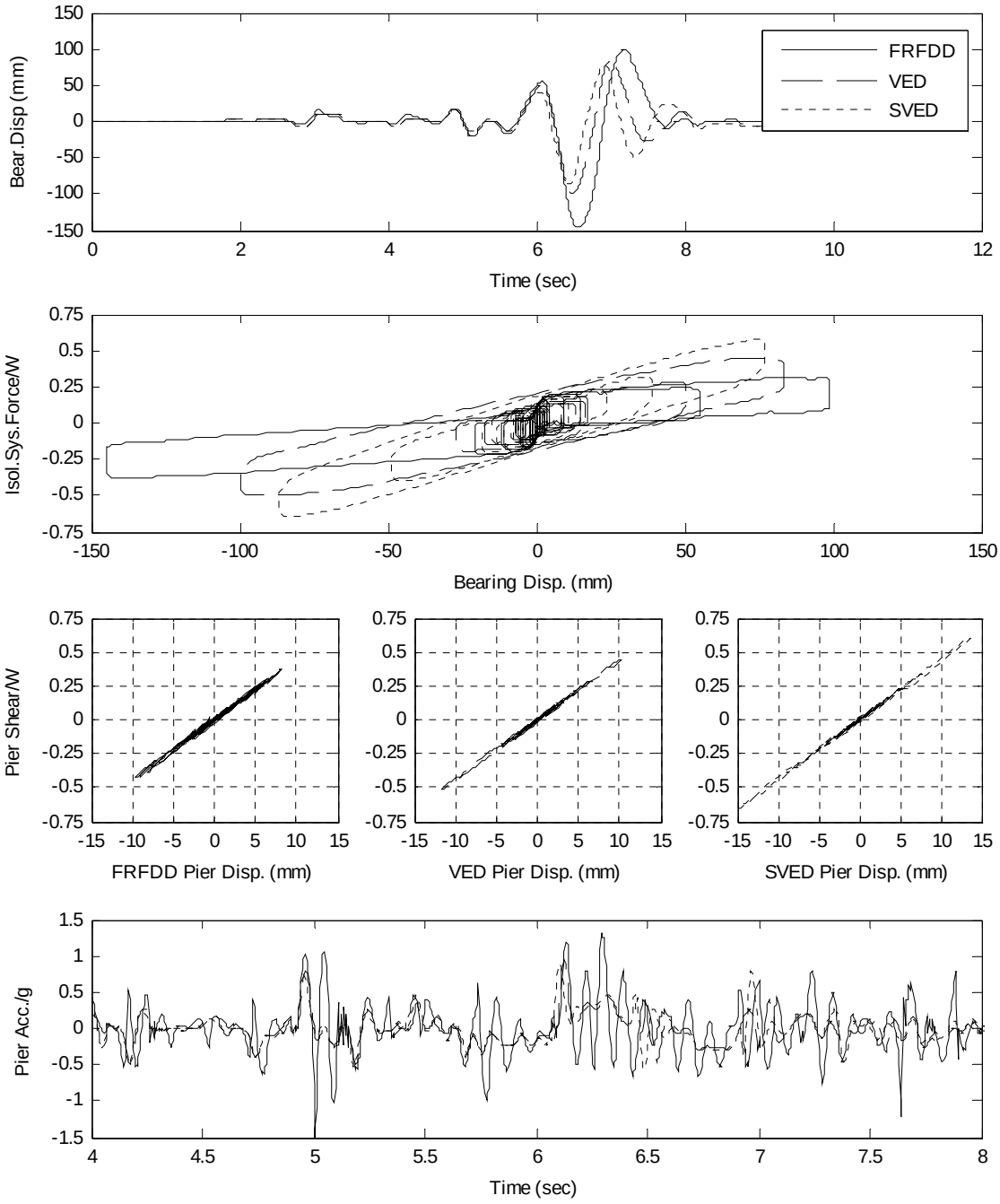

Figure (8-36) Comparison in response for isolation systems with FRFDD, VED, SVED subjected to 1987 Superstition Hills USA earthquake, station PTS. Sliding bearing with low friction.

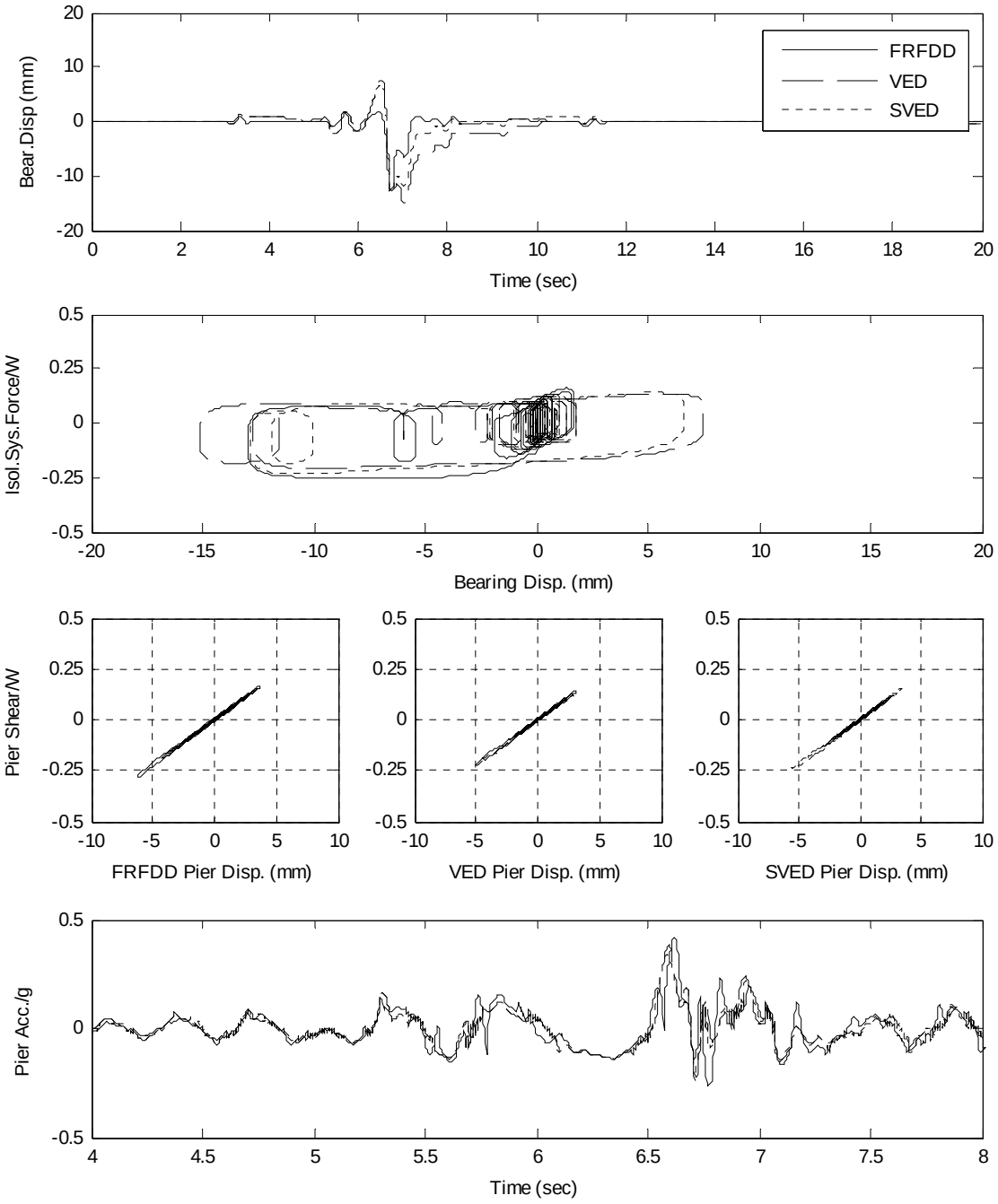

Figure (8-37) Comparison in response for isolation systems with FRFDD, VED, SVED subjected to 1987 Superstition Hills USA earthquake, station ELC.

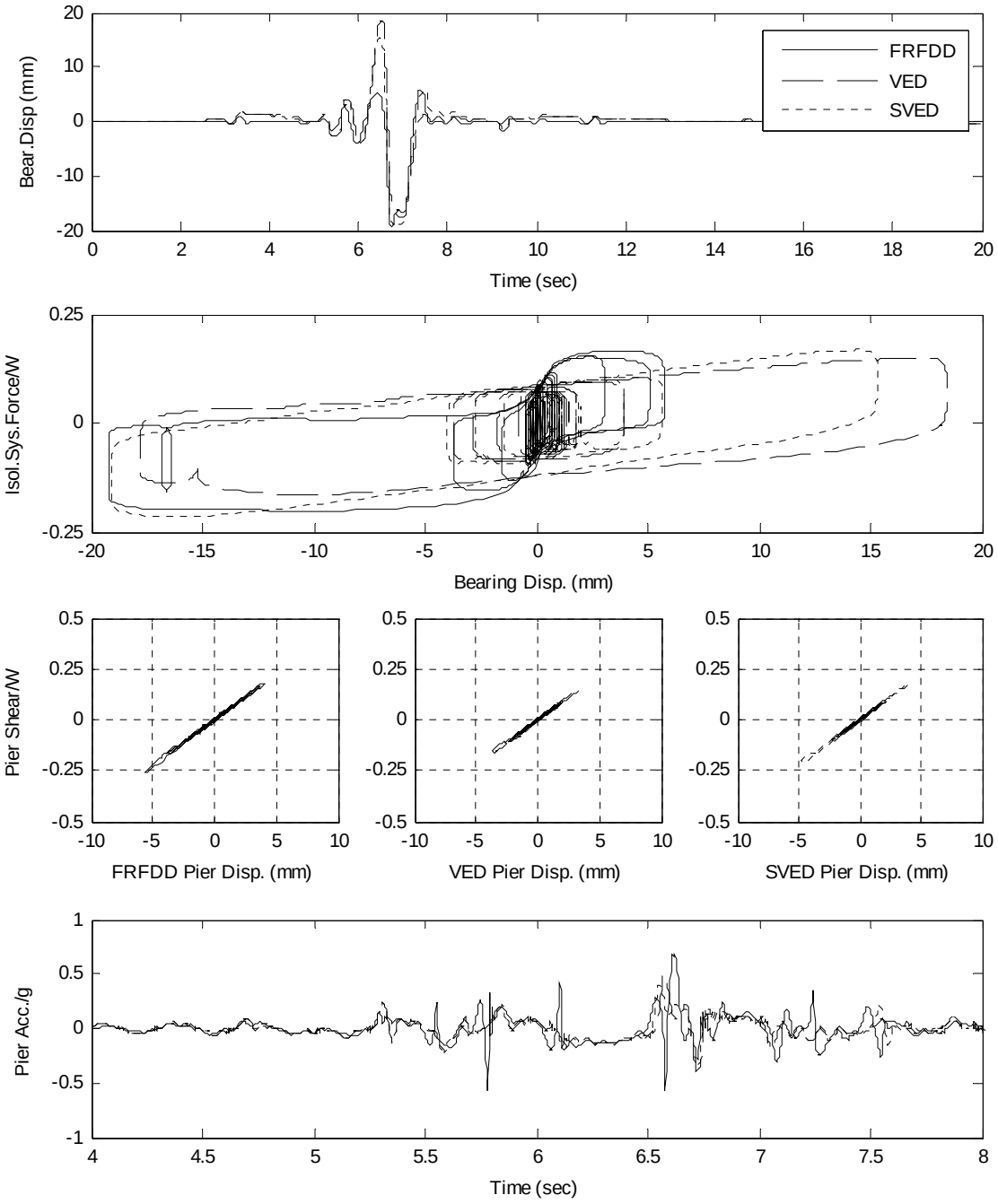

Figure (8-38) Comparison in response for isolation systems with FRFDD, VED, SVED subjected to 1987 Superstition Hills USA earthquake, station ELC. Sliding bearings with low friction.

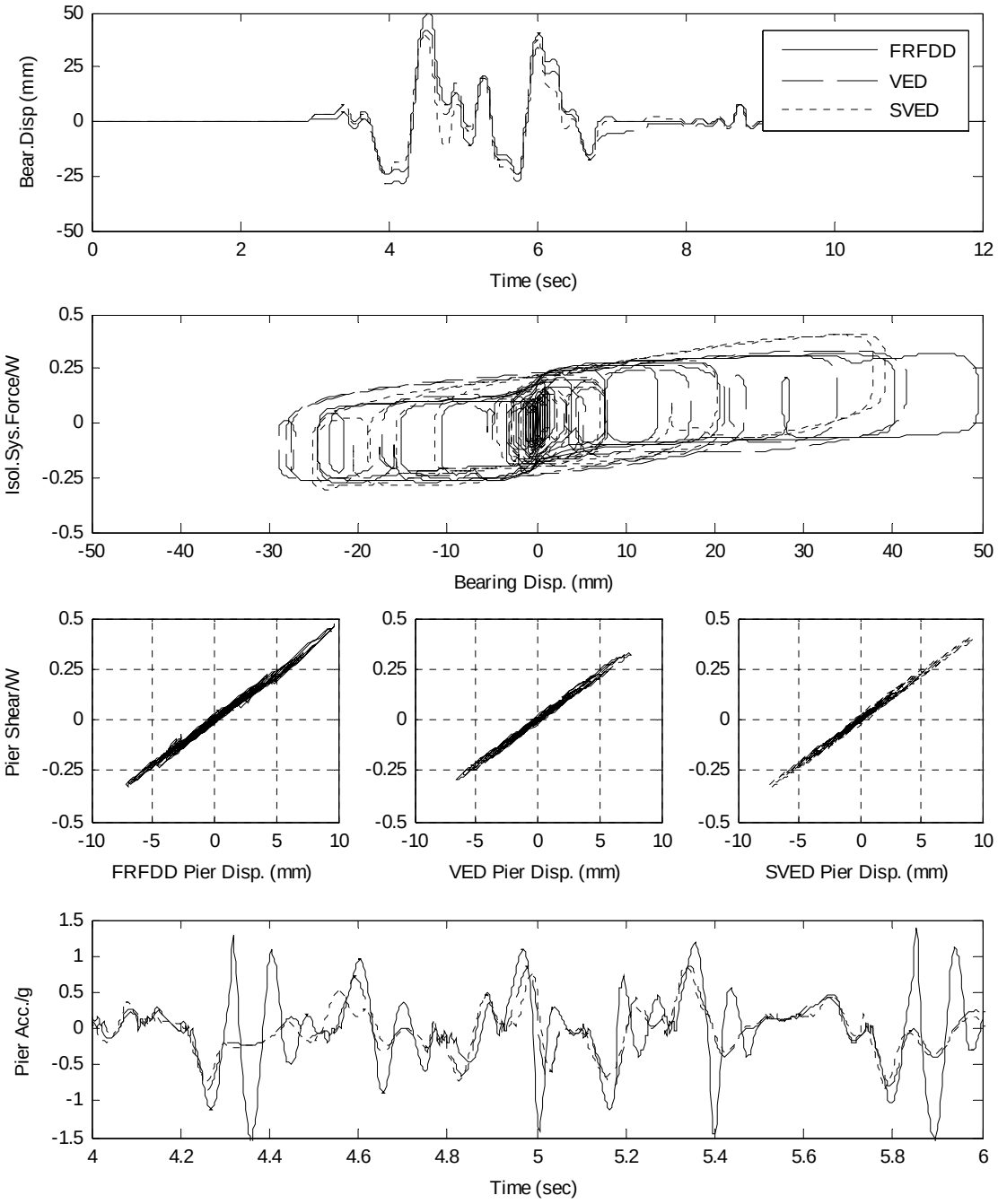

Figure (8-39) Comparison in response for isolation systems with FRFDD, VED, SVED subjected to 1989 Loma Prieta USA earthquake, station LGP.

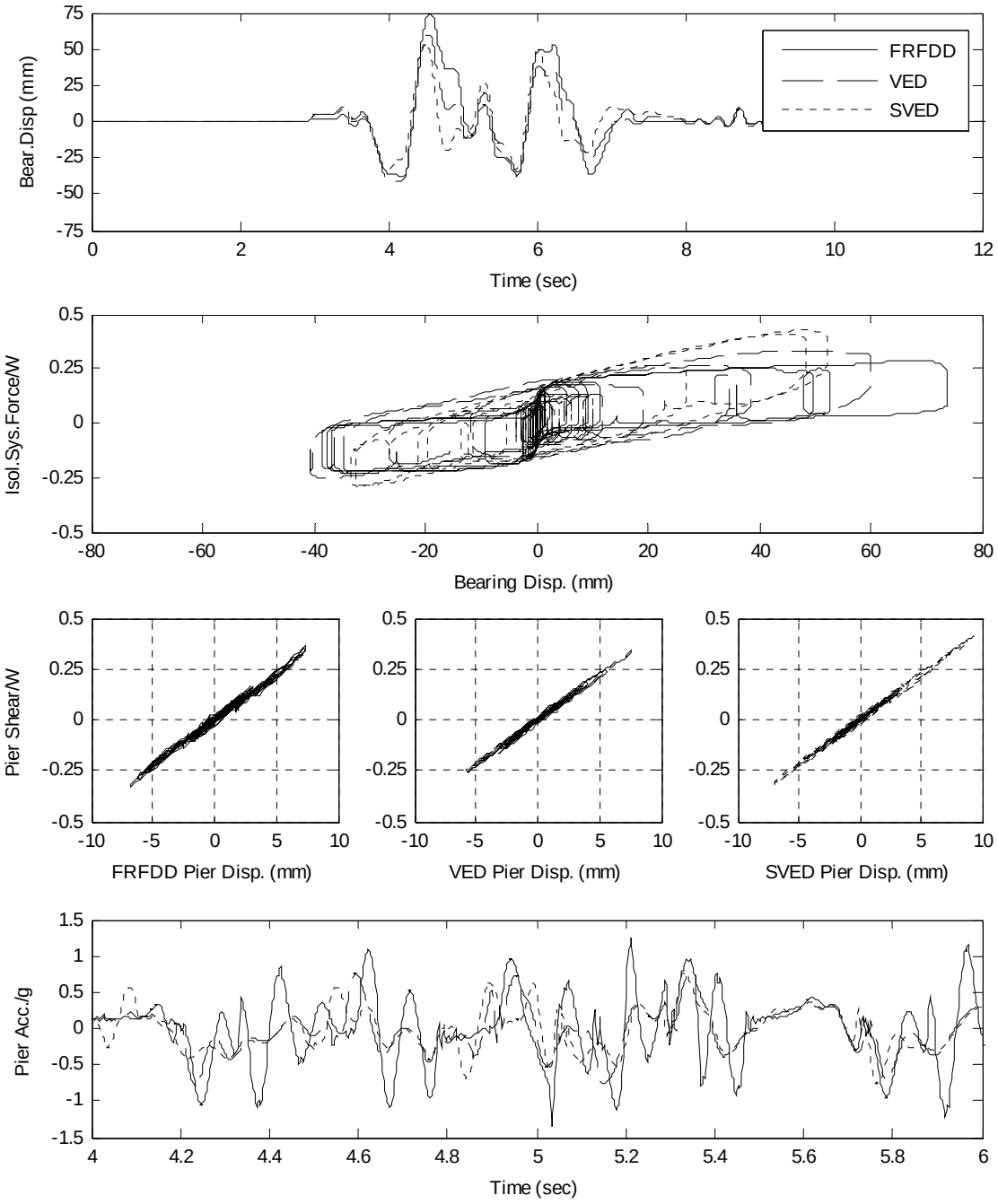

Figure (8-40) Comparison in response for isolation systems with FRFDD, VED, SVED subjected to 1989 Loma Prieta USA earthquake, station LGP. Sliding bearings with low friction.

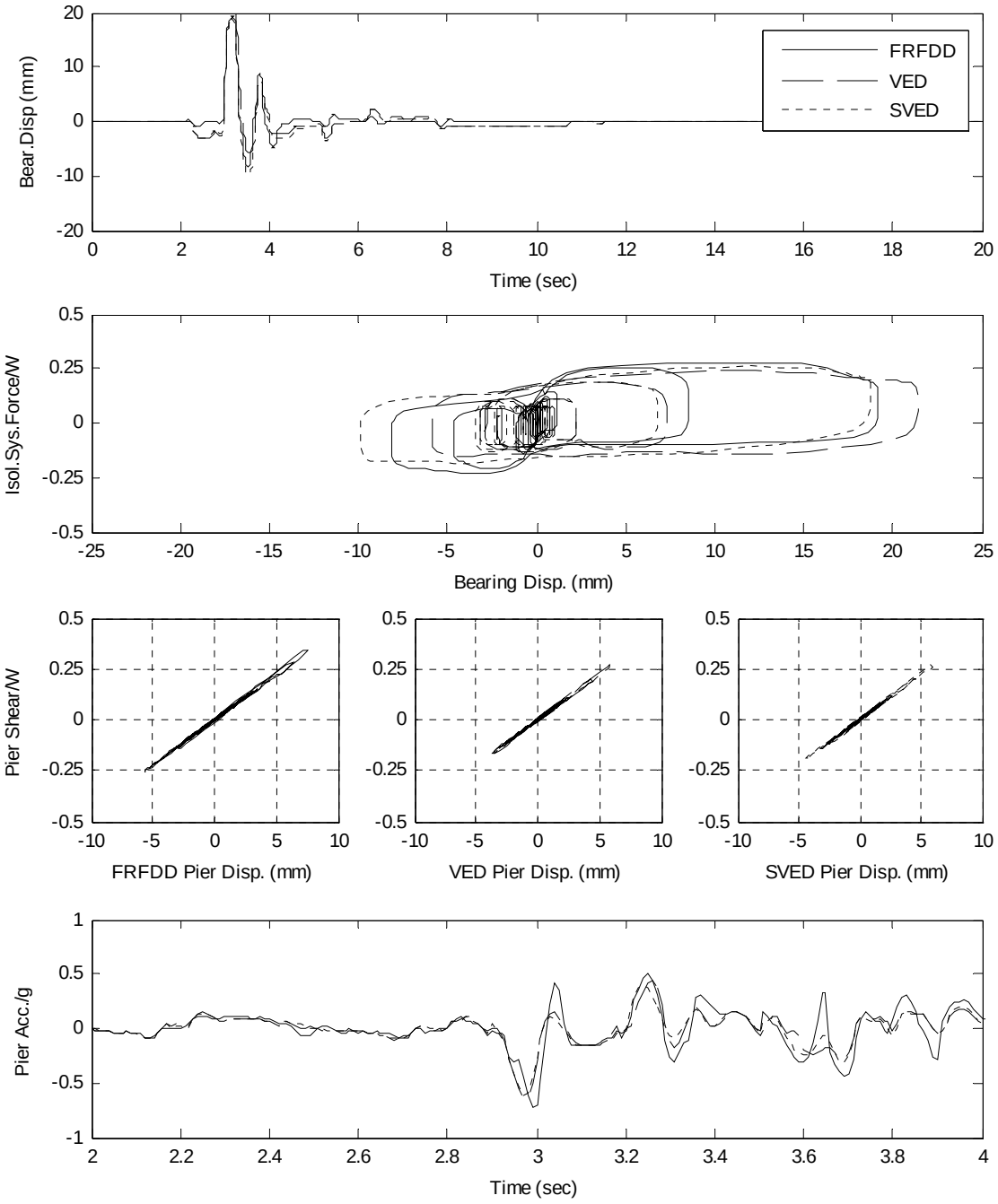

Figure (8-41) Comparison in response for isolation systems with FRFDD, VED, SVED subjected to 1989 Loma Prieta USA earthquake, station STG.

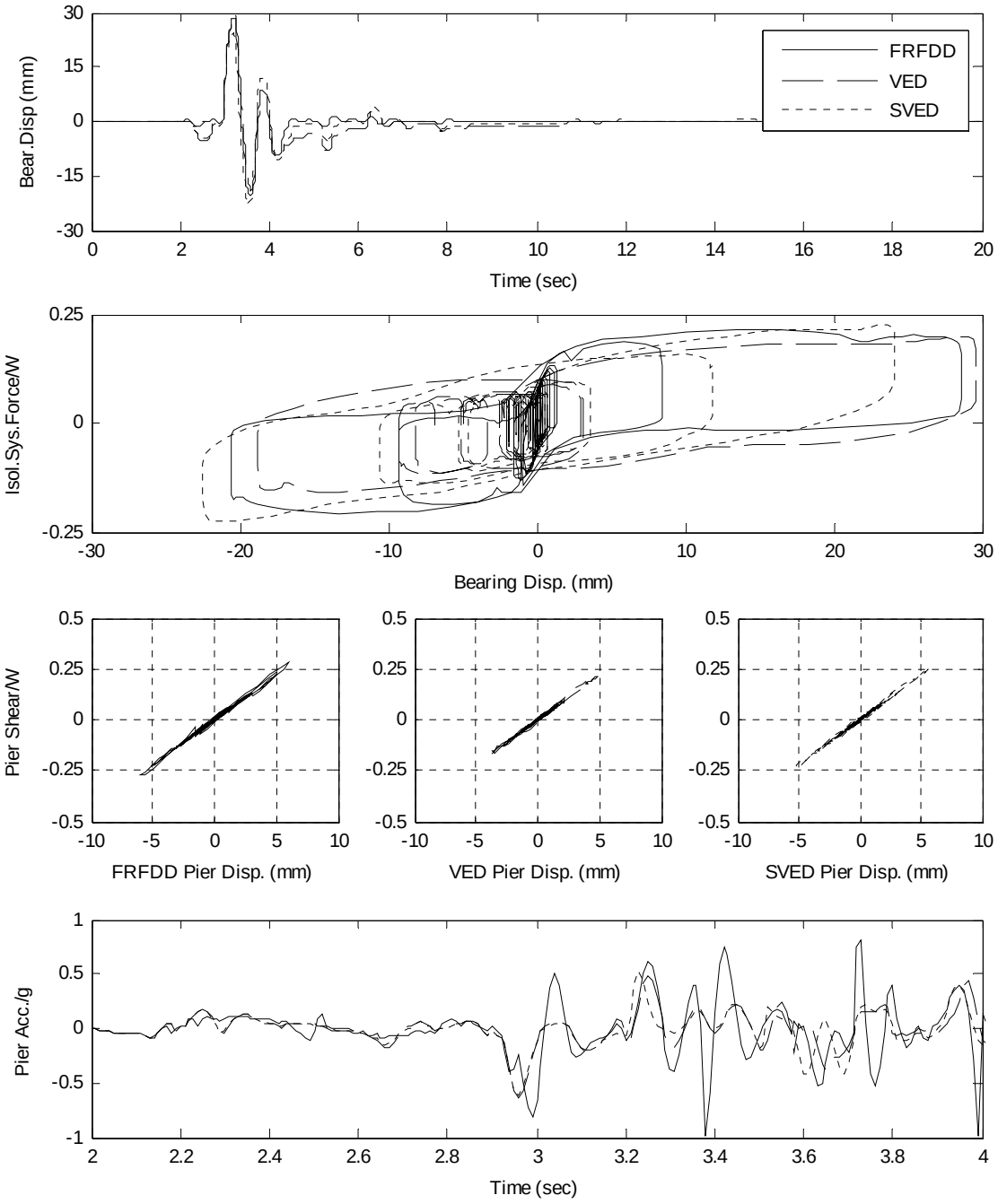

Figure (8-42) Comparison in response for isolation systems with FRFDD, VED, SVED subjected to 1989 Loma Prieta USA earthquake, station STG. Sliding bearings with low friction.

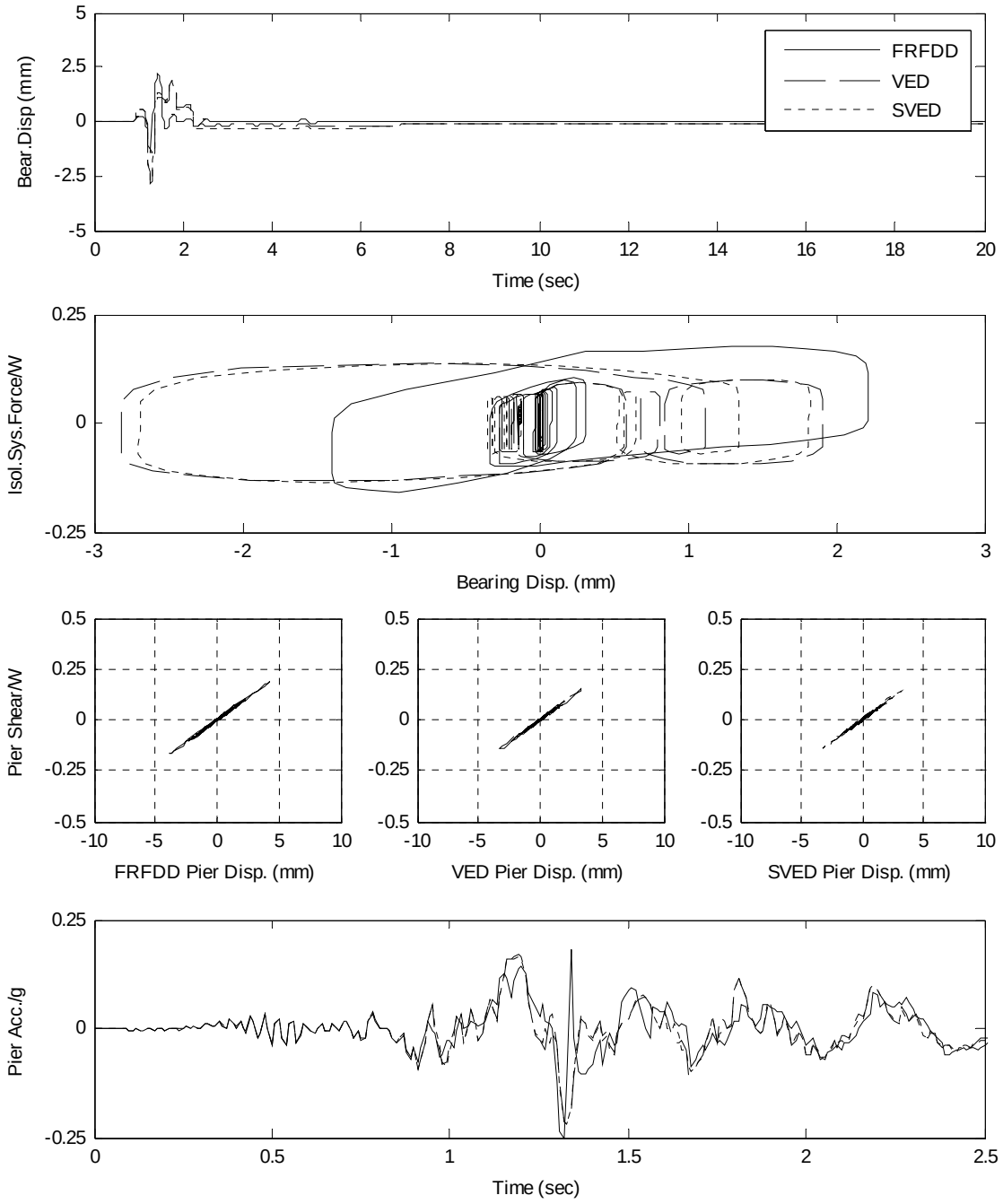

Figure (8-43) Comparison in response for isolation systems with FRFDD, VED, SVED subjected to 1991 Sierra Madre USA earthquake, station COG.

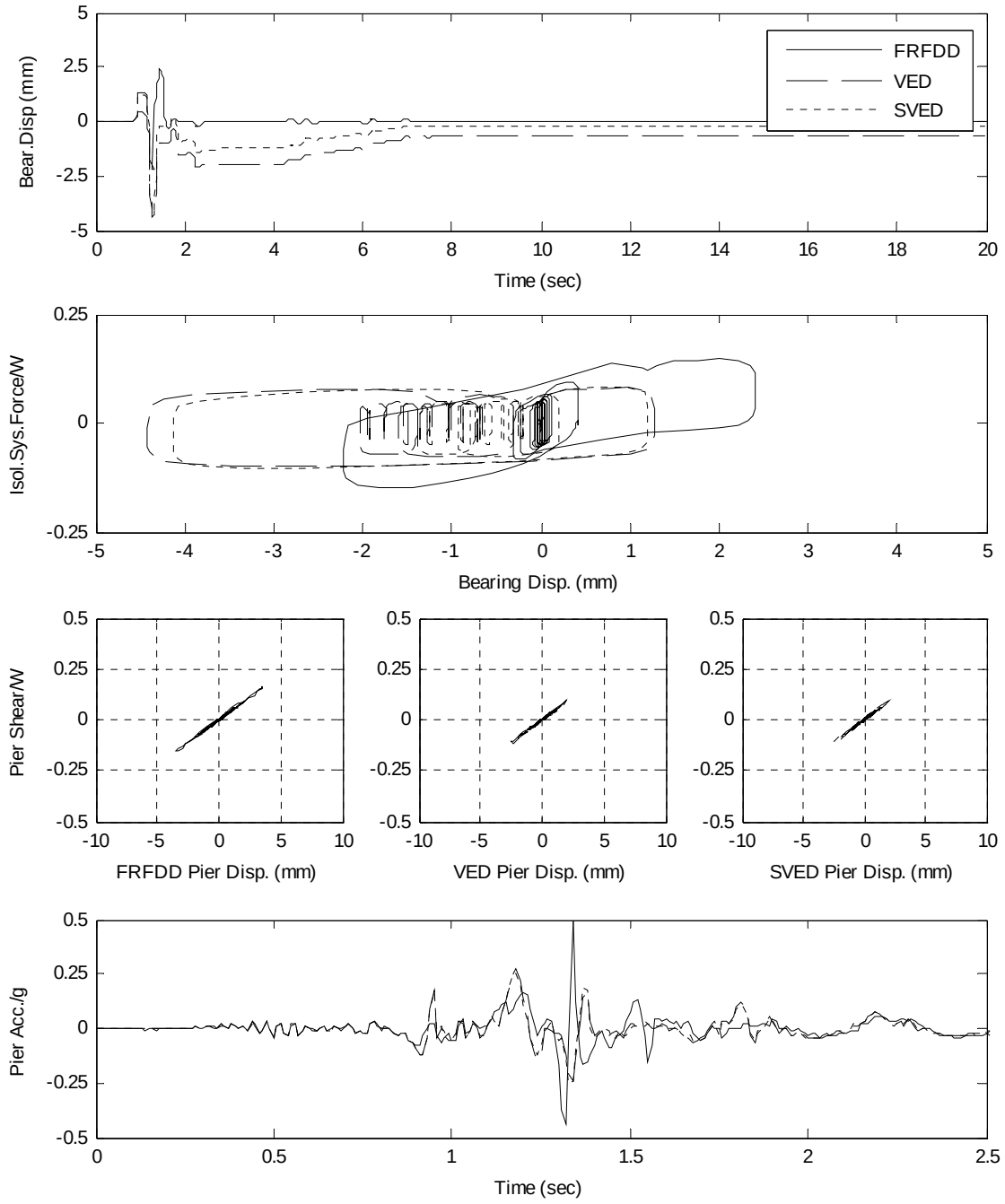

Figure (8-44) Comparison in response for isolation systems with FRFDD, VED, SVED subjected to 1991 Sierra Madre USA earthquake, station COG. Sliding bearing with low friction.

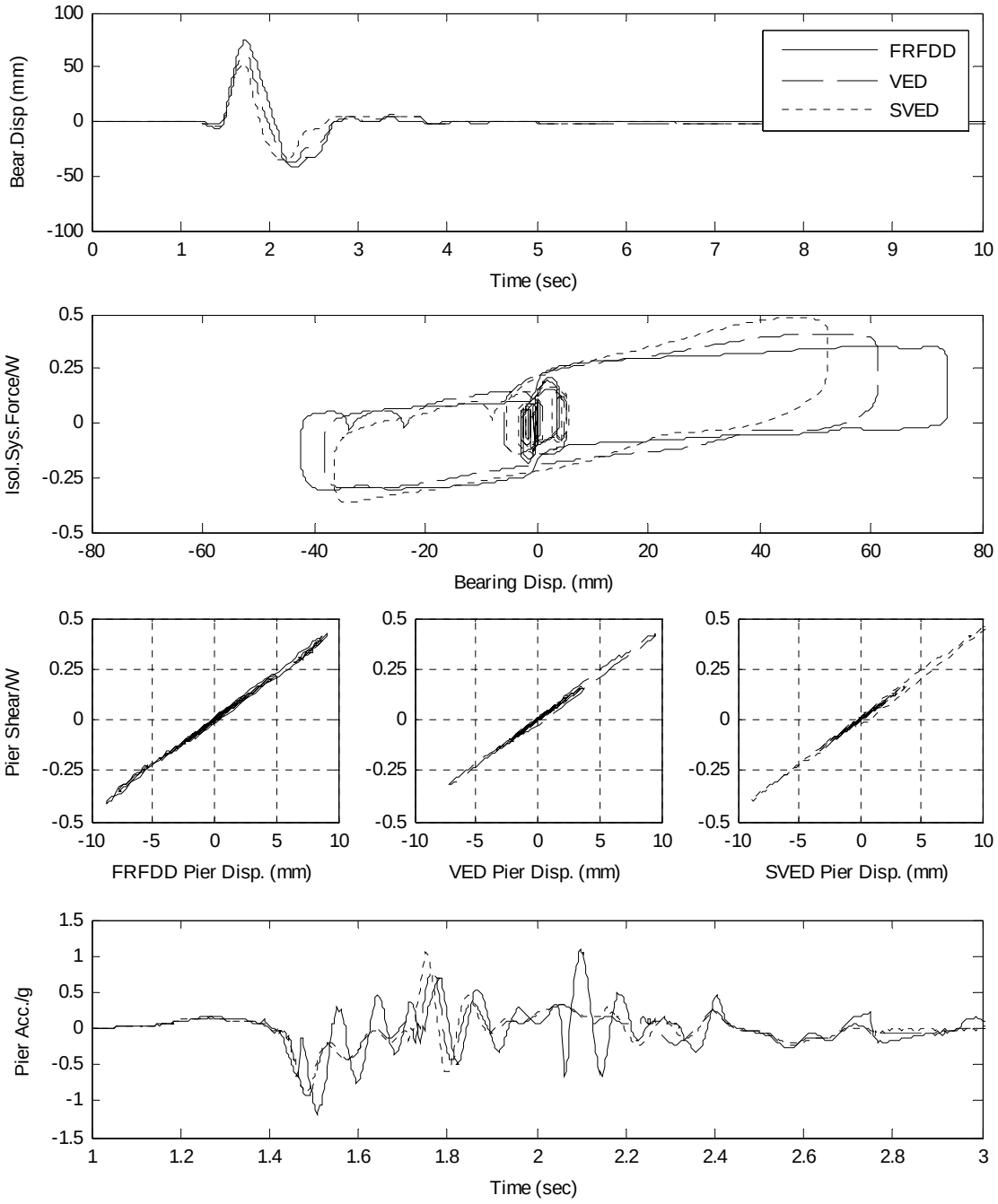

Figure (8-45) Comparison in response for isolation systems with FRFDD, VED, SVED subjected to 1992 Erzincan Turkey earthquake, station ERZ.

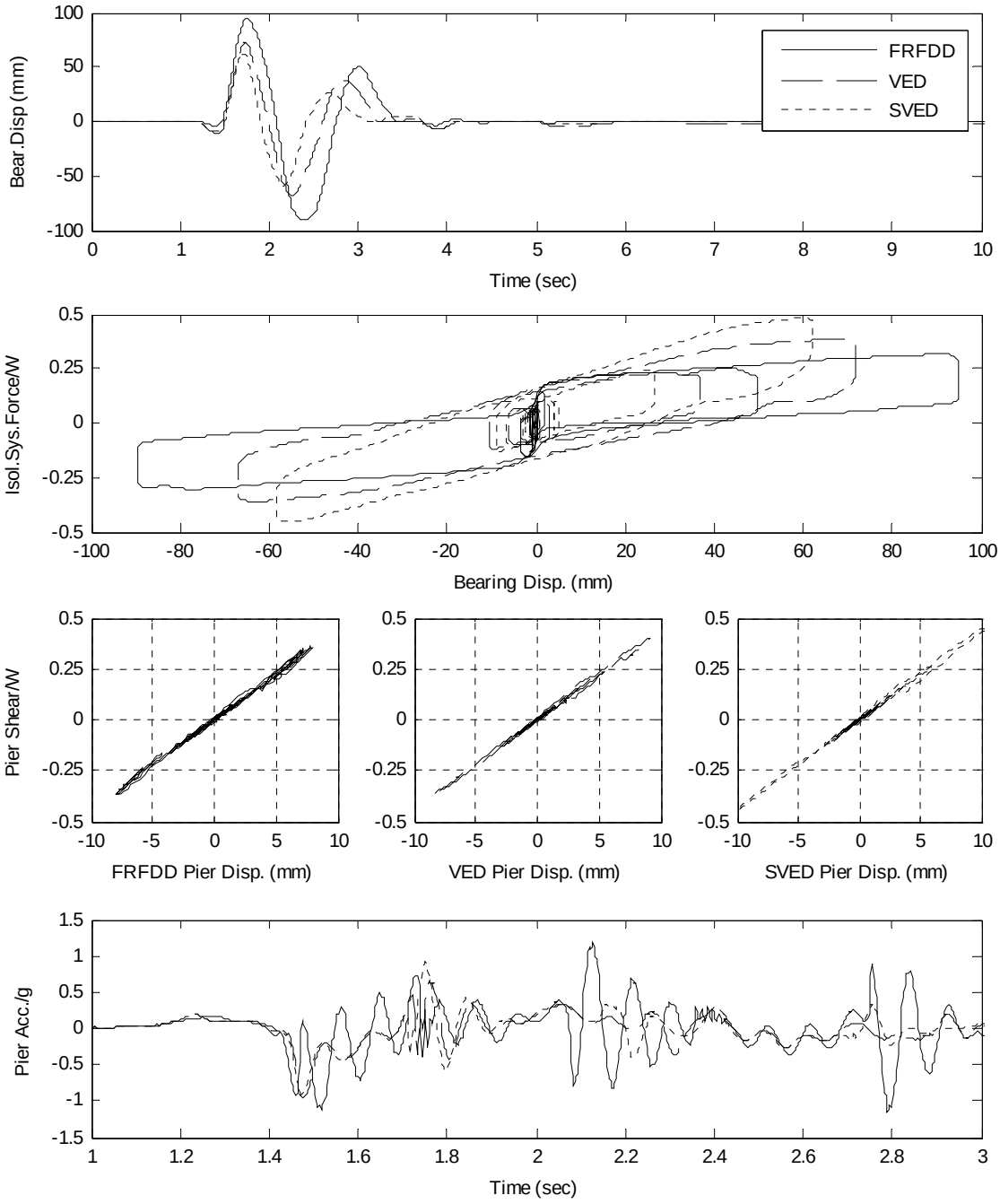

Figure (8-46) Comparison in response for isolation systems with FRFDD, VED, SVED subjected to 1992 Erzincan Turkey earthquake, station ERZ. Sliding bearings with low friction.

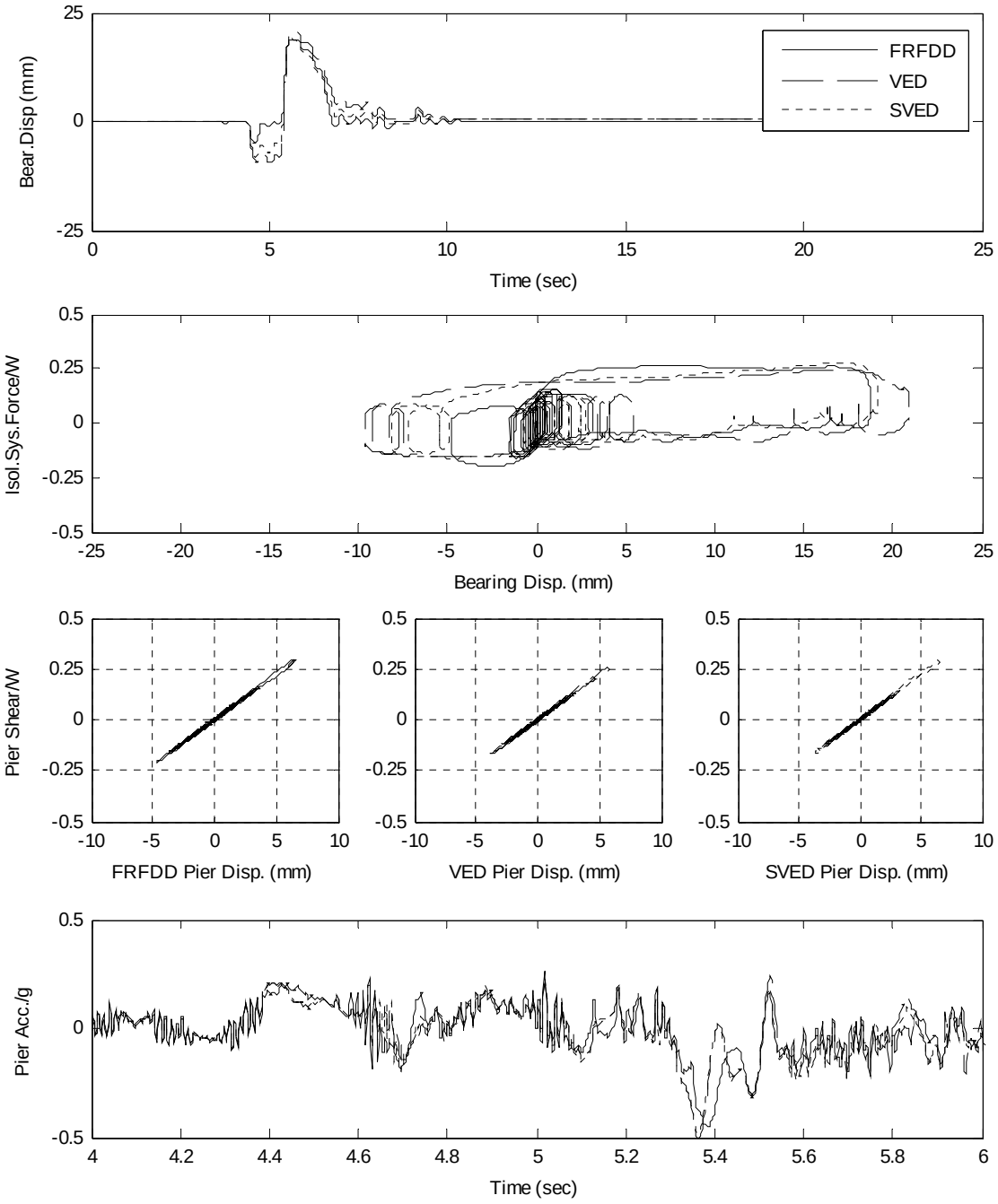

Figure (8-47) Comparison in response for isolation systems with FRFDD, VED, SVED subjected to 1992 Landers USA earthquake, station LUC.

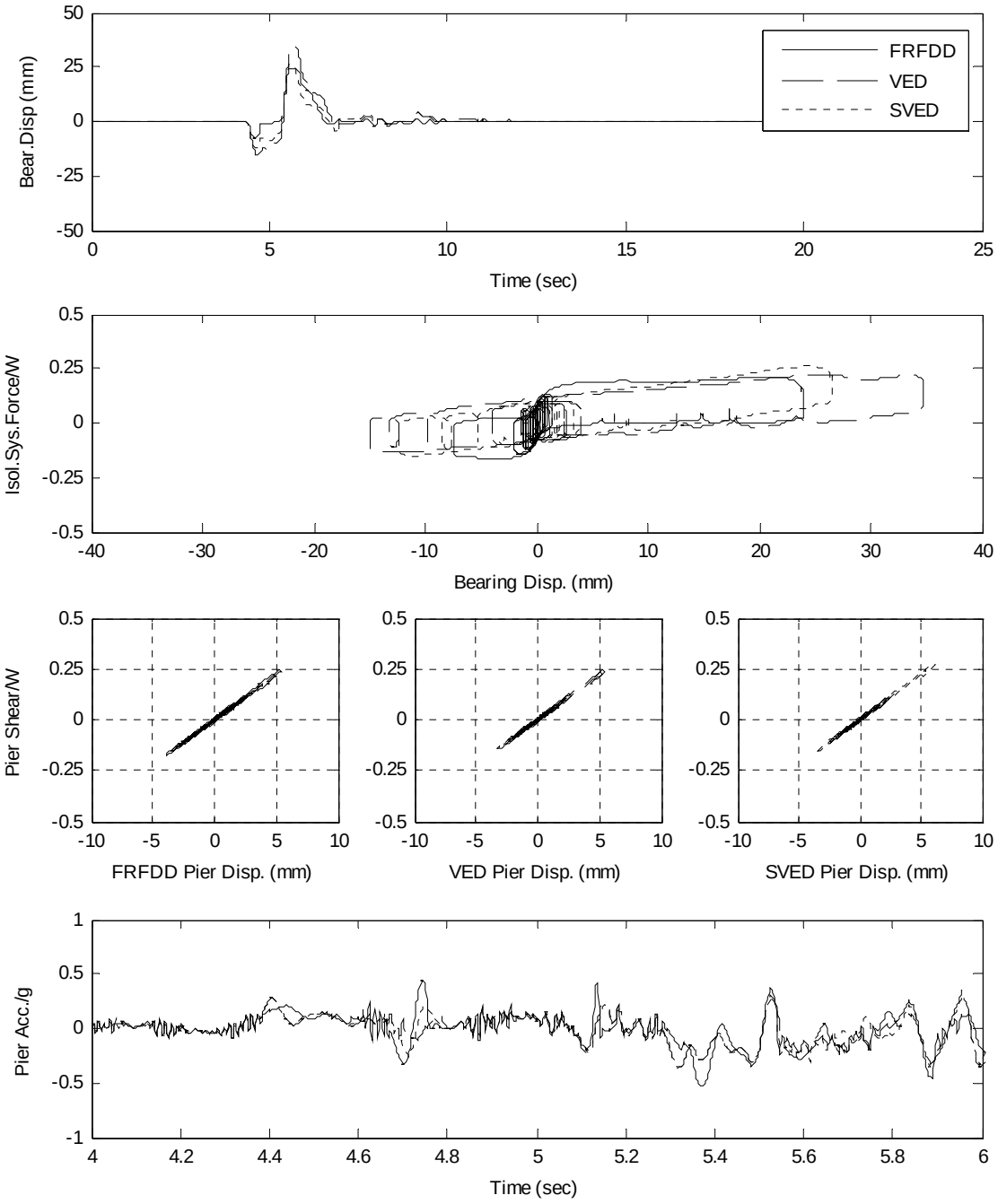

Figure (8-48) Comparison in response for isolation systems with FRFDD, VED, SVED subjected to 1992 Landers USA earthquake, station LUC. Sliding bearings with low friction.

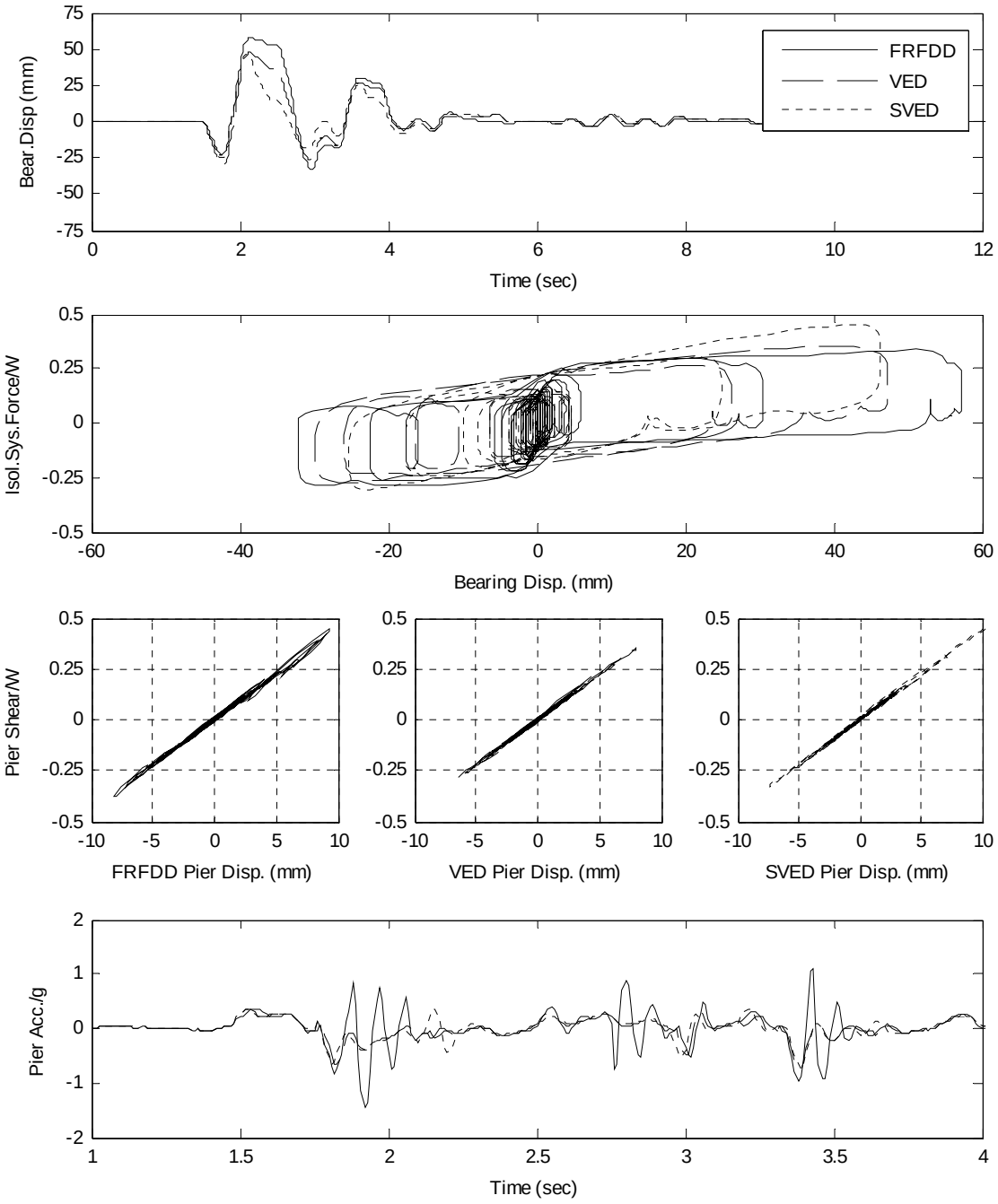

Figure (8-49) Comparison in response for isolation systems with FRFDD, VED, SVED subjected to 1994 Northridge USA earthquake, station JFA.

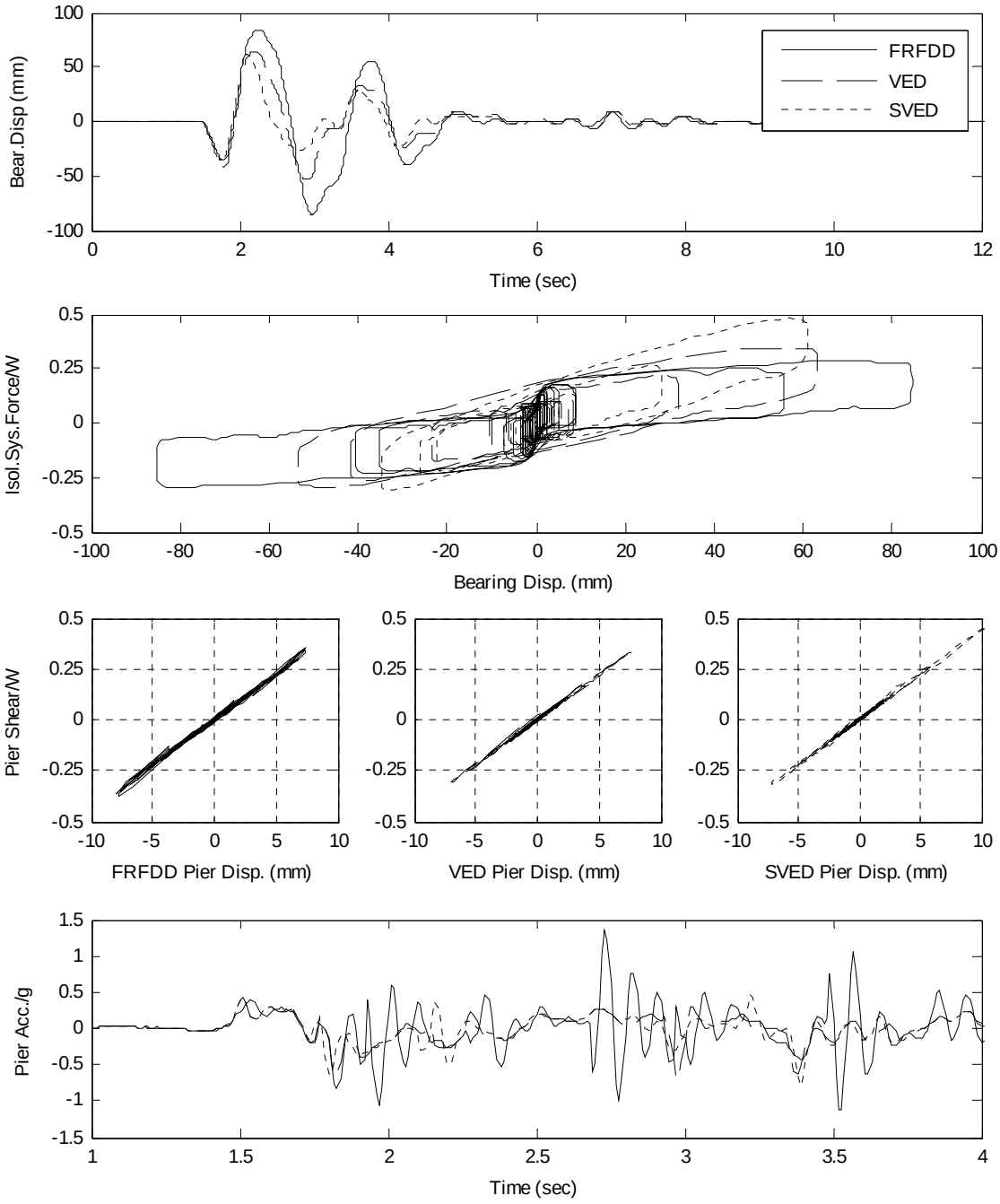

Figure (8-50) Comparison in response for isolation systems with FRFDD, VED, SVED subjected to 1994 Northridge USA earthquake, station JFA. Sliding bearings with low friction.

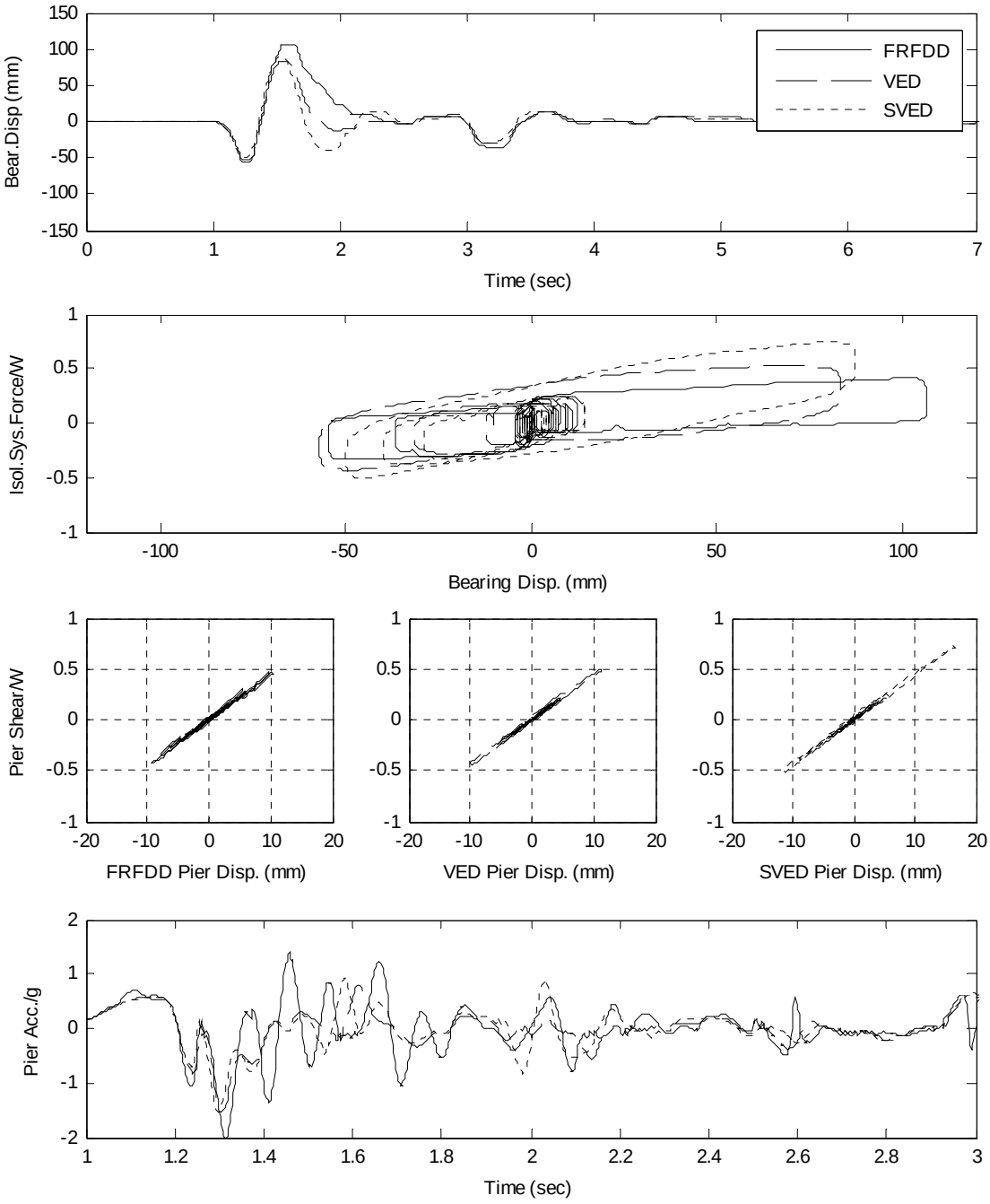

Figure (8-51) Comparison in response for isolation systems with FRFDD, VED, SVED subjected to 1994 Northridge USA earthquake, station RRS.

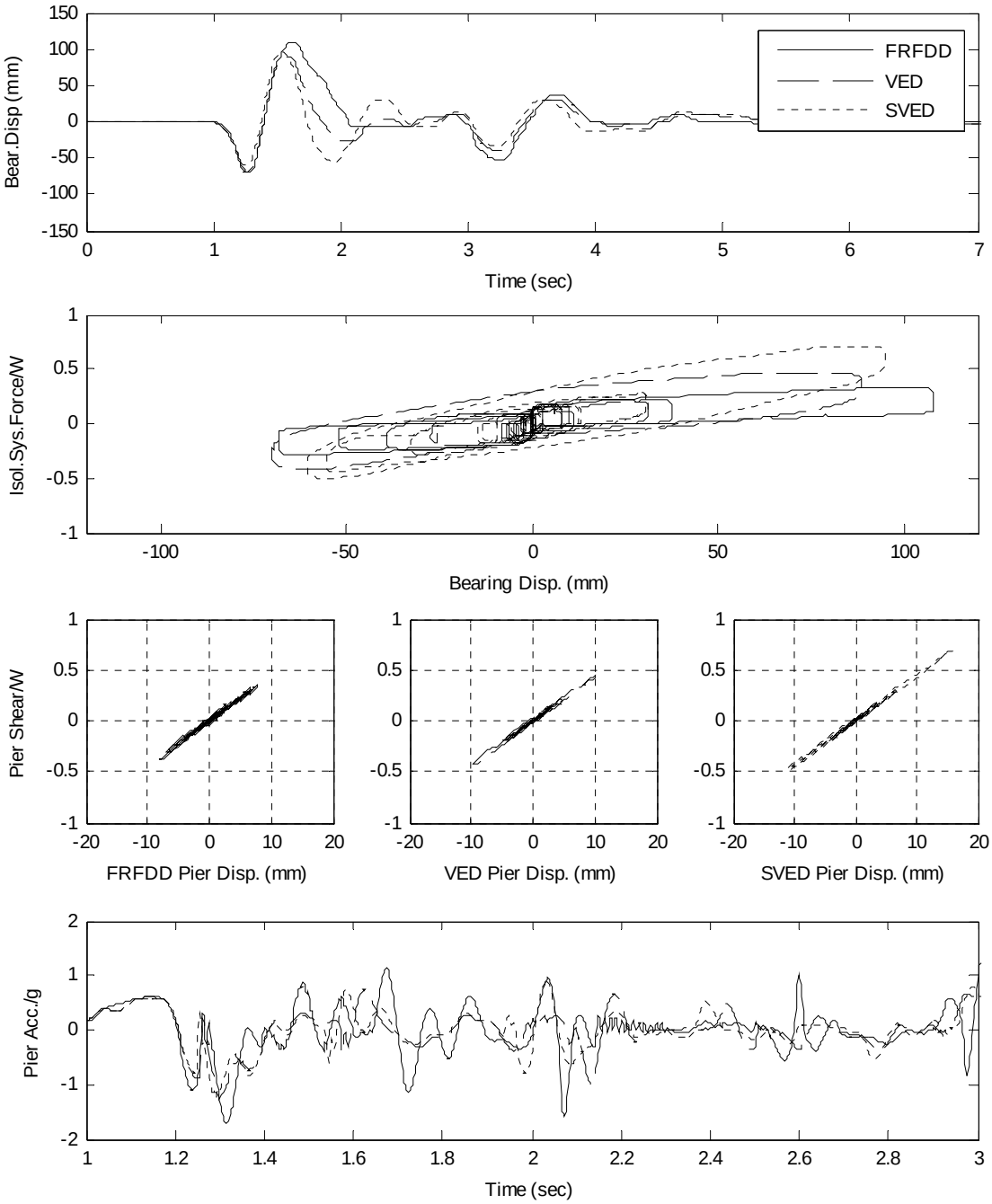

Figure (8-52) Comparison in response for isolation systems with FRFDD, VED, SVED subjected to 1994 Northridge USA earthquake, station RRS. Sliding bearings with low friction.

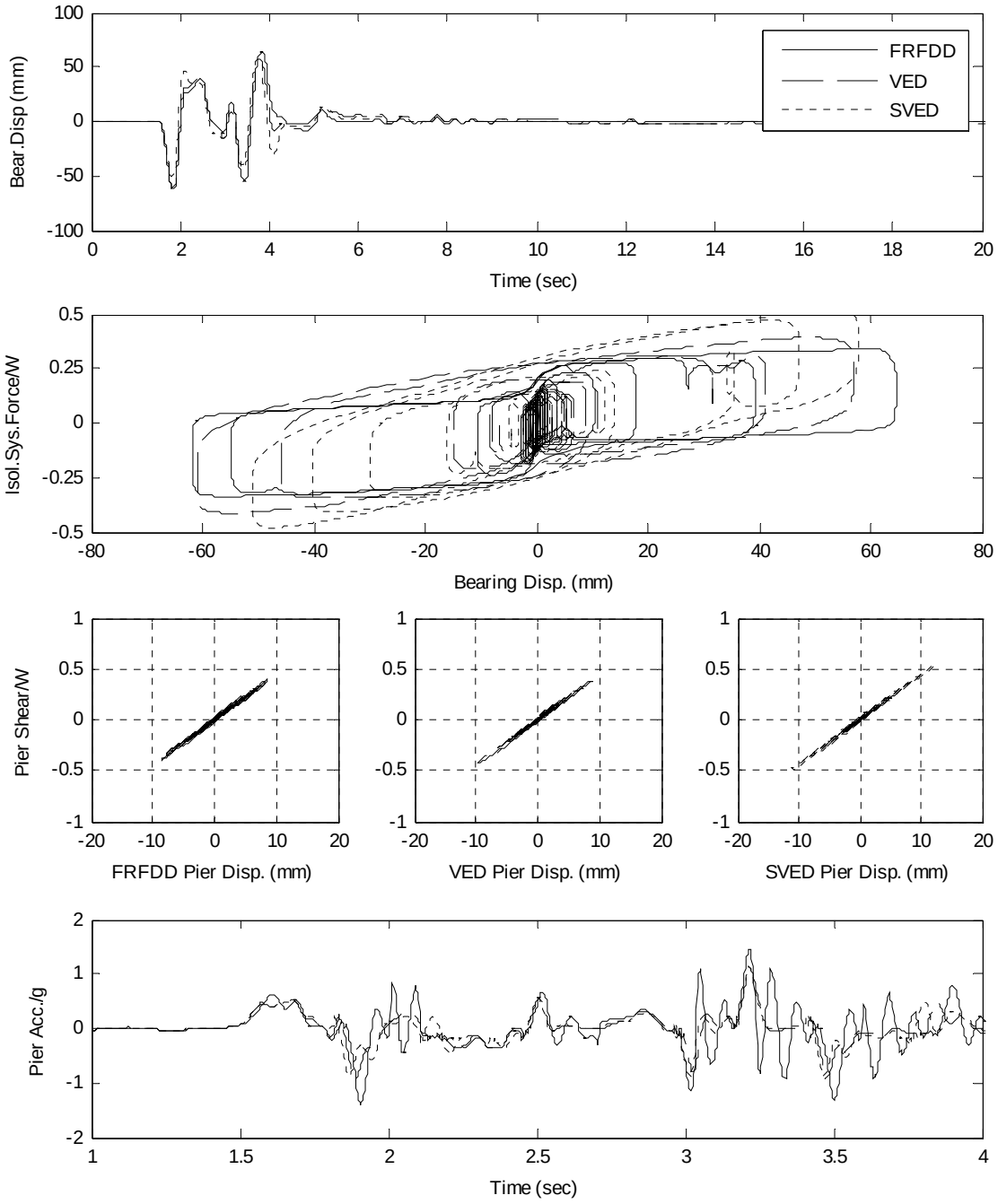

Figure (8-53) Comparison in response for isolation systems with FRFDD, VED, SVED subjected to 1994 Northridge USA earthquake, station SCG.

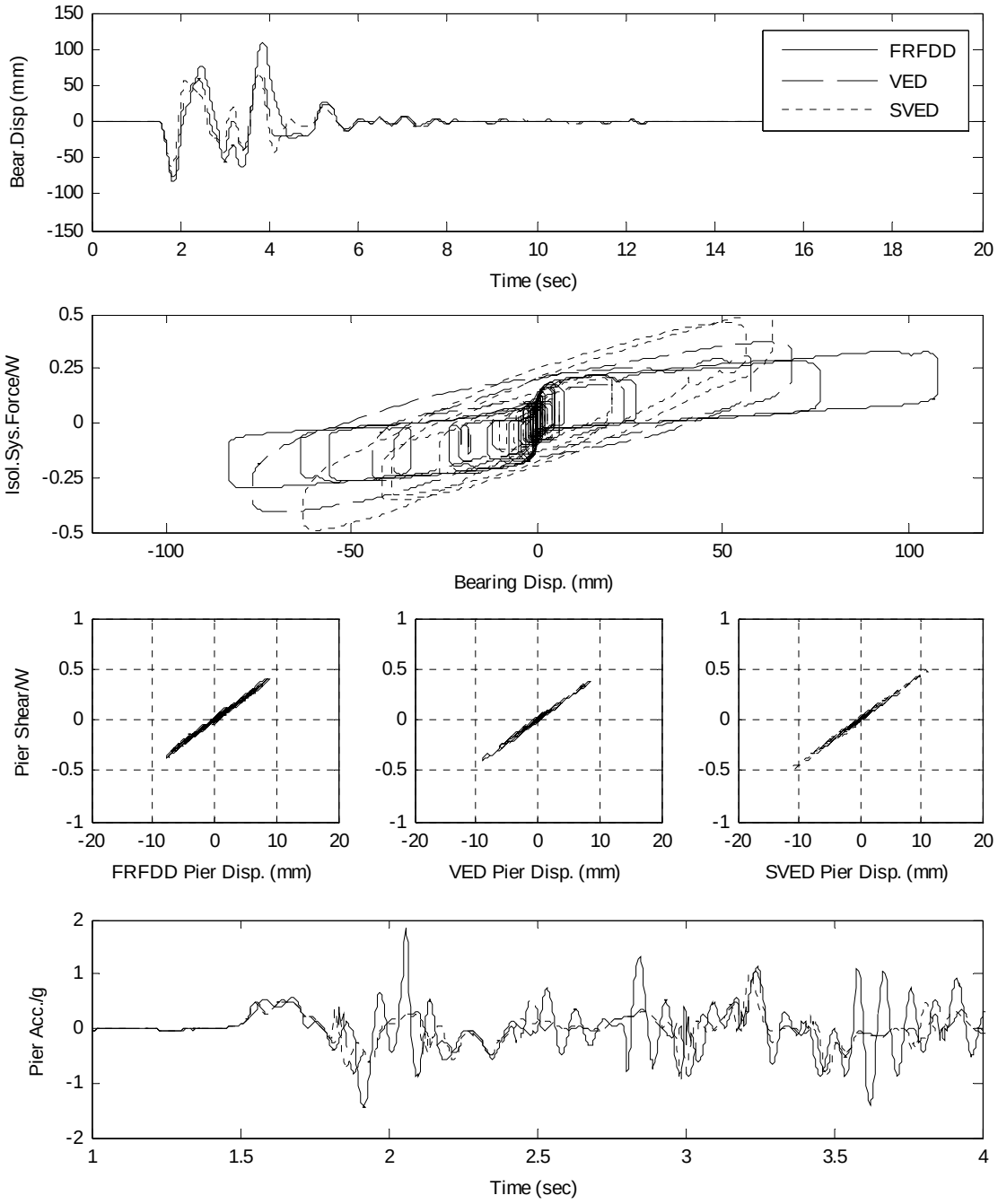

Figure (8-54) Comparison in response for isolation systems with FRFDD, VED, SVED subjected to 1994 Northridge USA earthquake, station SCG. Sliding bearings with low friction.

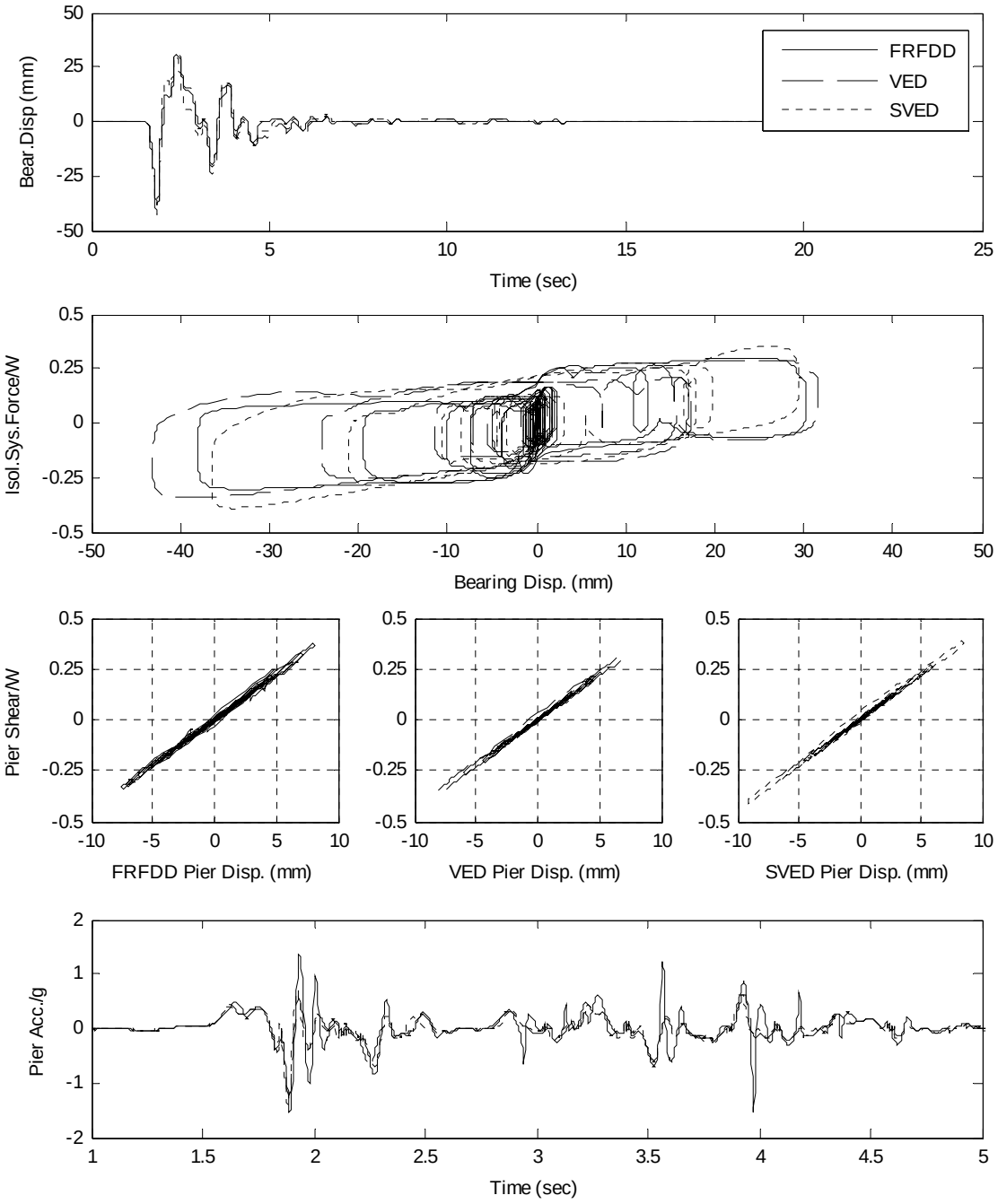

Figures (8-55) Comparison in response for isolation systems with FRFDD, VED, SVED subjected to 1994 Northridge USA earthquake, station SCH.

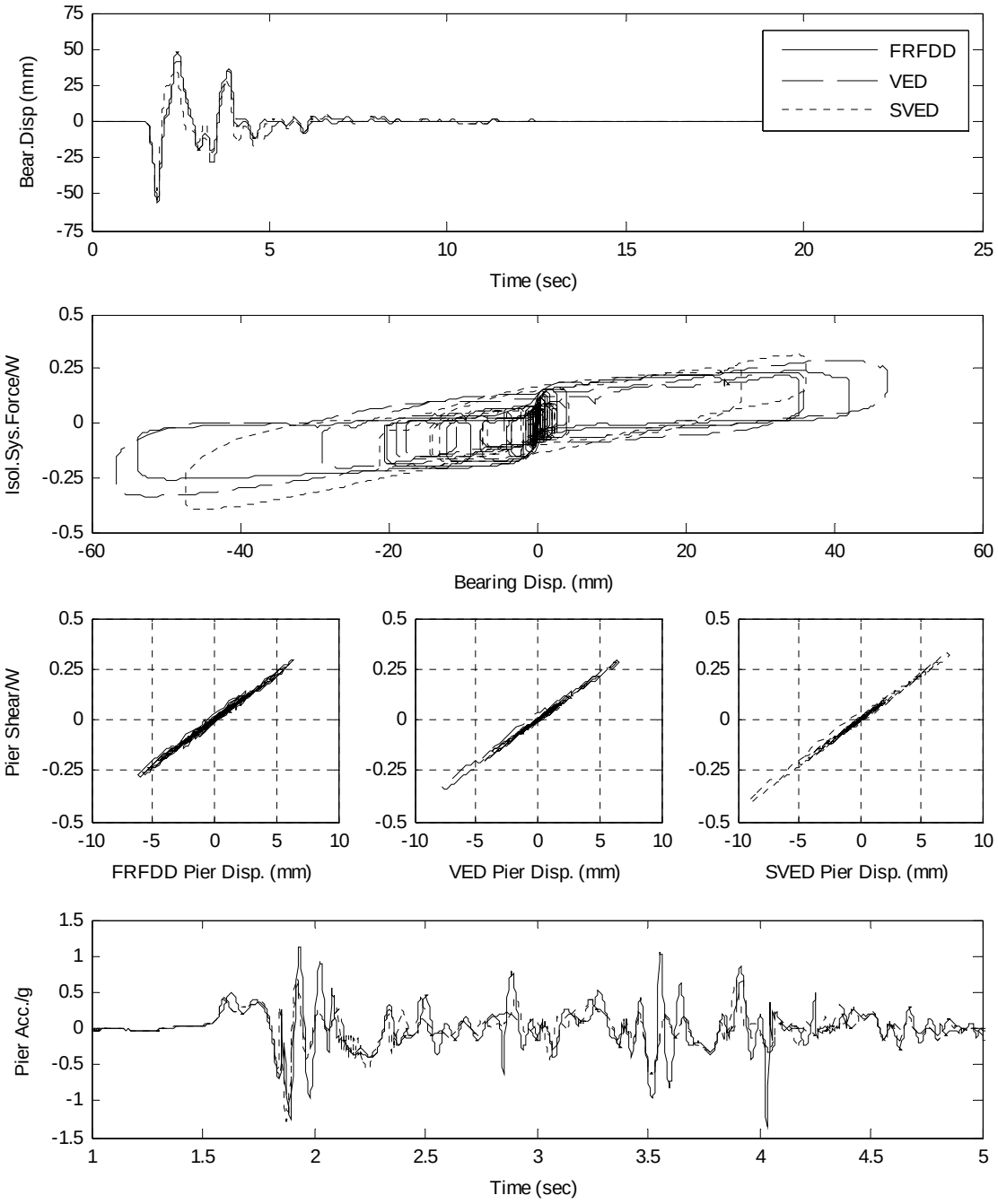

Figure (8-56) Comparison in response for isolation systems with FRFDD, VED, SVED subjected to 1994 Northridge USA earthquake, station SCH. Sliding bearings with low friction.

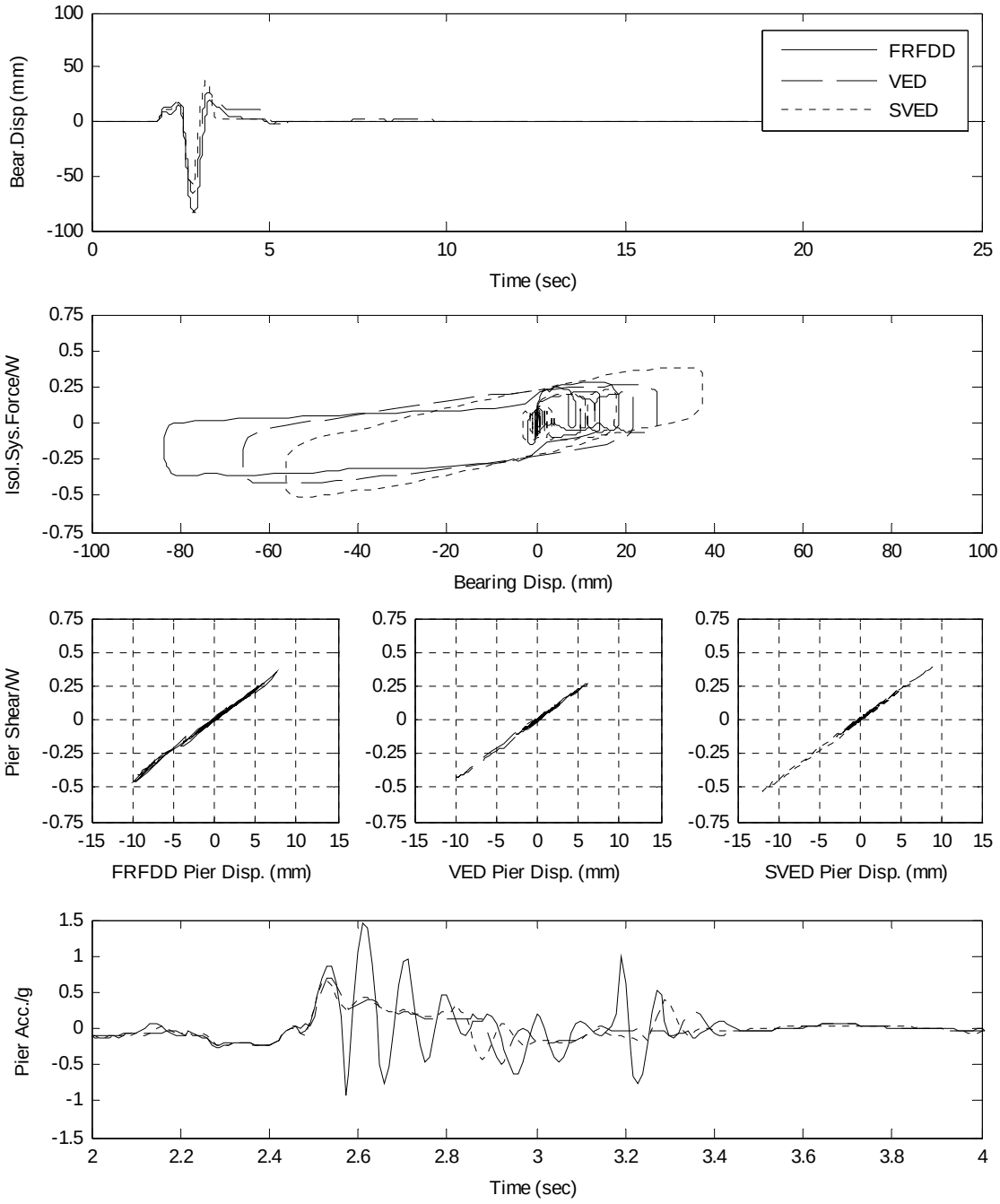

Figure (8-57) Comparison in response for isolation systems with FRFDD, VED, SVED subjected to 1994 Northridge USA earthquake, station NWS.

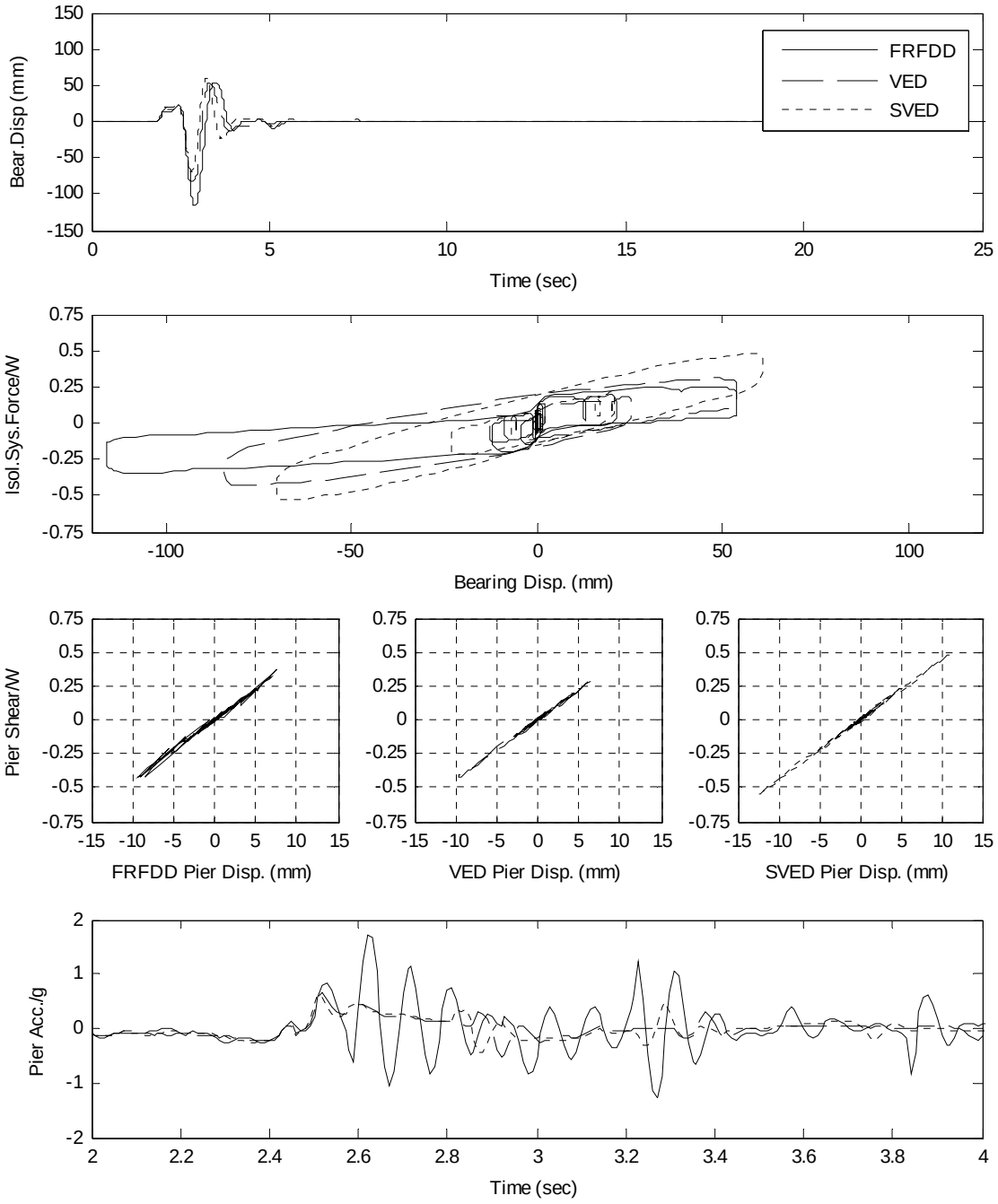

Figure (8-58) Comparison in response for isolation systems with FRFDD, VED, SVED subjected to 1994 Northridge USA earthquake, station NWS. Sliding bearings with low friction.

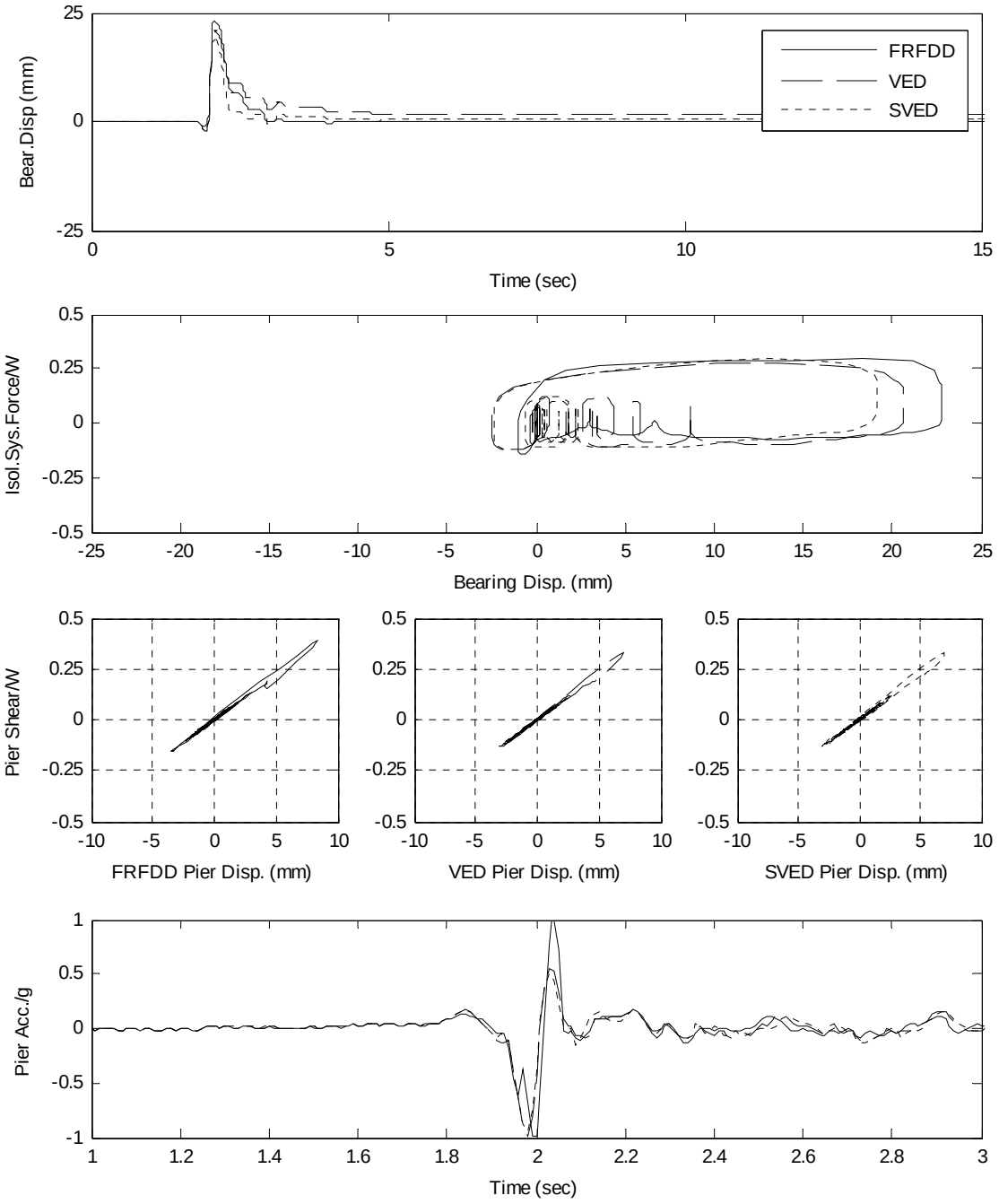

Figure (8-59) Comparison in response for isolation systems with FRFDD, VED, SVED subjected to 1995 Aigion Greece earthquake, station AEG.

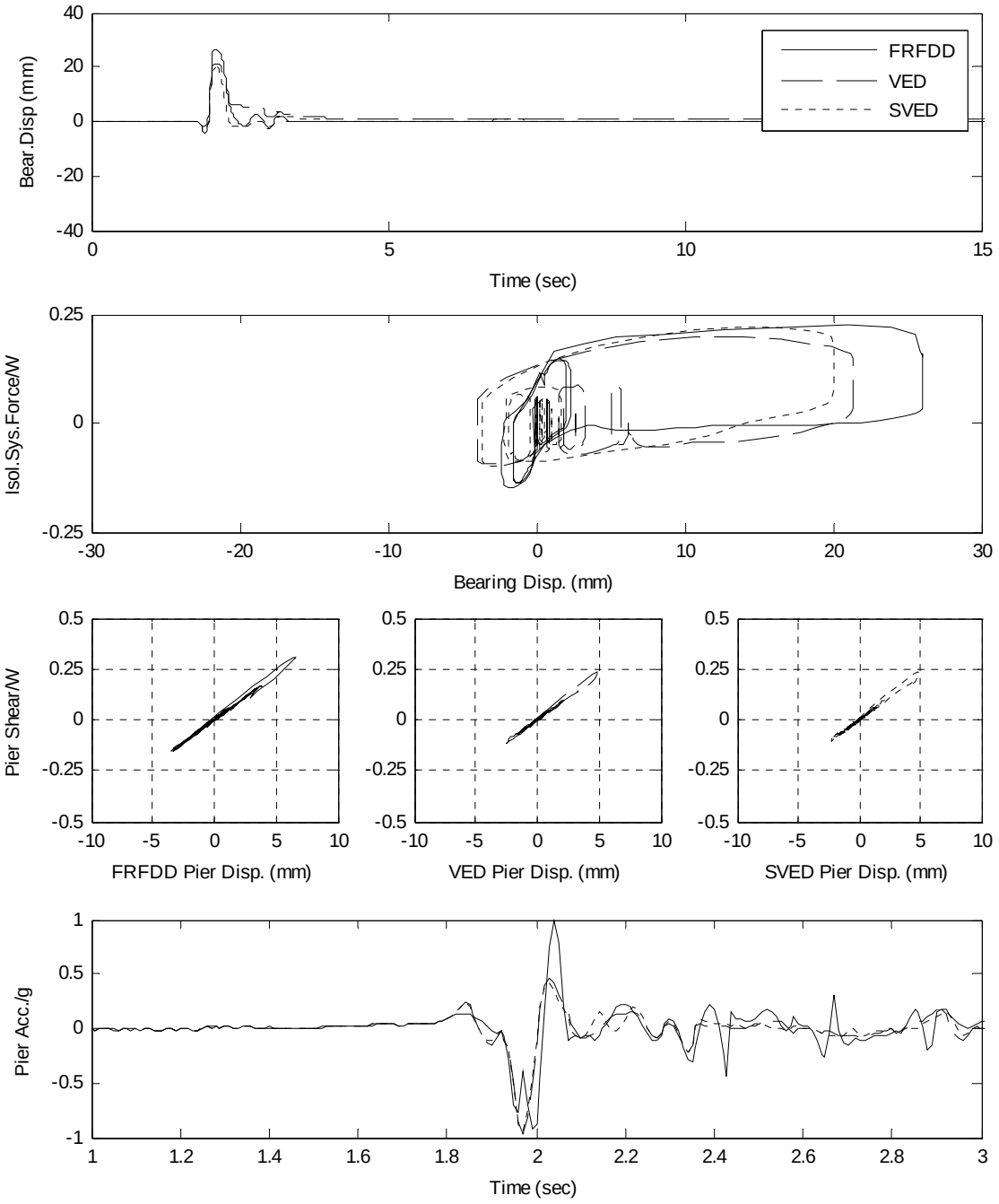

Figure (8-60) Comparison in response for isolation systems with FRFDD, VED, SVED subjected to 1995 Aigion Greece earthquake, station AEG. Sliding bearings with low friction.

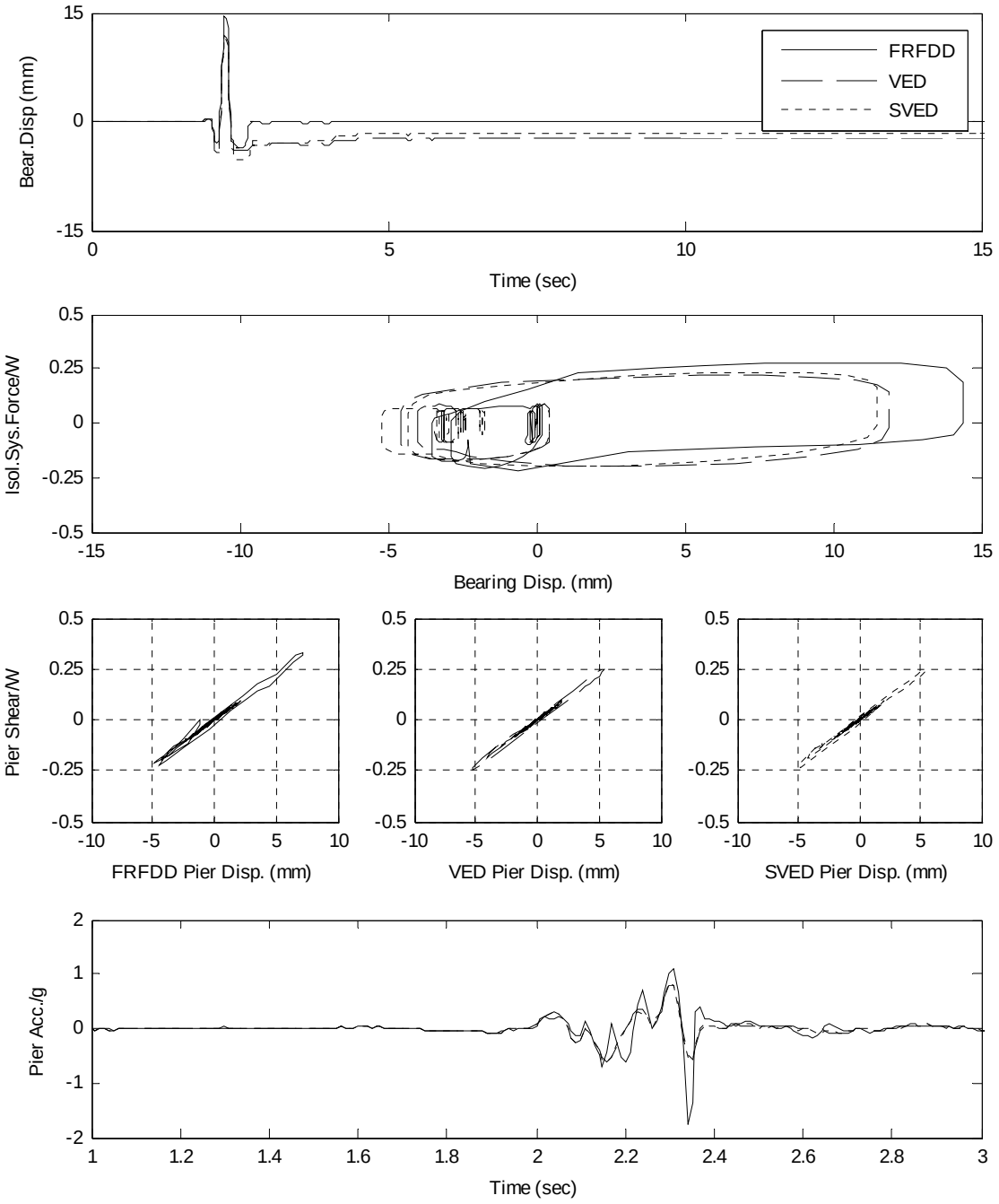

Figure (8-61) Comparison in response for isolation systems with FRFDD, VED, SVED subjected to 1995 Aigion Greece earthquake, station AEG.

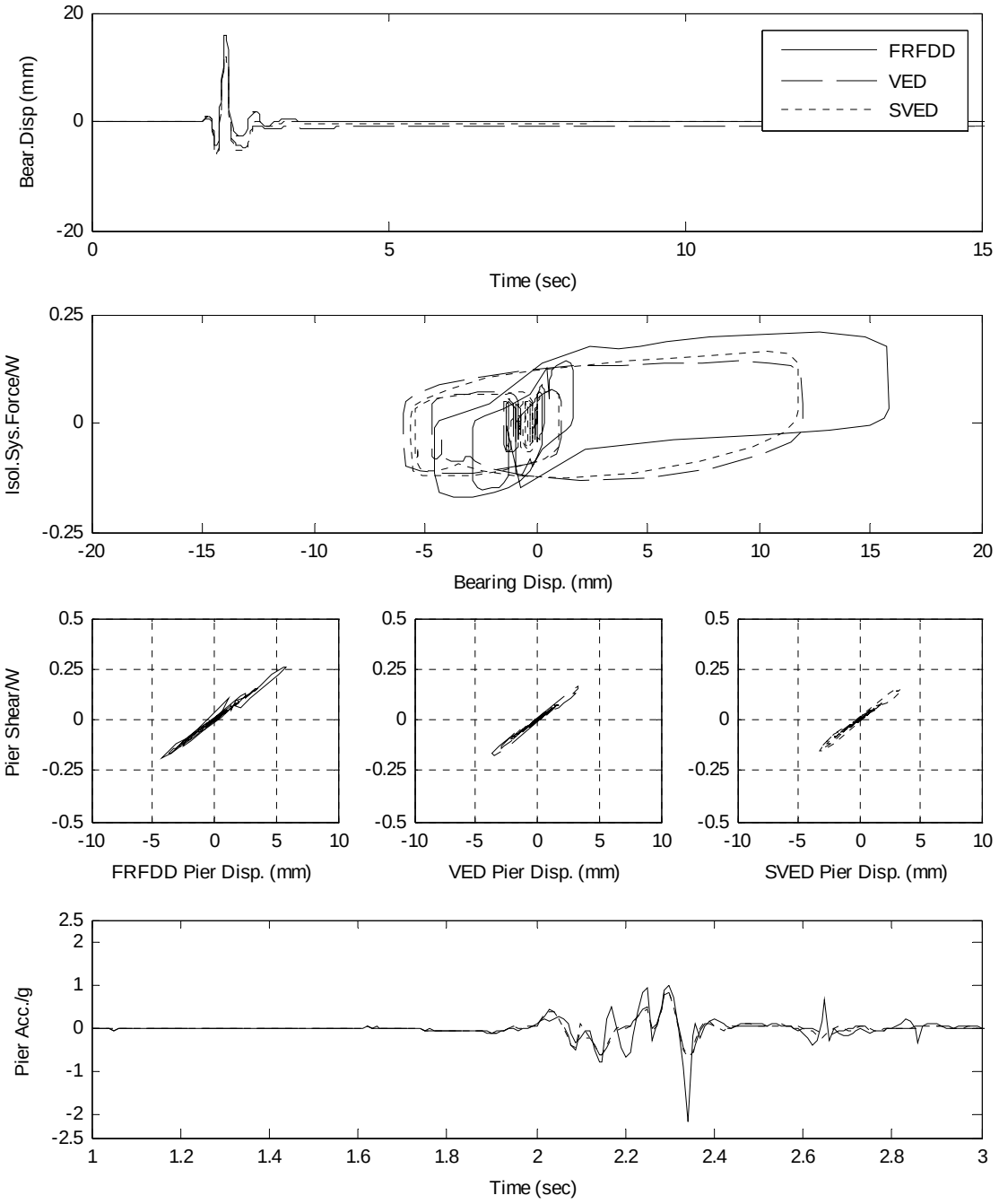

Figure (8-62) Comparison in response for isolation systems with FRFDD, VED, SVED subjected to 1995 Aigion Greece earthquake, station AEG. Sliding bearings with low friction.

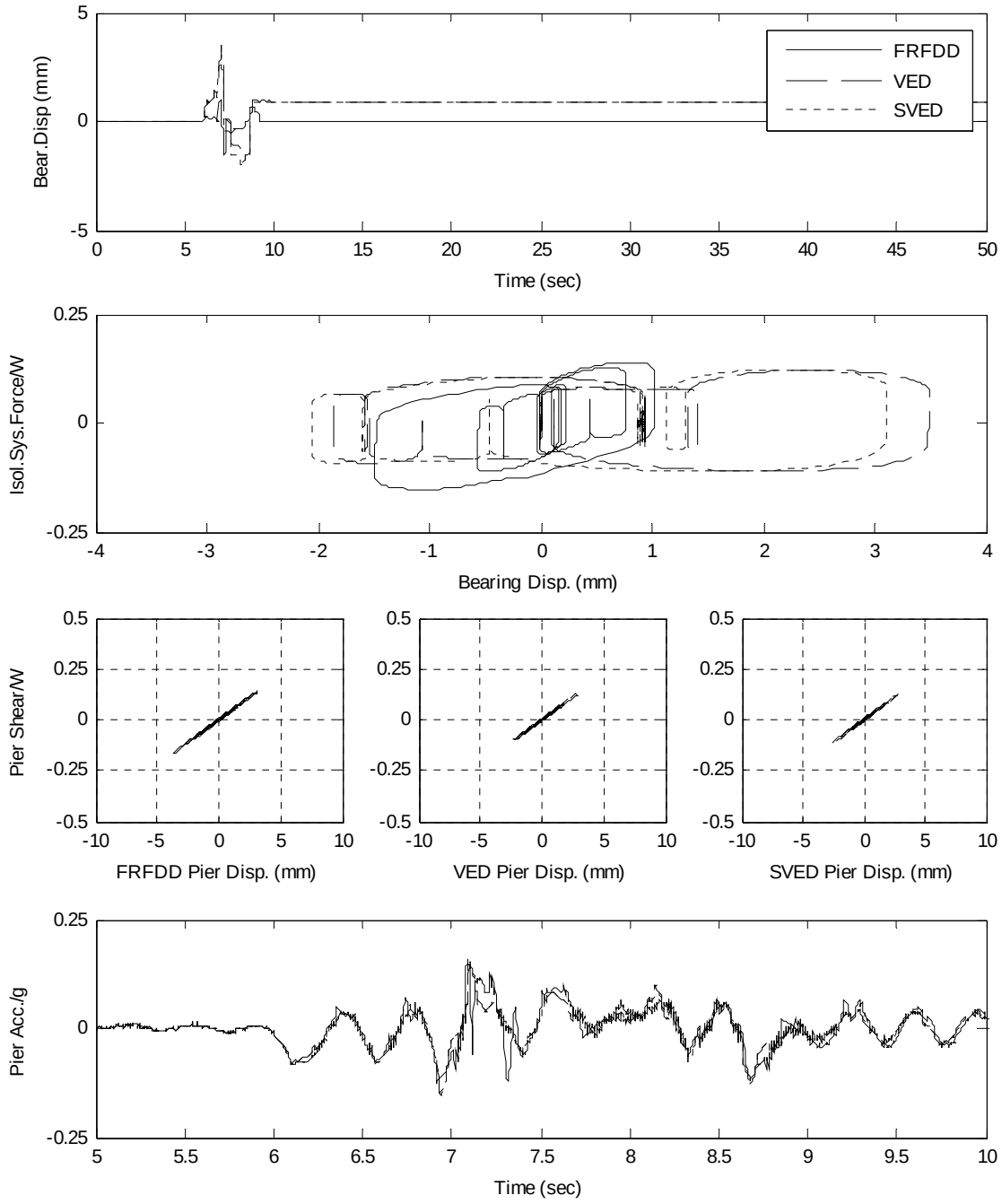

Figure (8-63) Comparison in response for isolation systems with FRFDD, VED, SVED subjected to 1999 Izmit Turkey earthquake, station ARC.

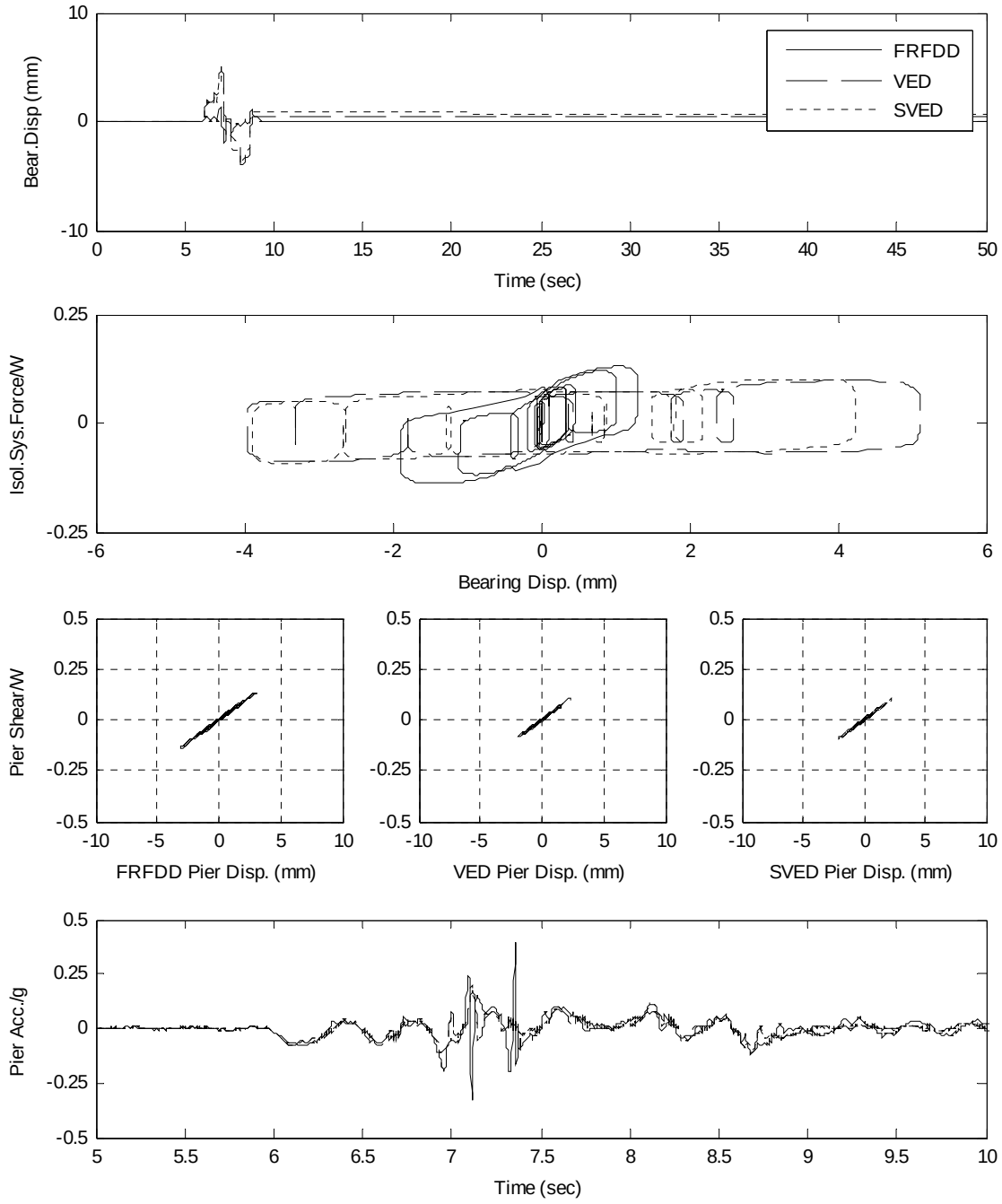

Figure (8-64) Comparison in response for isolation systems with FRFDD, VED, SVED subjected to 1999 Izmit Turkey earthquake, station ARC. Sliding bearings with low friction.

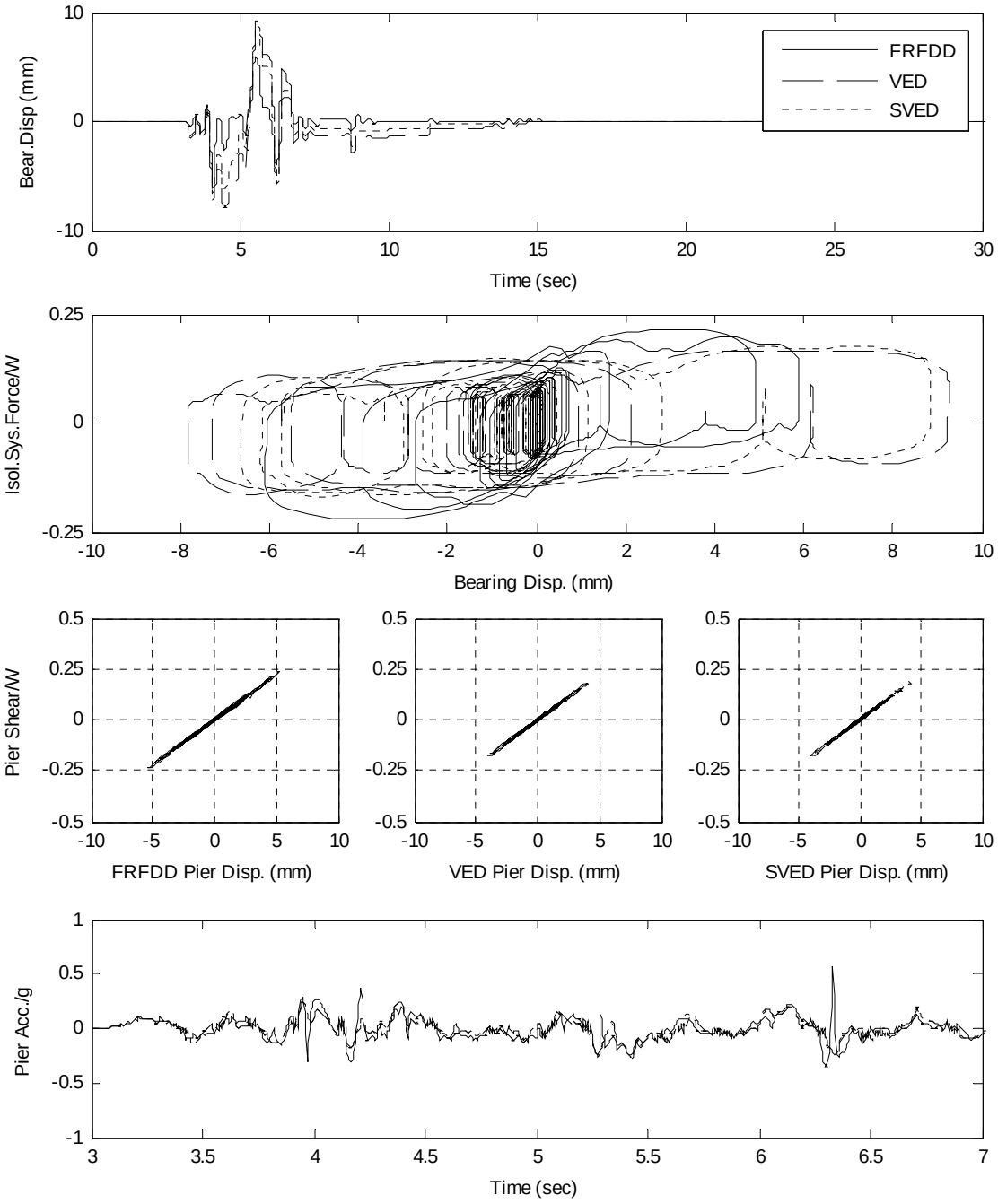

Figure (8-65) Comparison in response for isolation systems with FRFDD, VED, SVED subjected to 1999 Izmit Turkey earthquake, station SKR.

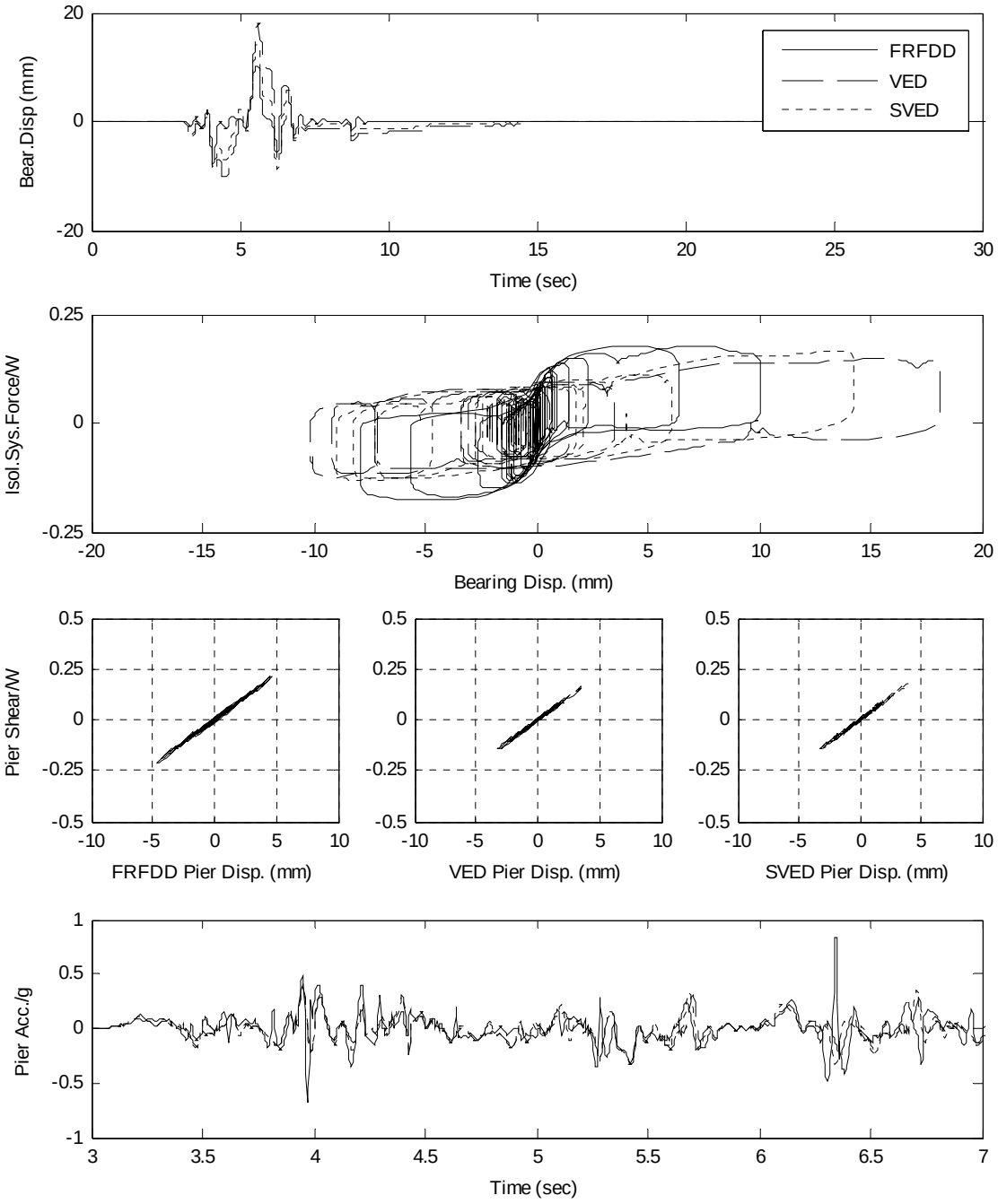

Figure (8-66) Comparison in response for isolation systems with FRFDD, VED, SVED subjected to 1999 Izmit Turkey earthquake, station SKR. Sliding bearings with low friction.

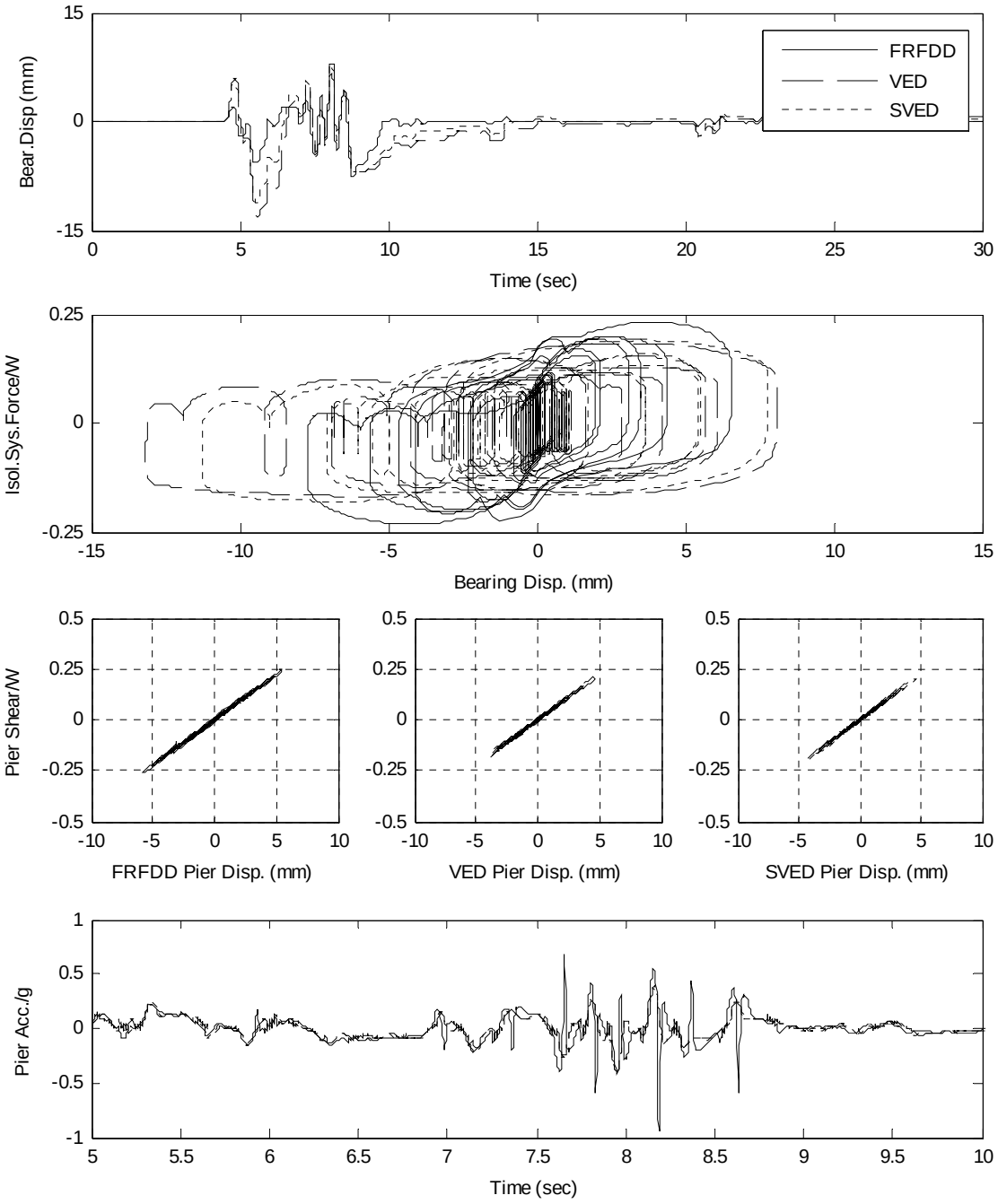

Figure (8-67) Comparison in response for isolation systems with FRFDD, VED, SVED subjected to 1999 Izmit Turkey earthquake, station YPT (first pulse).

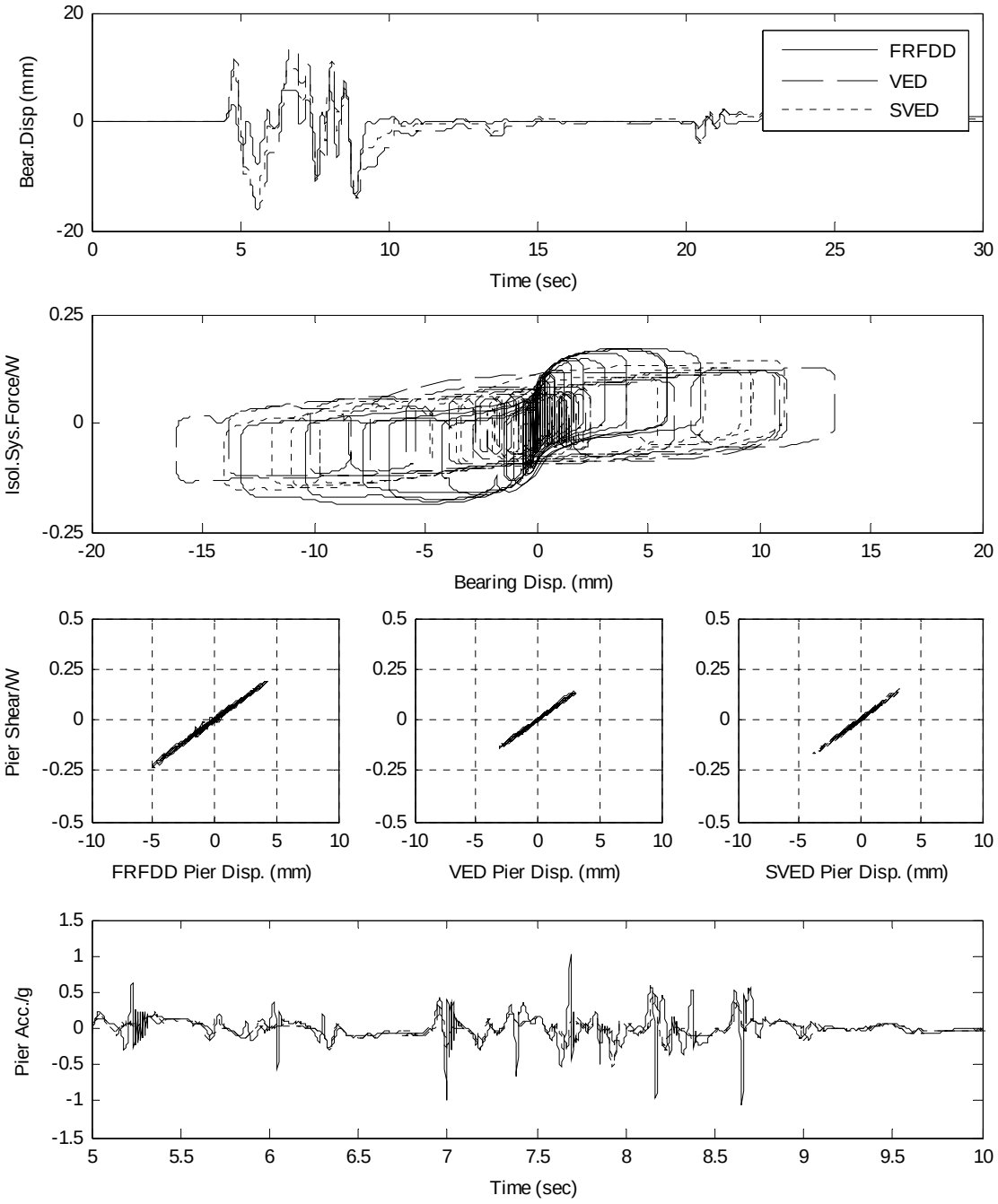

Figure (8-68) Comparison in response for isolation systems with FRFDD, VED, SVED subjected to 1999 Izmit Turkey earthquake, station YPT (first pulse). Sliding bearings with low friction.

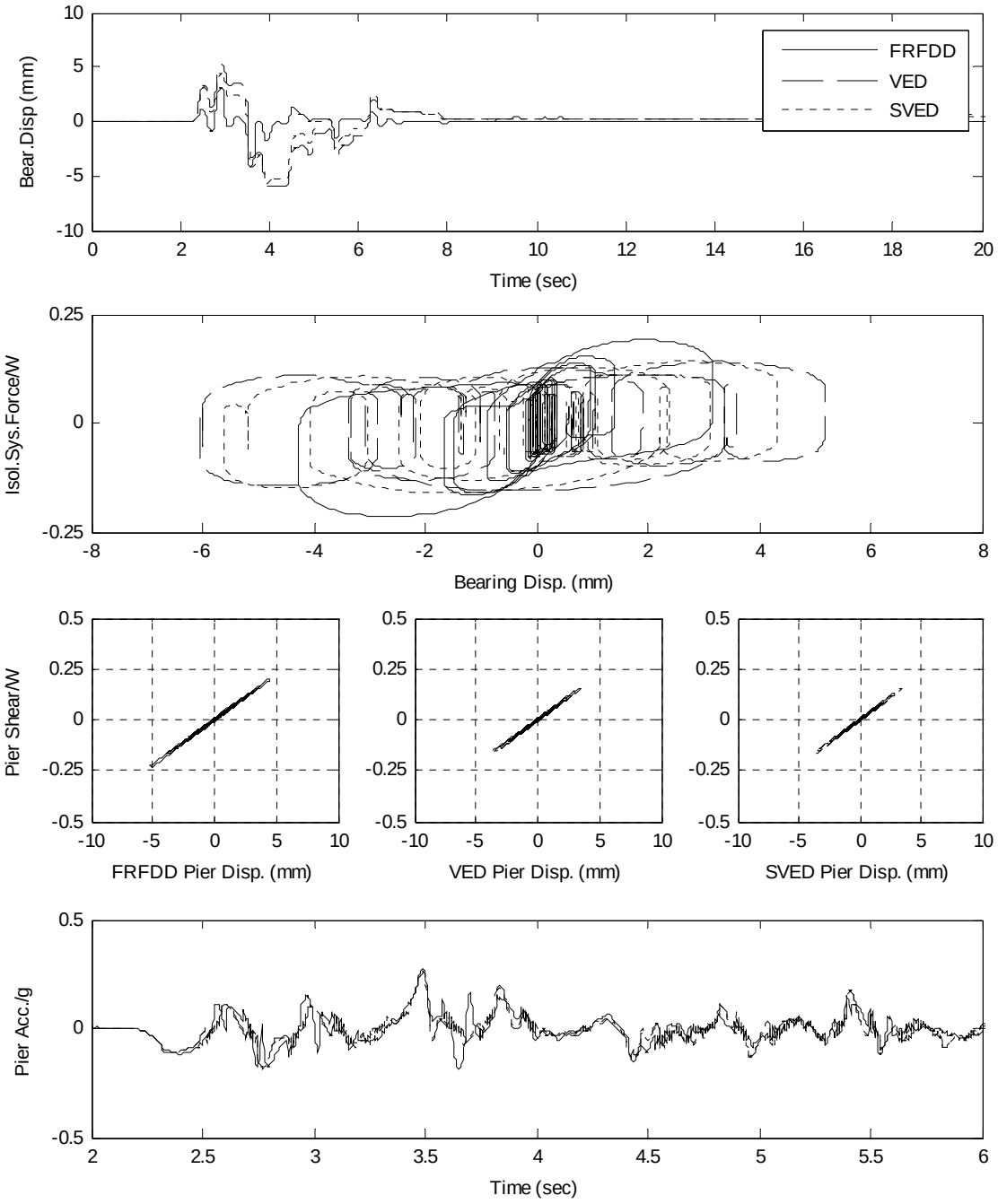

Figure (8-69) Comparison in response for isolation systems with FRFDD, VED, SVED subjected to 1999 Izmit Turkey earthquake, station GBZ (SN component).

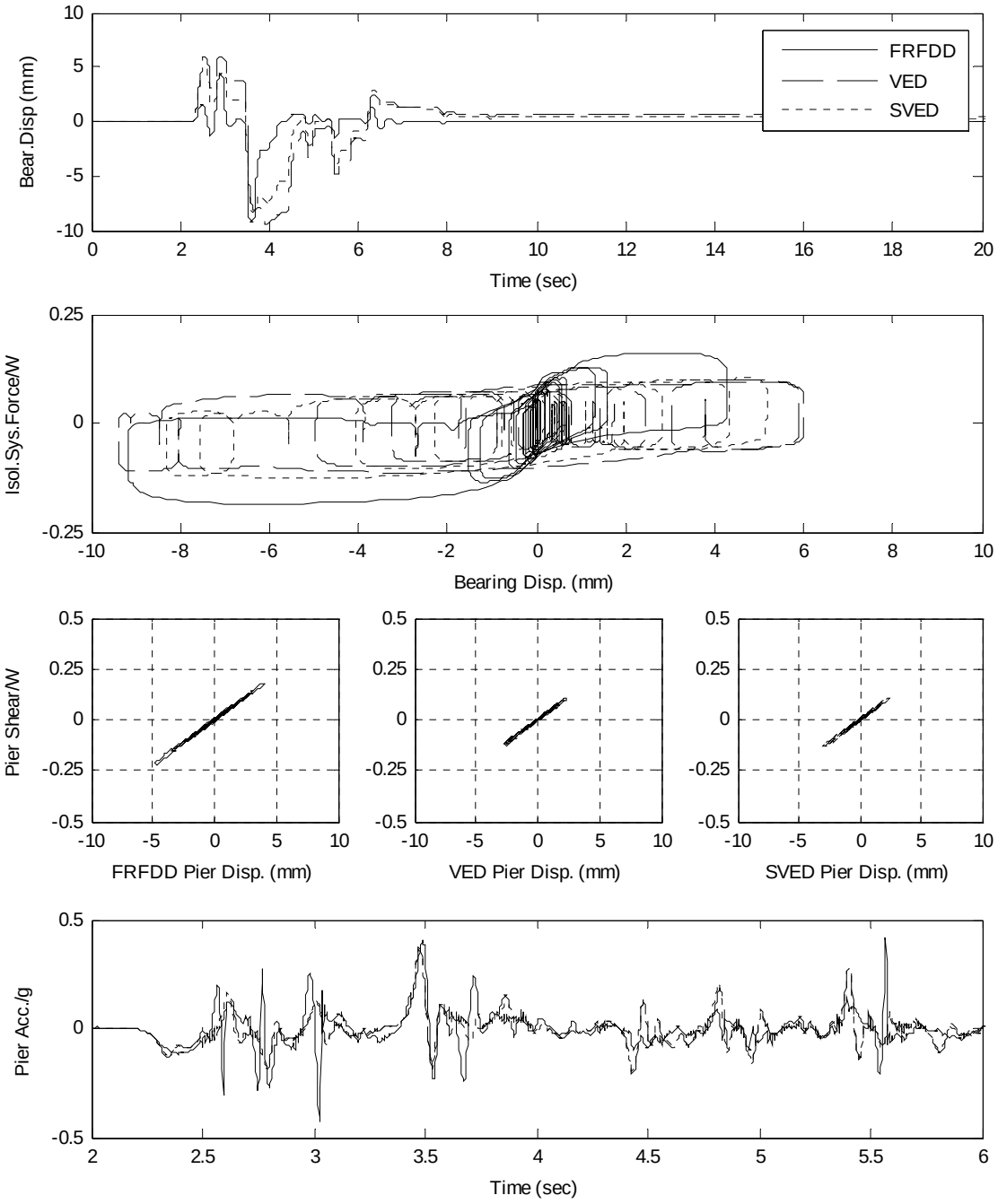

Figure (8-70) Comparison in response for isolation systems with FRFDD, VED, SVED subjected to 1999 Izmit Turkey earthquake, station GBZ (SN component). Sliding bearing with low friction.

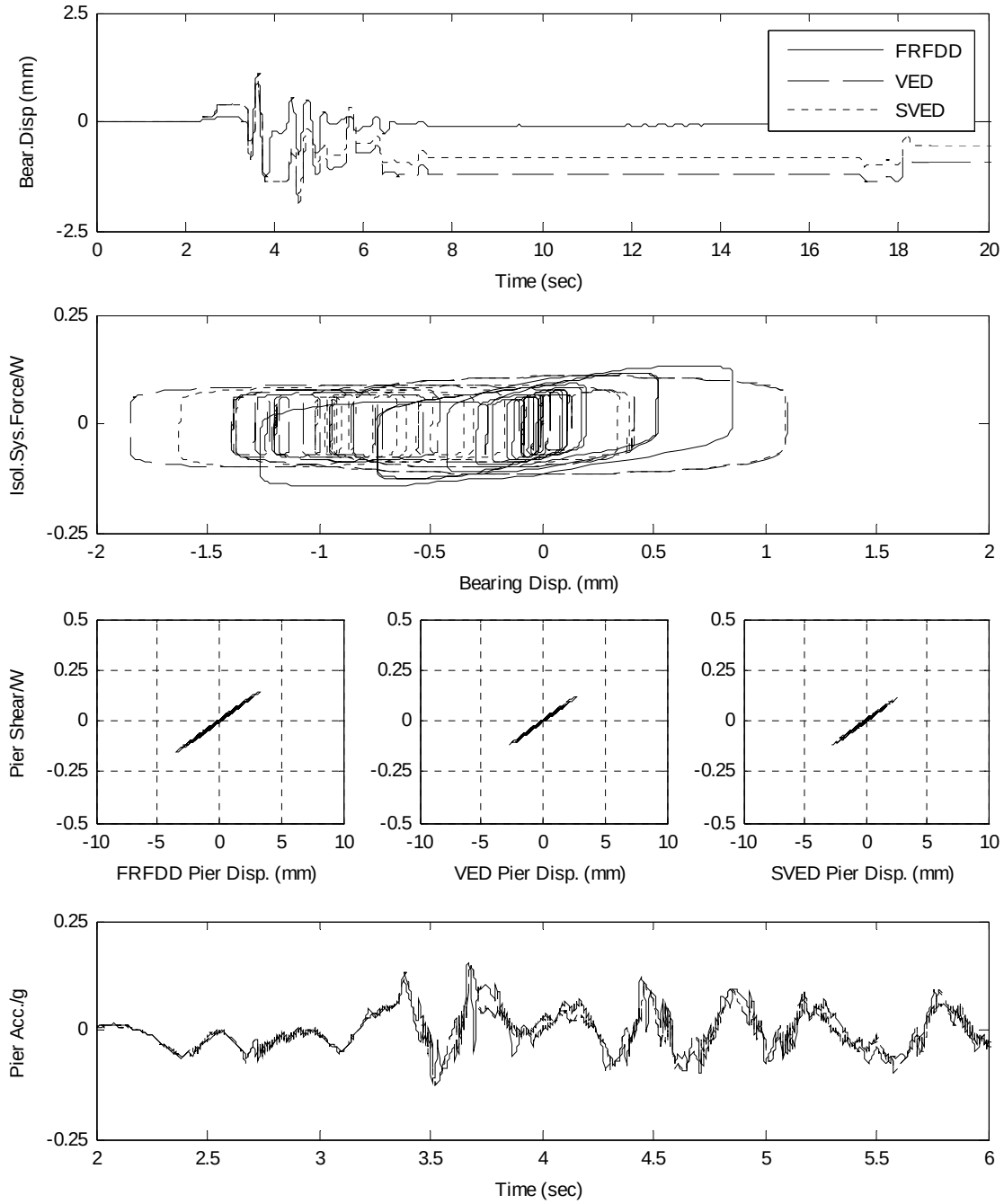

Figure (8-71) Comparison in response for isolation systems with FRFDD, VED, SVED subjected to 1999 Izmit Turkey earthquake, station GBZ (SP component).

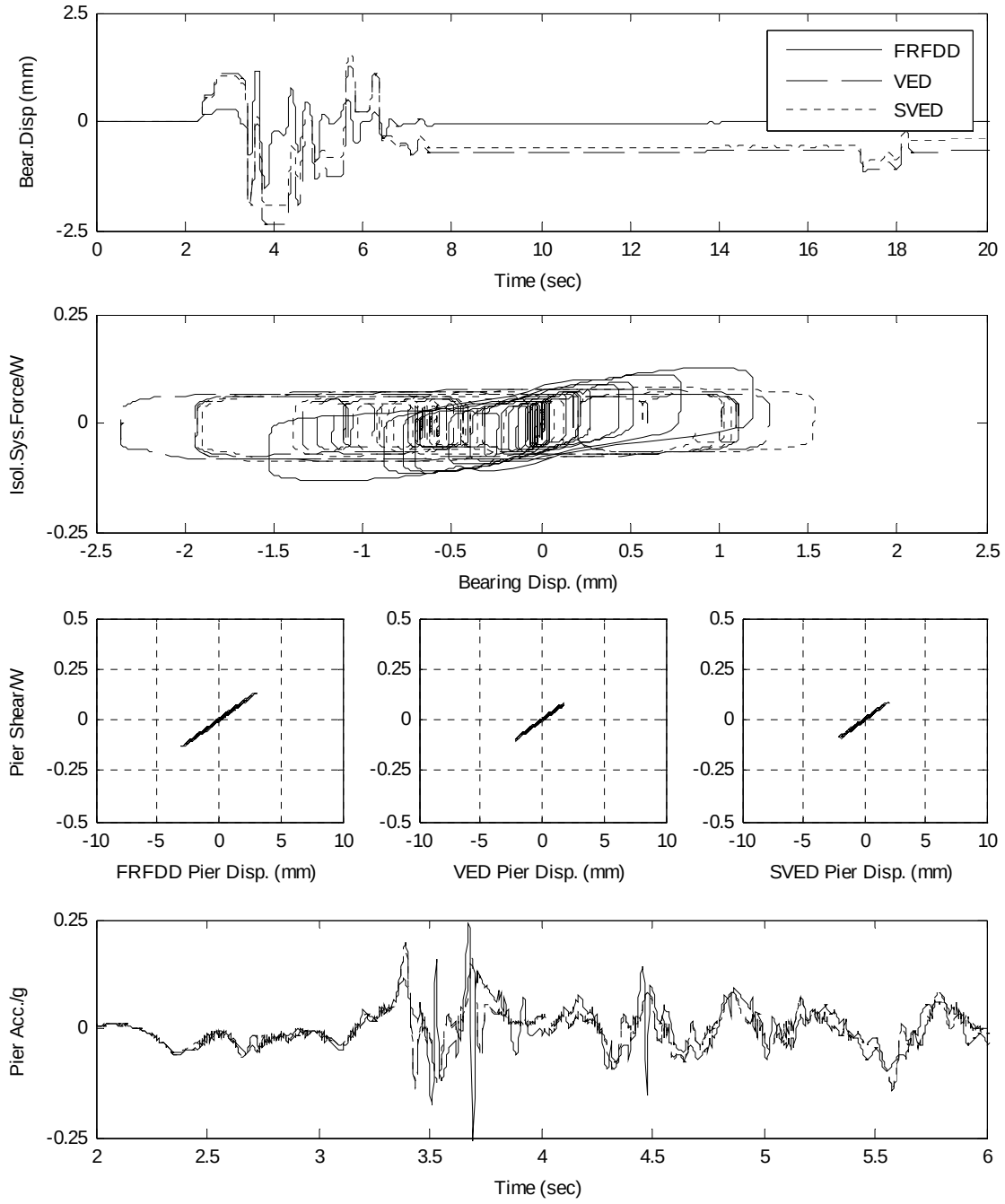

Figure (8-72) Comparison in response for isolation systems with FRFDD, VED, SVED subjected to 1999 Izmit Turkey earthquake, station GBZ (SP component). Sliding bearings with low friction.

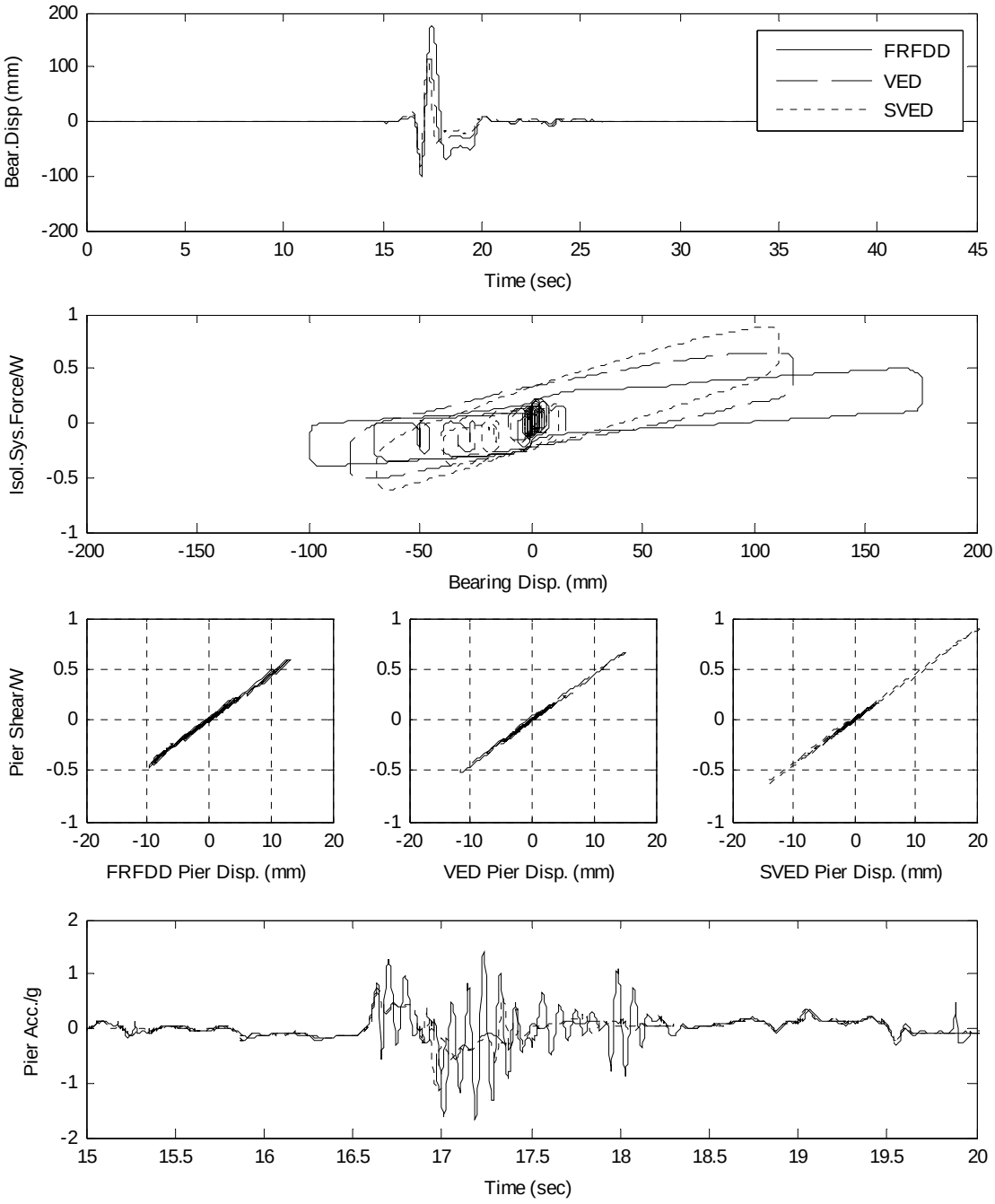

Figure (8-73) Comparison in response for isolation systems with FRFDD, VED, SVED subjected to 1999 Chi-Chi Taiwan earthquake, station TCU052.

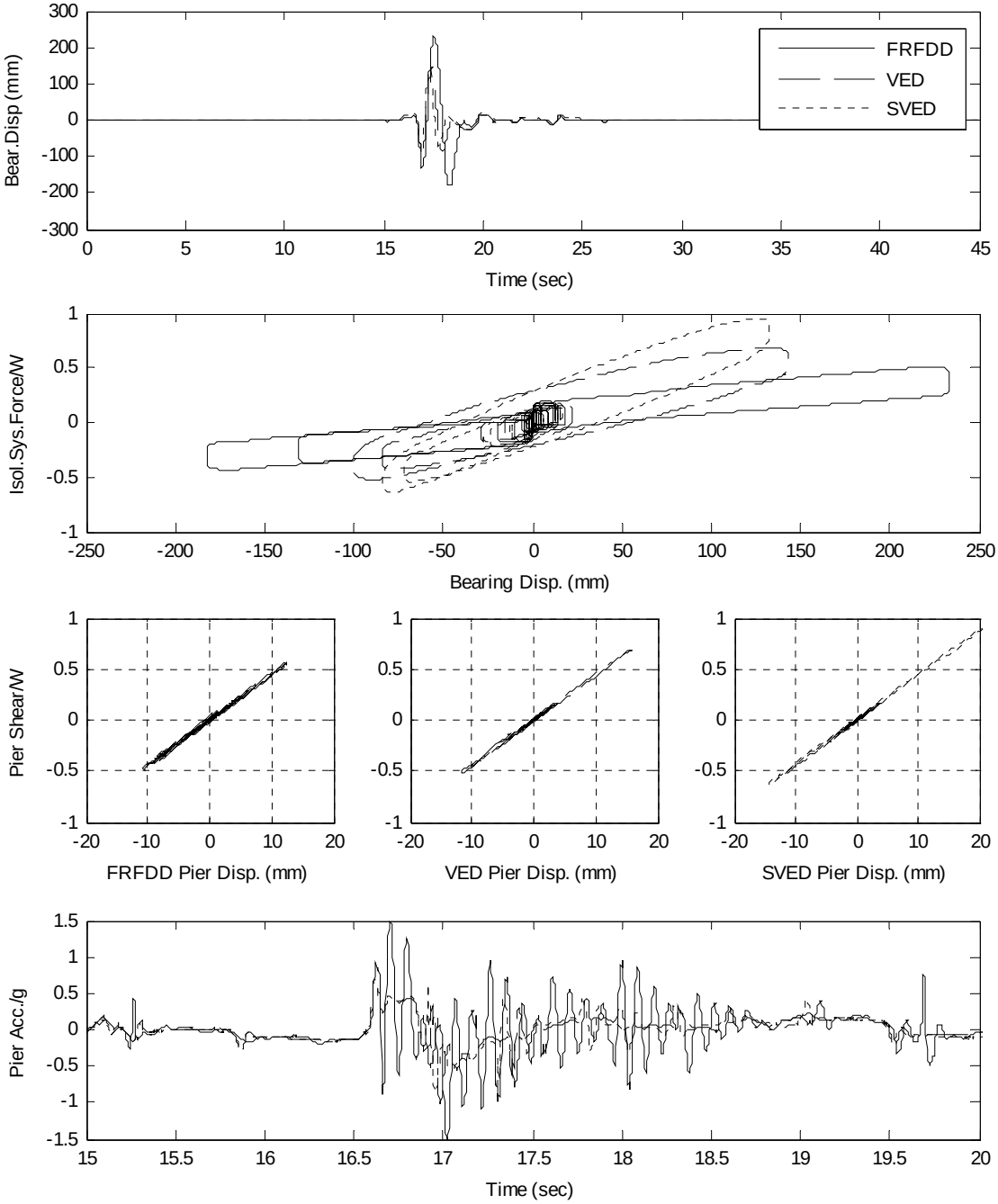

Figure (8-74) Comparison in response for isolation systems with FRFDD, VED, SVED subjected to 1999 Chi-Chi Taiwan earthquake, station TCU052. Sliding bearing with low friction.

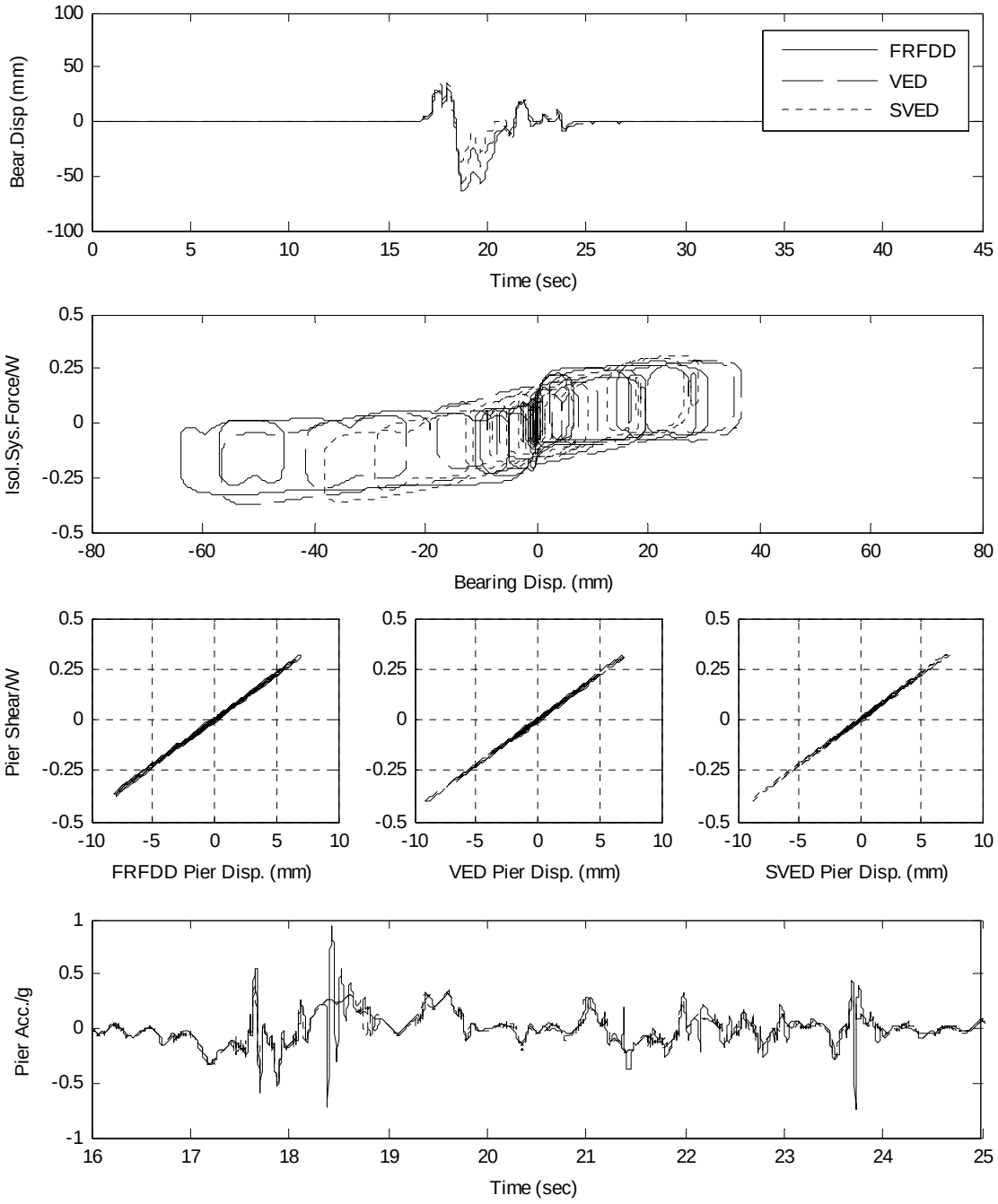

Figure (8-75) Comparison in response for isolation systems with FRFDD, VED, SVED subjected to 1999 Chi-Chi Taiwan earthquake, station TCU068.

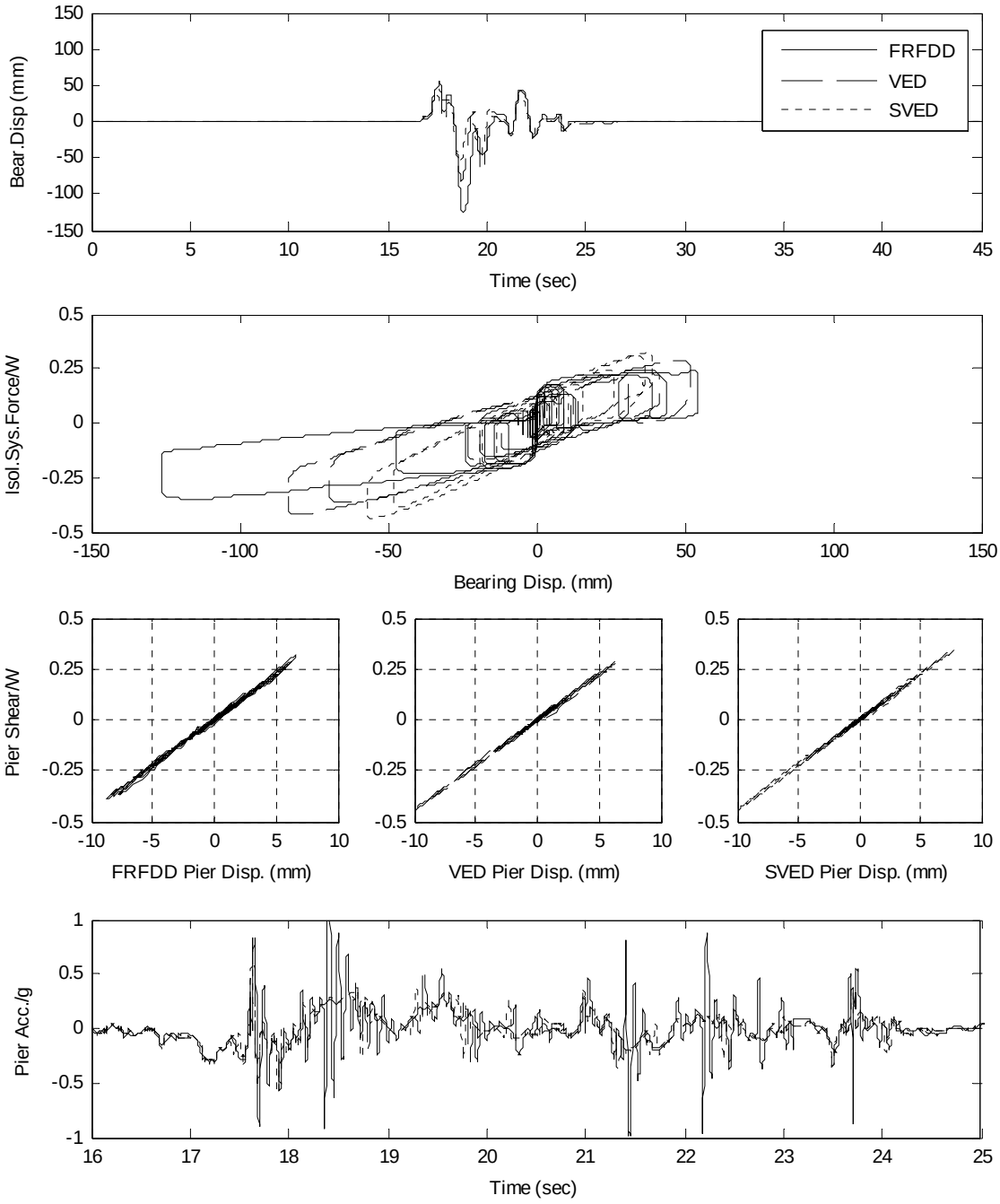

Figure (8-76) Comparison in response for isolation systems with FRFDD, VED, SVED subjected to 1999 Chi-Chi Taiwan earthquake, station TCU068. Sliding bearings with low friction.

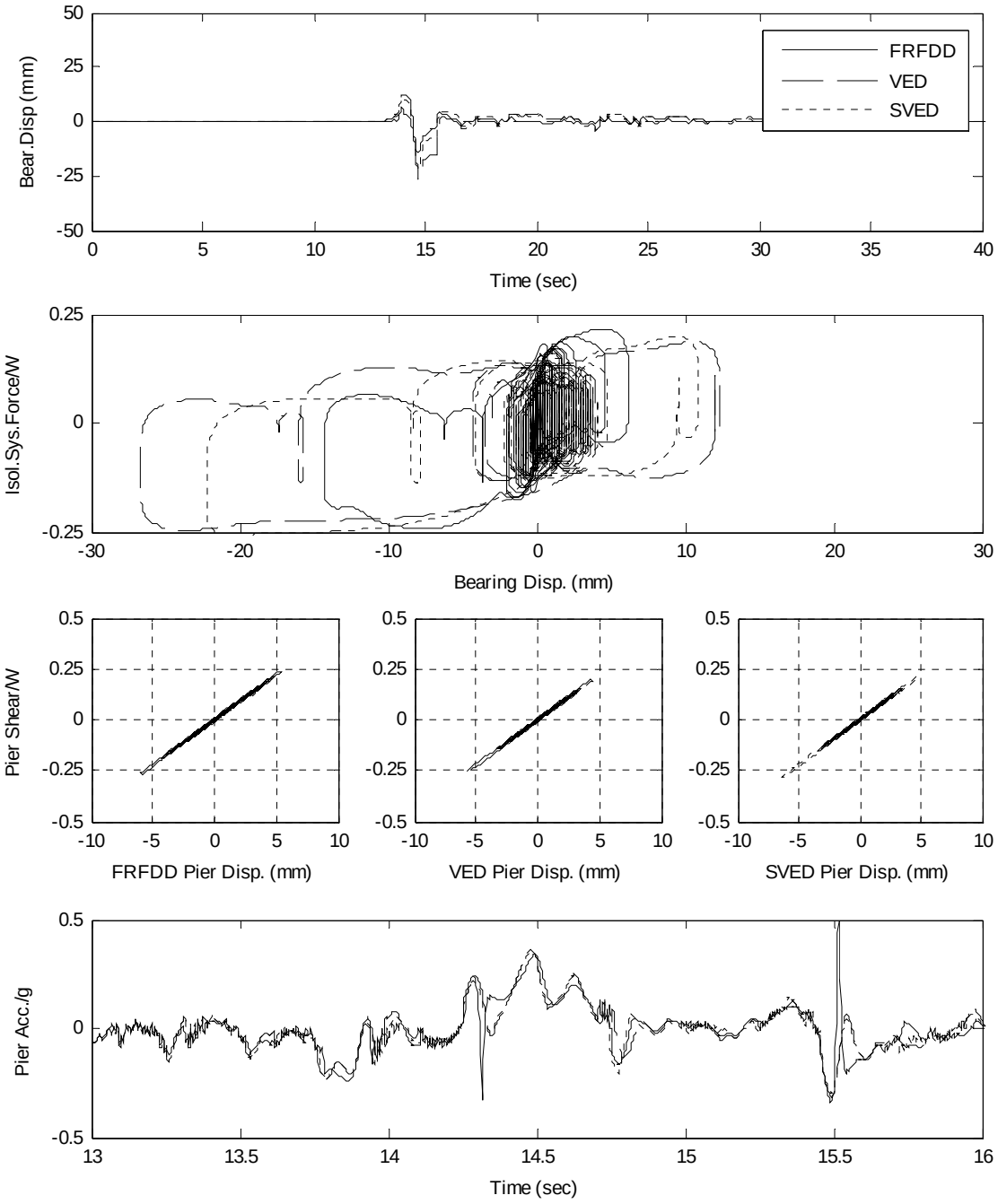

Figure (8-77) Comparison in response for isolation systems with FRFDD, VED, SVED subjected to 1999 Chi-Chi Taiwan earthquake, station TCU05.

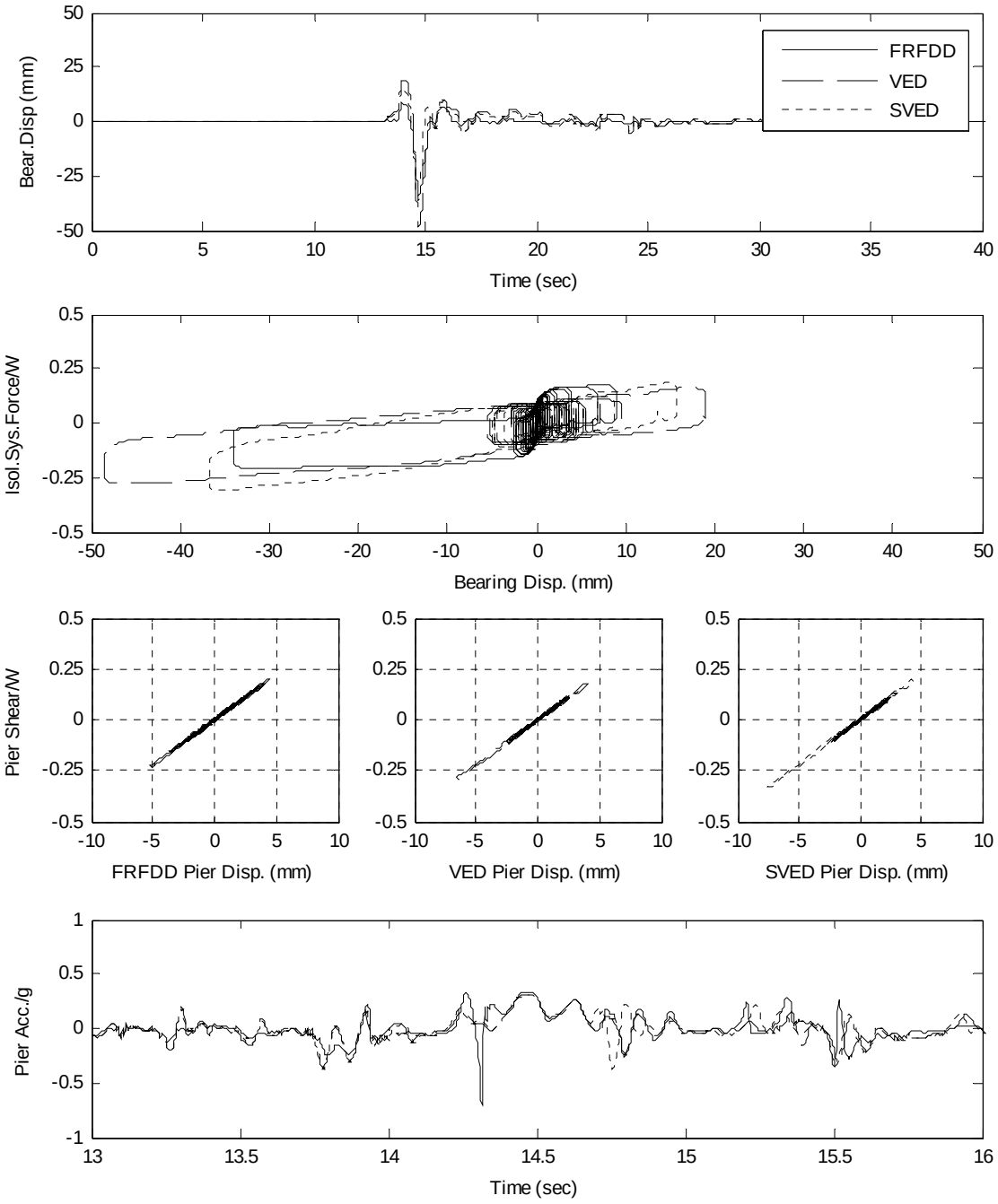

Figure (8-78) Comparison in response for isolation systems with FRFDD, VED, SVED subjected to 1999 Chi-Chi Taiwan earthquake, station TCU05. Sliding bearings with low friction.

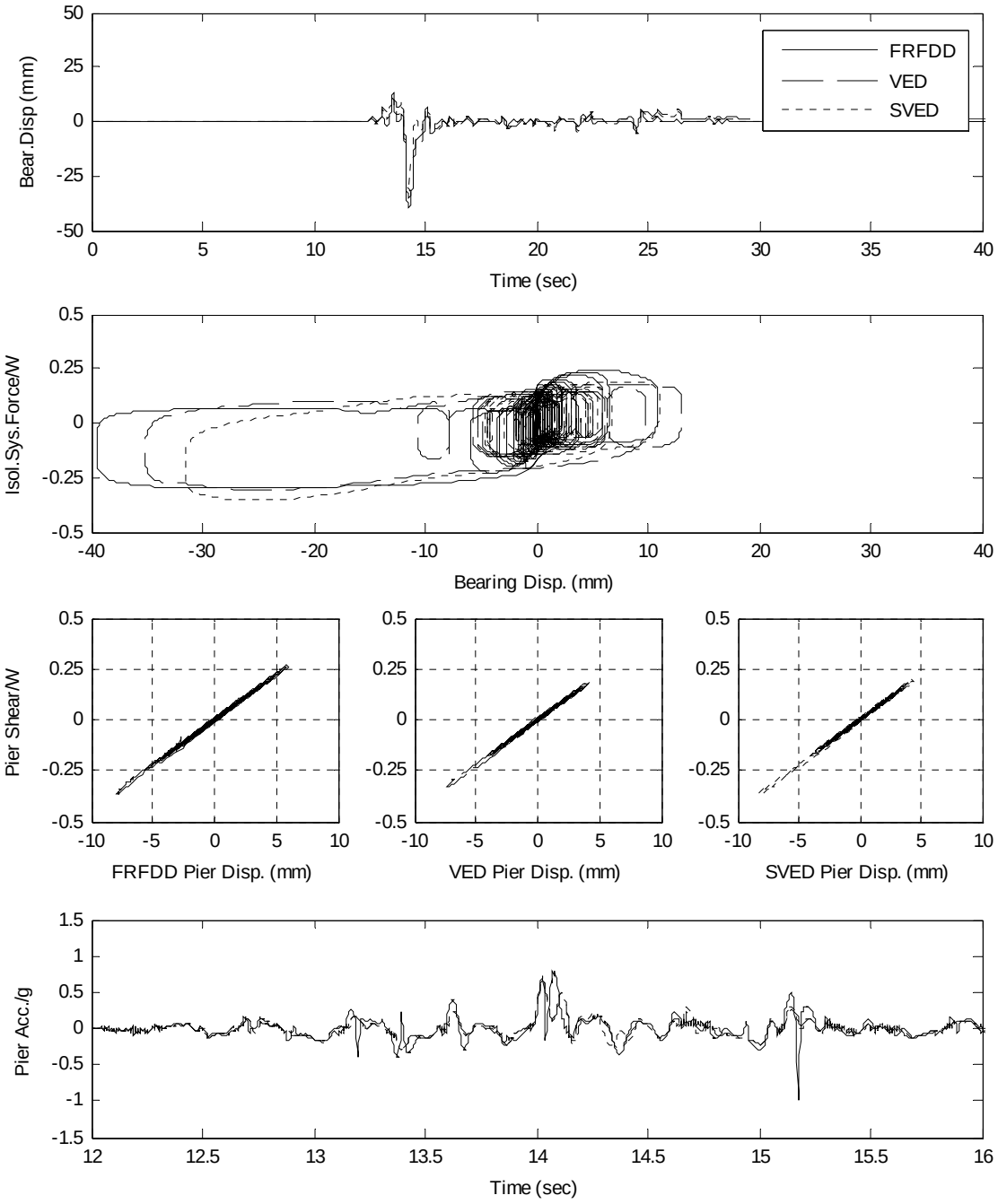

Figures (8-79) Comparison in response for isolation systems with FRFDD, VED, SVED subjected to 1999 Chi-Chi Taiwan earthquake, station TCU076.

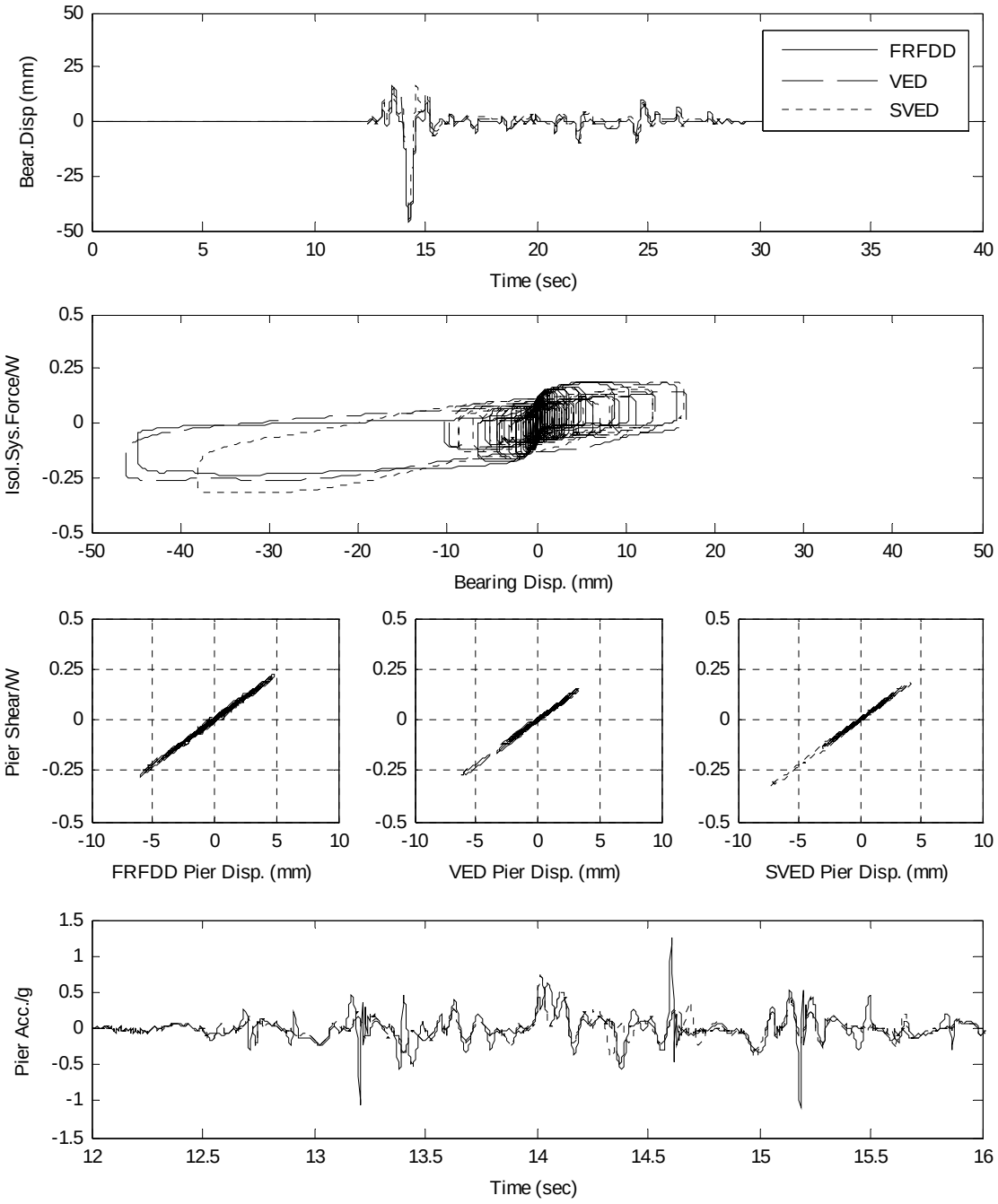

Figure (8-80) Comparison in response for isolation systems with FRFDD, VED, SVED subjected to 1999 Chi-Chi Taiwan earthquake, station TCU076. Sliding bearings with low friction.

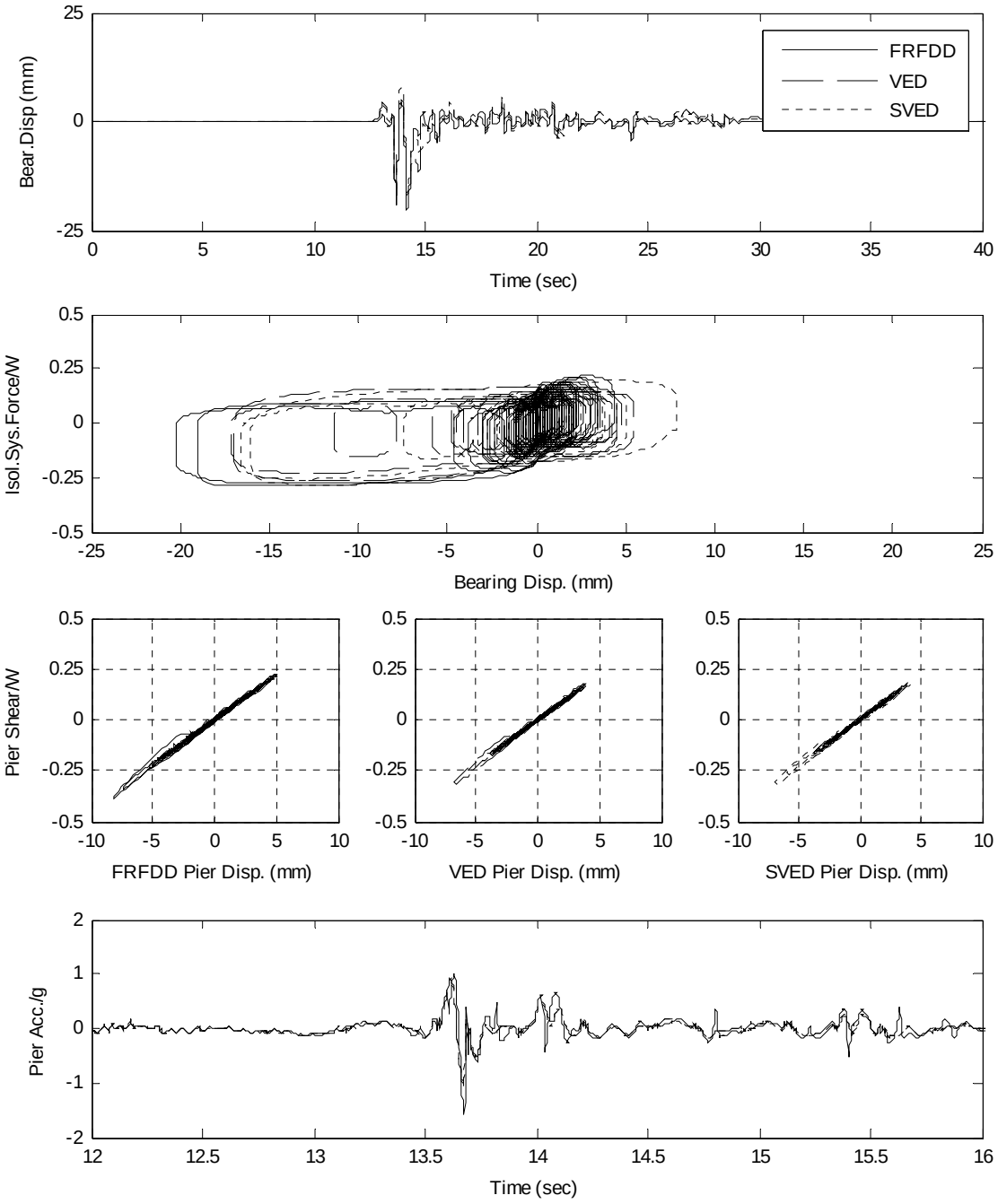

Figure (8-81) Comparison in response for isolation systems with FRFDD, VED, SVED subjected to 1999 Chi-Chi Taiwan earthquake, station TCU129.

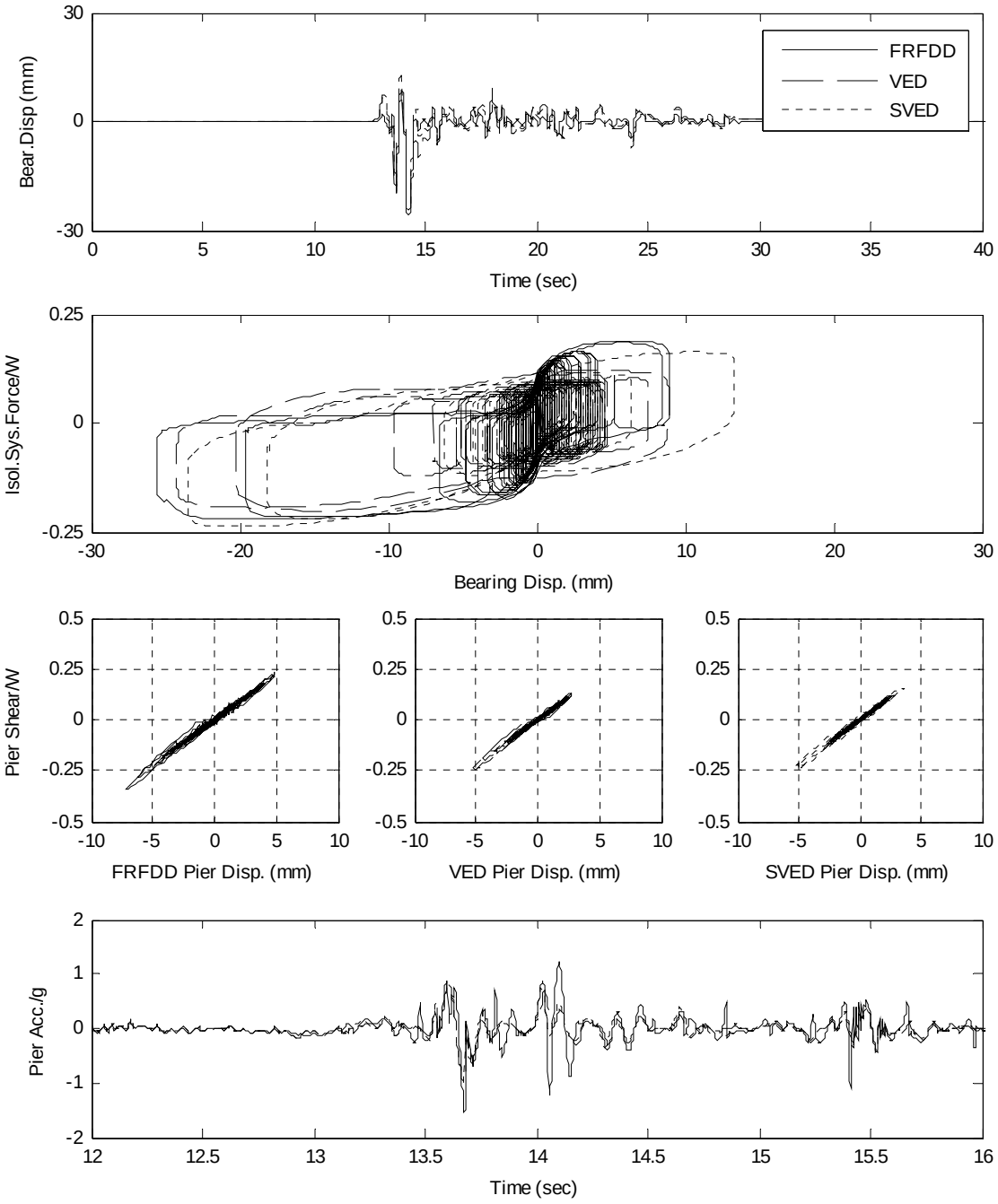

Figure (8-82) Comparison in response for isolation systems with FRFDD, VED, SVED subjected to 1999 Chi-Chi Taiwan earthquake, station TCU129. Sliding bearings with low friction.